



LUND UNIVERSITY

Systematic Antenna Design Using the Theory of Characteristic Modes

Miers, Zachary

2016

Document Version:

Publisher's PDF, also known as Version of record

[Link to publication](#)

Citation for published version (APA):

Miers, Z. (2016). *Systematic Antenna Design Using the Theory of Characteristic Modes*. Lund University.

Total number of authors:

1

Creative Commons License:

CC BY-SA

General rights

Unless other specific re-use rights are stated the following general rights apply:

Copyright and moral rights for the publications made accessible in the public portal are retained by the authors and/or other copyright owners and it is a condition of accessing publications that users recognise and abide by the legal requirements associated with these rights.

- Users may download and print one copy of any publication from the public portal for the purpose of private study or research.
- You may not further distribute the material or use it for any profit-making activity or commercial gain
- You may freely distribute the URL identifying the publication in the public portal

Read more about Creative commons licenses: <https://creativecommons.org/licenses/>

Take down policy

If you believe that this document breaches copyright please contact us providing details, and we will remove access to the work immediately and investigate your claim.

LUND UNIVERSITY

PO Box 117
221 00 Lund
+46 46-222 00 00

Systematic Antenna Design Using the Theory of Characteristic Modes

—

Zachary Thomas Miers

Lund 2016

Department of Electrical and Information Technology
Lund University
Box 118, SE-221 00 LUND
SWEDEN

This thesis is set in Computer Modern 10pt
with the L^AT_EX Documentation System

Series of licentiate and doctoral theses
No. 88
ISSN 1654-790X
ISBN 978-91-7623-910-0 (print)
ISBN 978-91-7623-911-7 (PDF)

© Zachary Thomas Miers 2016
Printed in Sweden by *Tryckeriet i E-huset*, Lund.
November 2016.

To my wonderful wife,

*Thank you for your adventurous spirit, kind gestures,
never-ending patience, and loving heart.*

&

To my family,

*Dad and Mom, thank you for your endless teaching, kindness, and love.
Josh and Seth, thanks for being my best friends.*

*The only person you should try to be better than,
is the person you were yesterday.*

~ Author Unknown

Abstract

The day Faraday moved a magnet in and out of a wire loop and detected the time-varying magnetic field, the first wireless transmitter / receiver system was created and the world was changed forever. However, it took almost fifty years for Heinrich Hertz to use Maxwell's equations and Faraday's insights in his professorship at Karlsruhe to create the first electromagnetic wireless communication system using a spark gap dipole transmitter and a loop antenna-based receiver. This simple system utilized the first non-optical human designed electromagnetic antenna, and since then, businesses, researchers, doctoral candidates, and hobbyists have been trying to determine the best way to design antennas for a variety of different applications. In almost all situations, antennas are designed using either intuition, closed-form equations, or information which can be obtained from Maxwell's equations and a set of boundary conditions. This thesis combines these three design techniques into one by using the Theory of Characteristic Modes (TCM). This theory allows for physics-based electromagnetic insights of an object to be obtained and combined with closed-form equations for all real media, limiting the overall design space, and allowing an engineer's intuition to be focused on an area with greater importance to antenna performance.

TCM is a unique amalgamation of many different theoretical concepts including Maxwell's equations, Sturm-liouville eigenvalue decomposition, Poynting's theorem, and in practical applications the Method of Moments (MoM). TCM was developed first by Garbacz in 1965 and then popularized by Harrington and Mautz in 1971. Many great researchers have put years of effort and hard work into advancing and popularizing TCM, and this thesis would not exist without the advances provided by these great women and men. The research that led to the initial idea of this thesis was based around the development of multiple-input multiple-output (MIMO) antennas for hand held devices, as this type of design environment is

challenging due to the electrical size of the device and the limited real-estate available. As TCM is uniquely suited for analyzing electrically compact systems which require orthogonal modes of radiation, it was a perfect candidate for studying how it can be better applied to this type of application.

The research contained within this thesis, as well as the articles published during the time of this doctoral study, analyze the practical and theoretical applications of TCM and present a set of theoretical proofs, which explain some of the shortcomings pertaining to MoM-based TCM analysis of dielectric or magnetic objects, and provide some solutions to many of these problems. Furthermore, a unique antenna design methodology was developed which allows for electrically compact MIMO terminal antennas to be designed in a fundamentally new way. As TCM provides a unique set of excitation-free attributes, as well as a set of orthogonal surface currents and far-fields, which are determined only by the object's shape and material. These orthogonal attributes can be used to determine how the object's characteristic modes (CMs) relate to a set of closed-form equations. Using the knowledge gained from each CM, and how the CMs link to these equations, small object alterations can be defined and used to adapt and feed the object, creating single or multiple optimized antennas from the object.

Popular Science

The popularity and acceptance of wireless communication technologies have grown substantially in the past twenty years. In 1996 there were 145 million active wireless subscriptions, and in January of 2016 there were over 7.3 billion. This considerable acceptance and integration of wireless devices into everyday life has forced the technologies within these systems to advance at an unprecedented rate. To support the huge demand, wireless communication technologies have to constantly evolve. One key evolutionary step in enabling high performance wireless communication systems was the introduction of multiple-input multiple-output (MIMO) systems. MIMO technology utilizes complex processing, intricate front-end systems, multiple antennas, and rich channel scattering to provide high data rates and link reliability. To meet the ever increasing needs of the fourth and upcoming fifth generation cellular systems, the design procedures of nearly all components in any wireless device have substantially changed. However, this has not been the case for one vital wireless component, i.e., integrated antennas.

In this thesis an antenna design paradigm which changes how integrated antennas are designed for many modern communication systems is formulated. This paradigm relies on the Theory of Characteristic Modes (TCM) to provide clear physical insights into an object's electromagnetic properties. TCM was originally developed in the late 1960's in an effort to fundamentally understand how an object scatters electromagnetic energy. However, this topic did not initially excite the electromagnetic community, and as such, the area did not advance significantly until recently when it was observed that TCM was uniquely suited for MIMO antenna design.

TCM calculates a set of surface currents that provide orthogonal far-fields. These currents can then be used to determine a wide variety of different radiation-related quantities, which can in turn be used to fully understand the electromag-

netic properties of any object. The developed antenna design paradigm utilizes the calculated quantities to determine the resonant characteristics of an object and how to alter any object into resonating at a defined frequency over a required bandwidth, without the need to define an excitation source. This is substantially different from the traditional integrated antenna design framework, which is based upon intuition and numerical optimization.

Preface

This doctoral thesis concludes my work as a Ph.D. student and is comprised of two parts. The first part gives an overview of the research field in which I have been working during my Ph.D. studies, and a brief summary of my contribution in it. The second part is composed of six included papers that constitute my most significant contributions to the field of characteristic mode analysis:

- [I] Zachary T. Miers and Buon Kiong Lau, “Wide band characteristic mode tracking utilizing far-field patterns,” *IEEE Antennas Wireless Propagation Letters*, vol. 14, pp. 1658-1661, 2015.
- [II] Zachary T. Miers and Buon Kiong Lau, “Computational analysis and verifications of characteristic modes in real materials,” *IEEE Transactions on Antennas and Propagation*, vol. 64, no. 7, pp. 2595-2607, Jul. 2016.
- [III] Zachary T. Miers and Buon Kiong Lau, “On characteristic eigenvalues of complex media in surface integral formulations,” *IEEE Antennas Wireless Propagation Letters*, Submitted.
- [IV] Zachary T. Miers and Buon Kiong Lau, “Antenna analysis and design using characteristic modes,” in preparation for submission to *IEEE Transactions on Antennas and Propagation*.
- [V] Zachary T. Miers, Hui Li, and Buon Kiong Lau, “Design of bandwidth enhanced and multiband MIMO antennas using characteristic modes,” *IEEE Antennas Wireless Propagation Letters*, vol. 12, pp. 1696-1699, 2013.
- [VI] Zachary T. Miers and Buon Kiong Lau, “Design of MIMO terminal antennas with user proximity using characteristic modes,” in *Proceedings of the 11th European Conference on Antennas and Propagation (EUCAP)*, Paris, France, 2017, Submitted.

During my Ph.D. studies, I have also contributed to the following publications. However, these publications are not included in the thesis:

- [VII] Hui Li, Zachary T. Miers, and Buon Kiong Lau, "Design of orthogonal MIMO handset antennas based on characteristic mode manipulation at frequency bands below 1 GHz," *IEEE Transactions on Antennas and Propagation*, vol. 62, no. 5, pp. 2756-2766, May. 2014.
- [VIII] Zachary T. Miers, Hui Li, and Buon Kiong Lau, "Design of bezel antennas for multiband MIMO terminals using characteristic modes," in *Proceedings of the 8th European Conference on Antennas and Propagation (EUCAP)*, The Hague, Netherlands, pp. 2556-2560, Sep. 2014.
- [IX] Zachary T. Miers and Buon Kiong Lau, "Effects of dielectrics and internal resonances on modal analysis of terminal chassis," in *Proceedings of the 10th European Conference on Antennas and Propagation (EUCAP)*, Davos, Switzerland, pp. 1-5, Apr. 2016.
- [X] Zachary T. Miers and Buon Kiong Lau, "Effects of internal components on designing MIMO terminal antennas using characteristic modes," in *Proceedings of the 10th European Conference on Antennas and Propagation (EUCAP)*, Davos, Switzerland, pp. 1-4, Apr. 2016.
- [XI] Zachary T. Miers, Hui Li, and Buon Kiong Lau, "Design of multi-antenna feeding for MIMO terminals based on characteristic modes," in *Proceedings of the IEEE International Symposium on Antennas and Propagation*, Orlando, FL, pp. 182-183, Jul. 2013.
- [XII] Hui Li, Zachary T. Miers, and Buon Kiong Lau, "Generating multiple characteristic modes below 1GHz in small terminals for MIMO antenna design," in *Proceedings of the IEEE International Symposium on Antennas and Propagation*, Orlando, FL, pp. 180-181, Jul. 2013.
- [XIII] Zachary T. Miers and Buon Kiong Lau, "Design of multimode multiband antennas for MIMO terminals using characteristic mode analysis," in *Proceedings of the IEEE International Symposium on Antennas and Propagation*, Memphis, TN, pp. 1429-1430, Jul. 2014.
- [XIV] Zachary T. Miers and Buon Kiong Lau, "Tracking of characteristic modes through far-field pattern correlation," in *Proceedings of the IEEE International Symposium on Antennas and Propagation*, Vancouver, Canada, pp. 1470-1471, Jul. 2015.
- [XV] Zachary T. Miers and Buon Kiong Lau, "Post-processing removal of non-real characteristic modes via basis function perturbation," in *Proceedings of the IEEE International Symposium on Antennas and Propagation*, Fajardo, Puerto Rico, pp. 419-420, Jul. 2016.

-
- [XVI] Zachary T. Miers and Buon Kiong Lau, "Antenna design using characteristic modes for arbitrary materials," in *Proceedings of the IEEE International Symposium on Antennas and Propagation*, Fajardo, Puerto Rico, pp. 9-10, Jul. 2016.
- [XVII] Zachary T. Miers and Buon Kiong Lau, "Far-field orthogonality of volume-based characteristic modes for real materials," in *Proceedings of the IEEE International Symposium on Antennas and Propagation*, Okinawa, Japan, Oct. 2016.

I contributed to following non peer-reviewed papers:

- [XVIII] Zachary T. Miers, Hui Li, and Buon Kiong Lau, "Designing and feeding multiple characteristic modes in small terminals at frequencies below 1 GHz," in *COST IC1004*, TD(13) 08041, Ghent, Belgium, Sep. 25 - 27, 2013.
- [XIX] Zachary T. Miers, Hui Li, and Buon Kiong Lau, "Multimode, multiband antennas for MIMO handsets with metal bezel," in *COST IC1004*, TD(14) 10075, Aalborg, Denmark, May 26 - 28, 2014.
- [XX] Zachary T. Miers and Buon Kiong Lau, "Characteristic mode tracking with farfield patterns," *COST IC1004*, TD(14)11048, Krakow, Poland, Sep. 24 - 26, 2014.
- [XXI] Zachary T. Miers and Buon Kiong Lau, "Tracking of characteristic modes over frequency with far-field correlation," in *COST IC1004*, TD(15) 13044, Valencia, Spain, May 5 - 7, 2015.
- [XXII] Zachary T. Miers, *et al.*, "On characteristic modes of MIMO terminals with real components," in *COST CA15104 (IRACON)*, TD(16) 01008, Lille, France, May 30 - Jun. 15, 2016.

I contributed as a section editor to the book:

- [XXIII] Narcis Cardona, *Cooperative Radio Communications for Green Smart Environments*. River Publishers, Gistrup, Denmark, 2016.

I contributed to the patent application:

- [XXIV] H. Li, Z. Miers, and B. K. Lau, "Orthogonal multi-antennas for mobile handsets based on characteristic mode manipulation," US Patent App. No. 14/050,761, Oct. 10, 2013.

I contributed to the following paper which was not in a subject matter pertaining to this thesis work:

- [XXV] J. Vieira, S. Malkowsky, K. Nieman, Z. Miers, N. Kundargi, L. Liu, I. Wong, V. Öwall, O. Edfors, and F. Tufvesson, “A flexible 100-antenna testbed for Massive MIMO,” in *Proceedings of the 2014 IEEE Globecom Workshops*, Austin, TX, pp. 287-293, Dec. 2014.

Acknowledgements

First and foremost, I would like to praise and thank God for giving his life so that I may live mine, and creating this wonderful unexplored universe in which we live.

Additionally, it is my pleasure to thank the many people who made this thesis possible.

It is difficult to overstate my sincere gratitude to my advisor, Prof. Buon Kiong Lau (Vincent Lau), for his continuous support during my Ph.D. studies. Without him I would not have moved to Europe and gained the knowledge and experiences that have shaped my life forever. Additionally, his guidance pertaining to which of my ideas has merit, the manuscripts which should be submitted for publication, as well as the edits, updates, and recommendations to each manuscript is critical to my success as a Ph.D. candidate.

Secondly, I am grateful to all the amazing people that have provided me with guidance and help over the past four years. I would like to thank my two co-advisors, Dr. Hui Li who provided me the initial tools that allowed me to begin my research, and Dr. Mats Gustafsson for his guidance, support, knowledge, and skepticism. I am forever indebted to both of you. I also would not be here today without the administrative and technical staff in the department. I am especially grateful to Pia Bruhn, Elisabeth Nordstrom, Jessica Nilsson, and Anne Andersson for their endless support and guidance during this process. I am also thankful for the support of Andreas Johansson, Josef Wajnblo, and Robert Johnsson for their technical support.

I am privileged that some of the best minds in this field of research have agreed to spend the time and travel here to evaluate my work. I would like to thank my opponent Prof. Jennifer Bernhard for the time and commitment involved in reviewing my doctoral work. I realize the time requirement for such a task is not small, and I appreciate the work you put into this task. Additionally, I would like to thank the members of my committee for their time and commitment: Prof. Dirk Manteuffel, Prof. Eva Antonino Daviu, Mr. Björn Johannisson, and Dr. Miloslav Čapek. I truly appreciate your willingness to fully analyze and critique my doctoral work.

I am extremely grateful for the financial support of the Swedish Research Council for providing the grants which allowed for my research to be accomplished. Additionally, I would like to thank Ericssons forskningsstiftelse, and Fysiografiska Sällskapet i Lund for the travel grants which allowed me to attend several conferences held around the world.

I am especially grateful to my colleagues in the Department of Electrical and Information Technology at Lund University. I am grateful for the guidance, friendship, and support provided to me by Nafiseh Seyed Mazloum, Fredrik Tufvesson, Carl Gustafson, Steffen Malkowsky, Irfan Yousaf, Ghassan Dahman, Doruk Tayli, Ove Edfors, Gerhard Kristensson, Peter Polfeldt, and everyone else in the department that has worked with me over the years.

I am so happy that I have had the support of all my friends in Sweden. I cannot thank you enough for all that you have done for me, thank you Carina Innings, Jenny, Jonas, Oscar and Oliver Bermin, Jenny, Wynter, and Greg Ruchti, Felix Johnny, Paula Dubbink, Martina Betakova, Belinda Jangren, and Jan Kjellstrom.

I would also like to thank the many friends from the United States that have come to visit me, and stayed in contact with me while I have been abroad. Thank you Derek Reese, Patrick Wagner, Jake Aho, Nick Schottler, Matt Keenan, Stephanie Turner, Katrina Baynes, Laura and Xing Shen, Molly Rose Rumery, Alex Waskiewicz, Chris Klepac, Chris Nicolaisen, and Benjamin Baker.

I am extremely grateful for the support and friendship of my officemate and good friend Ivaylo Vasilev. You supported me, and were friendly to me, the very first day I arrived in Lund. I am thankful for all the time we spent working together, gossiping, and traveling. Those moments will never be forgotten.

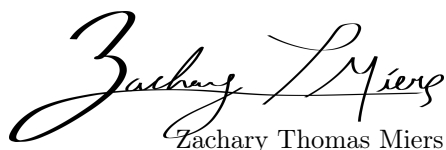
Additionally, I could not have finished, or enjoyed my final years at Lund University, without the great friendships of Dimitrios Vlastaras, Muris Sarajlic, and João Vieira. I have enjoyed all the sights we have seen together, adventures we have taken, and the wonderful lunches we have eaten.

Bill and Anne Horlbeck, you two have been so kind and caring to me since the day I met your wonderful daughter. Thank you for coming to visit us on so many occasions and for sending us cards on holidays and birthdays. Being so far away but knowing that you care and love us has truly helped us to have a much better life here in Sweden. Aunt Donna, thank you for visiting us, supporting us, and keeping in contact with us. Courtney, Scott, and Eloise, I thank you for supporting Brittany and me on this adventure, for keeping in contact with us, and including us in your life events while we were here. I am also very grateful for your gifts of K-cups when we first arrived; it meant more to us than you could have known. Will, thank you for being my brother and friend; your texts, jokes, and pictures made me happy during many difficult days.

I could not be here today without the love and support of my family. Dad, your wisdom, love, and guidance has made me the man I am today. You taught me that I can do anything I set my mind to, and that God, integrity, family, and honesty is all that matters in life; everything else is important, but comes second, including my doctoral degree. Mom, you taught me how to love and care for other people, to be truthful, the importance of my self-worth, and how to be chivalrous and respectful towards others. Because of you, I was able to make friends in Sweden that I will have for the rest of my life. Josh, you are my bigger brother, friend, and roommate. Thank you for supporting me while I was so far away, for always picking up the phone when I called, and coming out every year to visit me; it meant more than you can imagine. Seth, you are my younger brother, the one person I have always wanted to think I was smart and cool, but I always find myself realizing that you are smarter and better than me in so many ways. Thanks for staying up late and playing Halo with me when I was stressed, caring for me,

and being my friend. I am so thankful to have brothers like both of you.

I owe one person more gratitude than any other, and that is my beautiful, perfect, and adventurous wife, Brittany. You, more than anyone, sacrificed so I could pursue my doctoral degree. Thank you for not complaining when I woke you up after working late, providing me a place to work at home, time to get work done, and so many warm meals. Thank you for traveling with me, we were able to go on more than thirty different trips and visit more than twenty different countries during our first four years of marriage. I love you more than I will ever be able to tell you. Thanks for supporting me on this crazy adventure.


Zachary Thomas Miers

List of Acronyms

2-D	Two-Dimensional
3-D	Three-Dimensional
ASIC	Application-Specific Integrated Circuit
CA	Characteristic Attribute
CCE	Capacitive Coupling Element
CE	Coupling Element
CFIE	Combined Field Integral Equation
CM	Characteristic Mode
CMA	Characteristic Mode Analysis
CP	Circularly Polarized
CTIA	Cellular Telecommunications Industry Association
ECC	Envelope Correlation Coefficient
ECIE	Electric Combined Integral Equation
EFIE	Electric Field Integral Equation
FDTD	Finite-Difference Time-Domain
FEM	Finite Element Method
FoM	Figure of Merit
GA	Genetic Algorithm
ICE	Inductive Coupling Element
IE	Integral Equation

LC	Inductive Capacitive Resonant Circuit
LHCP	Left Hand Circular Polarized
LTE	Long Term Evolution
MCIE	Magnetic Combined Integral Equation
MFIE	Magnetic Field Integral Equation
MIMO	Multiple-Input Multiple-Output
MoM	Method of Moments
MS	Modal Significance
PEC	Perfect Electric Conductors
PMC	Perfect Magnetic Conductors
PMCHWT	Poggio-Miller-Chang-Harrington-Wu-Tsai
Q-factor	Quality Factor
RADAR	RAdio Detection And Ranging
RCS	RADAR Cross-Section
RFID	Radio-Frequency Identification
RHCP	Right Hand Circular Polarized
RLC	Resistive, Inductive, Capacitive
RWG	Rao-Wilton-Glisson
SEP	Surface Equivalence Principle
SIE	Surface Integral Equation
SNR	Signal to Noise Ratio
TCM	Theory of Characteristic Modes
TE	Transverse Electric
TM	Transverse Magnetic
UWB	Ultra-WideBand
VEP	Volume Equivalence Principle
VIE	Volume Integral Equation

Contents

Abstract	vii
Popular Science	ix
Preface	xi
Acknowledgements	xv
List of Acronyms and Abbreviations	xix
Contents	xxi
Part I: Overview of Characteristic Modes	1
1 Overview of Characteristic Modes	5
1.1 Founding Historical Concepts of TCM	6
1.2 Modern Applications and Updates to CMs	11
1.2.1 Antenna Synthesis	11
1.2.2 Electrically Small/Compact Antennas	11
1.2.3 MIMO Systems	12
1.2.4 Pattern Synthesis and Scattering Analysis	13
1.2.5 Reactive Loading	13
1.2.6 Theoretical and Mathematical Concepts	14
1.3 Thesis Overview	15
2 Mathematics of Characteristic Modes	21
2.1 Maxwell's Equations	21
2.1.1 Radiation and Scattering - Helmholtz Equation	24
2.1.2 Complex Power - Poynting's Theorem	26

2.2	Solving Maxwell's Equations Using MoM	28
2.2.1	The Integral Equation	29
2.2.2	Solving $\mathcal{L}(f) = g$	31
2.3	The Theory of Characteristic Modes	34
2.3.1	Solving for TCM in PEC Objects (EFIE)	34
2.3.2	Solving for TCM in Real Media (VIE)	39
2.3.3	Solving for TCM in Real Media (SIE)	43
2.3.4	Solving for TCM in Mixed Media (SIE)	47
2.4	Summary	48
3	Characteristic Attributes	53
3.1	Characteristic Eigenvalues	53
3.1.1	CM Eigenvalue Example	54
3.2	Modal Significance (Modal Solutions)	56
3.2.1	Modal Significance Example	58
3.3	Characteristic Currents	59
3.3.1	CM Currents Example	59
3.4	Characteristic Phase	60
3.4.1	Characteristic Phase Example	62
3.5	Modal Quality Factor	65
3.5.1	Modal Quality Factor Example	66
3.6	Characteristic Fields	67
3.6.1	Near- and Far-Field Example	68
4	Eigenvalue Tracking	73
4.1	Eigenvector Correlation Tracking	76
4.2	Weighted Current Correlation Tracking	77
4.3	Far-Field Correlation Tracking	78
4.4	Hybrid Tracking	80
5	TCM in Real Media	85
5.1	Analyzing VIE TCM Solutions	85
5.1.1	Computational Limitations of Volume Integral Equation (VIE)	86
5.1.2	Non-Orthogonal Far-Fields	87
5.2	Analyzing SIE TCM Solutions	89

5.2.1	Problems with Surface Integral Equation (SIE) Theory of Characteristic Modes (TCM) Solutions	90
	Internal Resonances Due to Forced Symmetry	90
	Eigenvalue's Relationship to Poynting's Theorem	93
5.2.2	Removal of SIE TCM Internal Resonances	94
5.2.3	Deriving the Correct TCM Eigenvalue	96
6	Systematic TCM Antenna Design	101
6.1	Characteristic Attribute Analysis	102
6.2	CM Excitation Analysis and Optimization	104
6.2.1	Visual Analysis	104
6.2.2	Computation of CM Interdependence	105
6.2.3	Point Excitation Analysis	106
6.2.4	CM Regional Frequency Evolution	108
7	Contributions, Conclusions, and Future Work	113
7.1	Overview of Included Papers	113
7.1.1	Paper I: Wide Band Characteristic Mode Tracking Utilizing Far-Field Patterns	113
7.1.2	Paper II: Computational Analysis and Verifications of Characteristic Modes in Real Materials	114
7.1.3	Paper III: On Characteristic Eigenvalues of Complex Media in Surface Integral Formulations	115
7.1.4	Paper IV: Antenna Analysis and Design Using Characteristic Modes	116
7.1.5	Paper V: Orthogonal Multi-band Antennas Designed Using Characteristic Modes	117
7.1.6	Paper VI: Design of Multiple-Input Multiple-Output (MIMO) Terminal Antennas with User Proximity Using Characteristic Modes	118
7.2	Not-Included, Notable Publications	118
	Design of Orthogonal MIMO Handset Antennas Based on Characteristic Mode Manipulation at Frequency Bands below 1 GHz	119
	Design of Bezel Antennas for Multi-band MIMO Terminals Using Characteristic Modes	119
	Effects of Dielectrics and Internal Resonances on Modal Analysis of Terminal Chassis	120

Effects of Internal Components on Designing MIMO Terminal Antennas Using Characteristic Modes	120
Post-processing Removal of Non-real Characteristic Modes Via Basis Function Perturbation	121
Far-Field Orthogonality of Volume-Based Characteristic Modes for Real Materials	121
7.3 Conclusions	122
7.4 Future Work	123
References	127
Part II: Included Papers	139
Paper I	141
Paper II	147
Paper III	163
Paper IV	169
Paper V	185
Paper VI	191

Part I

Thesis Overview

Chapter 1

Overview of Characteristic Modes

Overview of Characteristic Modes

RESONANT objects are encountered in our everyday lives, from the vibrating guitar string to the receiving antenna. Even with a fundamental understanding of how resonant structures function, electromagnetic antenna design, which is based around electric waves interacting with a resonant structure, is often referred to as a form of black magic. There are many reasons for this, but one may be the sheer fear of the unknown, as the wave-like resonant properties of antennas are unobservable. Additionally, many well-known antenna systems are complex, and thus it may be difficult to determine their exact resonant properties. For example, a modern cellular telephone has as many as seven different antennas, each with multiple parts including matching circuits, stub-tuners, parasitic couplers, and isolation elements. These types of antenna are often developed using computationally complex optimization algorithms, where the antenna's shape is determined through a set of predefined requirements. As a result, the design engineer has only a simplistic understanding of how these antennas truly function. This lack of insight leads to difficulties when utilizing existing designs in new problems. Furthermore, many antenna textbooks overview how basic antennas work by analyzing them using a set of electromagnetic equations (Maxwell's equations), providing little more than an intuitive set of numbers. However, there is an analysis tool which allows resonant antennas to be understood in the same way as a resonating string played on a guitar, and that tool is the Theory of Characteristic Modes (TCM).

TCM provides insights into the natural resonant phenomena of any electromagnetic object, providing a much needed link between Maxwell's equations and the observable world. When TCM is applied to an object, a set of currents are found (i.e., current distributions); each current is unique in the same sense that each string on a guitar is unique. If one string is excited (plucked) it will sound different than any of the other strings. As such, if one of the TCM derived currents are excited, it will resonate differently than any of other derived currents. This is one of the many advantages of TCM.

Other major advantages of TCM are better explained in relation to other com-

putational electromagnetic tools. While all computational electromagnetic solvers have advantages in specific areas, TCM is unique as it is unlike any other. This is due in part to TCM not requiring the placement of excitation sources when determining the electromagnetic properties of an analyzed object. The majority of computational electromagnetic solvers, including but not limited to Finite Element Method (FEM), Finite-Difference Time-Domain (FDTD), and Method of Moments (MoM), provide brute force solutions to antenna design based on numerical approximations of Maxwell's Equations. These solvers often require a physical excitation, or feeding element, to excite an object before insights can be obtained. Once solutions are obtained from these types of computational solvers, only a single current distribution that produces a specific radiation pattern will be obtained. This is not the case when analyzing an object using TCM. TCM produces a theoretically infinite number of currents that correspond to the same number of orthogonal radiated fields (far-field patterns). Moreover, the Characteristic Attributes (CAs) of an object (characteristic eigenvalues, characteristic currents, Quality Factors (Q-factors), near-fields, and far-fields) can be used to obtain many physical insights including: proper location of an excitation element, variability between structures, isolation between Multiple-Input Multiple-Output (MIMO) elements, RAdio Detection And Ranging (RADAR) cross section, and more. However, even with the significant number of advantages when analyzing an object using TCM, the entire field received relatively little attention in the first few decades following its initial introduction.

1.1 Founding Historical Concepts of TCM

The Theory of Characteristic Modes has a short but complicated history. The notion that an object's electromagnetic properties can be described through a linear combination of modal field patterns, which are determined only by the object's shape and material makeup, was originally theorized by Garbacz in 1965 [1]. This original definition utilized a scattering matrix which is a mathematical representation describing the interaction of an object with an exciting wave. This definition provided a theoretical proof showing that any excitable current on an object can be decomposed in to an infinite set of radiating currents, with the most significant having the lowest magnitude eigenvalue (λ). In Garbacz's scattering definition of Characteristic Modes (CMs), each eigenvalue is defined in terms of the radiation resistance of the corresponding current. However, this theoretical

introduction to CMs required prior knowledge of characteristic far-field radiation patterns and their associated eigenvalues. In this work Garbacz provided two possible solutions to finding the unknown modes; both methods are difficult to implement and not possible to utilize on all object geometries. With this significant drawback there was no published research into this topic for another six years.

In May 1971, Garbacz once again introduced the subject of scattering-based TCM to the academic community [2]. In [2], a clear definition to TCM is stated to be *“At a given frequency every perfectly conducting obstacle has associated with it a particular set of surface currents and corresponding radiated fields which are characteristic of the obstacle shape and independent of any specific excitation.”* This general definition to TCM has since remained with only one minor change, that TCM is no longer associated with only Perfect Electric Conductors (PEC). While [2] provides more information on the implications of the scattering eigenvalue and how this eigenvalue could relate the phase of an incoming field to the scattered field, this work has been relatively overlooked due to the works of Harrington et al. published in September 1971 [3, 4]. Even though Garbacz pioneered the work of TCM, the works in [3] and [4] are often considered to provide the mathematical basis of TCM due to the use of a MoM impedance matrix in determining the characteristic currents and their associated eigenvalues.

In [3, 4], the computational method for determining both the characteristic currents and eigenvalues is based on the Sturm-Liouville theory for weighted eigenvalue problems [5]. The Sturm-Liouville theory is also the basis for solving Greens’ function using a direct approach [6]. In this context Harrington et al. found that the characteristic far-fields can be determined using a weighted eigenvalue problem which utilizes both the real and imaginary parts of the impedance operator. Through this approach the currents are derived to correspond with a set of radiated fields and the eigenvalues are directly related to the reactive power. Electromagnetic theory states that the reactive power determines whether or not a CM is in, or near resonance. This provided evidence to Garbacz’s prediction in [1], that for any sufficiently small object, only a few modes are necessary to synthesize a radiated or scattered pattern. The computational method outlined in [3, 4] allowed for TCM to be applied by anyone in the electromagnetic community.

Between 1965 and 2000 only a few electromagnetic researchers investigated potential applications of TCM. Although relatively few papers were published during this period, the majority of research after 2000 is based on these founding works, and it is important to understand the significance of these contributions.

During this period the field of electromagnetic research focused on its application in RADAR and communication systems, particularly RADAR scattering of aircraft and short wave communications. As such, TCM found its first applications in these areas. The first known usage of TCM was developed to obtain a desired RADAR scattering pattern through the reactive loading of an object [7]. To obtain the desired results, this work derived many of the main formulations still in use today, including: modal Q-factor, TCM-based current synthesis for maximizing platform gain and gain over quality factor (G/Q), as well as TCM for pattern synthesis of an arbitrarily shaped object. Additional early works in this area include [8–14]. This body of work focused more on scattering rather than antenna applications, where quality factor is often utilized. This may be in-part due to the initial lack of knowledge in deriving feed locations from TCM analysis. This problem was first outlined and partially solved by Garbacz et al. in [15].

The theoretical and practical work developed in [15] found simple quadratic equations for the self- and mutual-admittances of delta-gaps between basis functions of thin wires. In this work the input impedance (admittance) of a wire antenna was derived as a weighted summation of its characteristic currents at a selected point on an object. This work showed many practical uses in determining the impedance of a delta gap. Furthermore, this initial idea allowed for the derivation of antenna input impedance in terms of CMs for the first time, this has been used extensively in TCM-based antenna synthesis. This work led to the first antenna shape synthesis using TCM [16]. In [16], simple structures were synthesized using known rotationally symmetric Transverse Electric (TE) and Transverse Magnetic (TM) fields. While the initial results were simple ideal structures, these concepts led to significant future work in antenna shape synthesis. Additional early works in this area can be found in [17–20]. These published works in antenna applications focused on the mathematical aspects of TCM, but other publications attempted to unite these mathematical concepts with real-world problems.

As TCM is comprised of a unique set of radiating currents, Borgiotti in [21] utilized measured antenna patterns and TCM to determine the dominant CMs of a physical antenna. This novel method of far-field modal reconstruction provided a mathematical link between a physical structure and the set of currents derived by TCM. This was the first TCM analysis that allowed for modal reconstruction without knowing either an incident electric field or the actual currents on the object. Further early research in this area was done on printed antennas in [22]. In this work a set of functions referred to as dynamic CMs were utilized to decompose

the CMs of entire domain systems, and shown to effectively decompose the modes of a simple arrayed antenna structure.

Newman's work in [23] presented an entirely new field of research within TCM, which focuses around antenna design. The practical applications of the theoretical work of [23] can be linked to almost one quarter of all TCM publications between 2000 and 2016. Specifically, [23] develops a TCM-based antenna design concept for maximizing the performance of antennas located on structures (i.e., platform antennas, small antennas with support structures, and integrated antennas). This work points out that most antennas are developed to work well in free space, but in reality they are often mounted on some type of support structure (airplane, building, car, human, ship, or any other larger object). As it turns out, the relatively many contributions of this work pointed out that a small antenna may not be the primary radiator in such a setup, but rather the larger structure. This is because the currents that couple from the antenna to the structure can lead to a more efficient antenna. This work developed not only a concept, but also the mathematical framework to properly locate a Capacitive Coupling Element (CCE) or Inductive Coupling Element (ICE) on an integrated structure. This idea was further expanded upon by Austin and Murray in [24].

TCM research on antennas did not only focus on the creation/synthesis of antennas, but also on the analysis, optimization, and understanding of many common antennas. Although common antennas have well known radiation properties, a complete understanding of these structures is still an ongoing study. Prior to many of the developments in TCM, most antennas were derived from, and analyzed by, closed-form expressions. These expressions often provide a limited understanding of the antenna structure. Furthermore, no direct physical intuitions into radiation, scattering, or coupling phenomena could be obtained through traditional port based electromagnetic solvers such as FDTD, FEM, or MoM. However, Pozar et al. noted in [25] that TCM could be used to analyze known antenna types to better understand their physical properties. This work analyzed the mutual coupling of dipole arrays to determine side-lobe errors. The work in [25] triggered further research into traditional antenna structures using TCM including the analysis of log-periodic structures [26], microstrip patches [27,28], wire grids [29], slots [30], and broad band systems [31]. These works showed that TCM can provide significant physical insights into well-known antennas.

While the theoretical foundations for these prior works were based on [1–4], other fundamental theoretical concepts were needed for future research. The the-

ory behind mode degeneracy was developed in [32]. Degenerate modes can produce inaccuracies in the solution to characteristic currents and often cause problems in modal tracking over frequency. In [32], Knorr developed mathematical concepts for the CMs of symmetric structures. This work showed why symmetry in structures causes identical eigenvalues, and that these specific eigenvalues should not cause degeneracy. While this work did not specifically discuss the tracking of CMs across frequency, the degeneracy concepts gave insights into some of the problems associated with modal tracking. Additionally, this work offered a mathematical basis for why degeneracy occurs at points of (non-symmetric) modal crossings, which produce inaccuracies in characteristic currents.

The first theoretical foundations for utilizing TCM in objects of any material were outlined in [33,34]. In [33], it is shown that the MoM based Volume Integral Equation (VIE) impedance matrix formulation could be utilized to determine the CMs of dielectric, magnetic, composite, and lossy composite objects. Different formulations are provided for obtaining the CMs of each type of object. One major drawback of the VIE approach is the high computational complexity required to form the MoM impedance matrix, even for relatively simple structures. These theoretical concepts were later applied to a MoM Surface Integral Equation (SIE) impedance operator [34]. The use of SIE in the computation of non-PEC materials facilitates a reasonable computational time for simple structures. However, due to the problems associated with the formulations in [33] and [34], further research into the CMs of non-PEC or non-Perfect Magnetic Conductors (PMC) objects were not further analyzed prior to 2012.

The fundamental concepts, applications, and derivations outlined in [1] - [34] are not the only theoretical or practical works developed around this time period. However, the outlined works are the cornerstones on which the research contained within this thesis was built. Without a thorough understanding of these concepts, the new theories, algorithms, and practical designs contained within this thesis could not have been developed. Additionally, some newer results in this field that were published between 2000 and the writing of this thesis also played a critical role in guiding the thesis work. Some of these works will be outlined according to their applications in Section 1.2, and many other critical works will be highlighted throughout the thesis.

1.2 Modern Applications and Updates to CMs

Research into both the theoretical, and practical applications of TCM grew significantly between the years 2000 and 2016. The majority of these new works applied the same concepts and ideas that were outlined in Section 1.1. Here, according to the concepts which are utilized in this thesis, these newer research outcomes are summarized in six different categories: antenna synthesis, electrically small/compact antennas, MIMO applications, pattern synthesis and scattering analysis, reactive loading, and new theoretical concepts.

1.2.1 Antenna Synthesis

Antennas are typically synthesized through a complex optimization procedure, where the feeding structure, feed location, and object are all changed independently in an effort to obtain the best antenna performance. Although an antenna's radiation performance is fundamentally limited by its shape and material, typical analysis tools are not well suited for this type of optimization as feeding structures are required. However, TCM is perfectly suited for antenna synthesis algorithms as it only analyzes the performance of the object and does not require any excitation structures [35]. Additionally, TCM-based algorithms can be developed to synthesize or optimize an object and predict the best locations to implement excitation structures [36–39]. After an object is optimized, other computational analysis tools can be utilized to synthesize and optimize feeding structures in the areas predetermined by TCM analysis.

1.2.2 Electrically Small/Compact Antennas

Electrically small objects are perfectly suited for TCM, as only a few modes can be effectively excited on such objects. As such, the total design space is limited, allowing for a nearly complete physical understanding of the electromagnetic properties of the object. In electrically compact antennas at most only one mode is near resonance, which implies that when an object is excited the current will spread across the object, as predicted by TCM [40–43]. The far-field pattern shape is determined only by the current on the object, and as TCM provides a unique set of currents that provide orthogonal far-field patterns, it can be used to better

understand multiple antenna systems [44–47]. Furthermore, when an object is analyzed, new modes can be forced into resonance through modifications to the object’s shape [48, 49], allowing for additional modes to be excited at a given frequency. TCM analysis of supporting structures, such as meta-materials, has been shown to help better understand how these affect an object’s performance [50]. As can be seen from these works, TCM analysis of electrically compact antennas is highly beneficial and will continue to develop with advances in TCM research.

1.2.3 MIMO Systems

MIMO systems became a hot research topic in the early 2000’s. The technology has since matured and is widely commercialized. MIMO is one of the main contributing factors for TCM’s emergence as a promising research topic, since it is perfectly suited to maximize a fundamental Figure of Merit (FoM) of MIMO, i.e., Envelope Correlation Coefficient (ECC). In particular, a reduction in ECC will increase system capacity and data throughput. Assuming a rich multipath channel with uniform 3D angular power spectrum, the ECC of two antenna radiation patterns is equal to the ECC of the MIMO channel. It was shown in [51, 52] that as TCM solves for an orthogonal set of radiated far-fields, if two different CMs are excited by different antenna ports, the ECC should theoretically be zero. This concept was further analyzed in [53, 54]. These articles presented some of the first pattern diversity MIMO antennas designed using TCM. Later in [55–57], the TCM concepts presented earlier in [23] was applied to the context of terminal antenna design. For a terminal operating at frequencies where it is electrically compact (less than $\lambda/3$, where λ is the free-space wavelength), the antenna will couple energy into the terminal’s ground plane; this effectively provides a path for currents to couple into other antenna ports. The unique currents solved by TCM show that antennas must be placed in specific areas on the chassis so not to couple to one another. This MIMO antenna design technique was taken further, providing insights into multi-port antennas [47, 49, 58], shape-optimized antennas [59], pattern reconfigurable antennas [46], MIMO user effects on TCM antenna designs [60], and massive MIMO Ultra-WideBand (UWB) antennas [61]. It can be seen from these works that MIMO systems have significantly benefited from TCM research.

1.2.4 Pattern Synthesis and Scattering Analysis

TCM provides a complete set of the orthogonal radiated far-field patterns that an object can radiate, making TCM perfectly suited for pattern synthesis and scattering analysis. Any outgoing radiation from an object due to scattering or excitation can be expressed as a superposition of the far-fields for a set of CMs. Often it is important to decompose an object into its orthogonal fields for a variety of purposes. A modern application to the basic scattering problem is the use of chipless Radio-Frequency Identification (RFID) tags, which scatter an incoming wave, thus passively providing information to an active RFID reader. This passive concept resolves one of the largest challenges to the wide-spread adoption of RFID systems, i.e., the significant cost of Application-Specific Integrated Circuits (ASICs). In [62], TCM was adopted to determine three major design factors of multi-bit RFID tags: Q-factor, resonant frequency, and RADAR Cross-Section (RCS). Additionally, other aspects of both RFID and RADAR systems can be determined through the knowledge of the scattering matrix. In [63] TCM was used to determine the generalized scattering matrix of an antenna, thus creating a link between [1] and [4]. Many new scattering problems which can be better understood through TCM analysis are emerging. One such new application uses TCM to determine the shape of different carbon nano-tube structures based on their CMs [64]. A scattered pattern is a representation of the currents generated on an object by an incoming wave. A parallel but different approach to analyzing the patterns produced by a scatterer is to analyze the far-field produced by an induced current [65]. In [65], a practical approach of decomposing an excited antenna's currents into a set of characteristic currents through far-field decomposition was proposed. Additionally, [42] created a multi-objective evolutionary algorithm to synthesize a desired pattern using TCM.

1.2.5 Reactive Loading

Reactive loading has been used almost since the introduction of the antenna, as lumped elements can force out-of-resonant objects into resonance. Previously this technology has been used in loading monopole and dipole type antenna structures, and more recently in compact small antennas, MIMO antenna systems, reflectors, and terminal antennas. TCM, and all tools based around MoM, are uniquely suited to utilize reactive loading as the impedance matrix provides valuable insights into how to modify a structure using reactive components. This is because the

resonant properties of a PEC object can be represented by a set of discrete reactive components (i.e., an equivalent circuit) [10], and as such the addition of a reactive component will change the current distribution of the structure. While there are several ways to analyze the location where reactive elements should be placed, the use of TCM offers many advantages over traditional methods. TCM provides a set of characteristic currents that provide critical insights into the optimal placement of reactive elements. This method has been used for analyzing a loaded electrically small dipole antenna [66], matching wide-band antennas [67,68], as well as enabling pattern reconfigurability [46,69], and frequency reconfigurability [70]. Reactive loading will remain a key component of antenna design, and as such TCM is expected to remain as a beneficial tool in determining the proper loading of a variety of structures.

1.2.6 Theoretical and Mathematical Concepts

While the basic theoretical concepts of TCM have not changed since 1971, many of the methods, approaches, and derivations have been expanded upon in recent years. The most important extensions include theoretical developments on TCM for dielectrics [71], modal weighting factor [71], quality factor [72], degenerated modes [73,74], and sub-structure decomposition [75].

The calculation of CMs for dielectric and magnetic objects has not been a topic of significant interest since its introduction in [33,34]. In [71], the original theoretical derivations were reviewed and observations were made on different problems associated with the previously developed theories. In [71], an attempt was made to develop a new theoretical approach to determining the CMs using an Integral Equation (IE)-based formulation. The observations in [76] showed that only the VIE method satisfied field orthogonality, and the SIE method did not. Additionally, not all of the solved CMs found using the SIE formulation radiate unitary power.

Contributions into the further development of determining the proper modal weighting factor of an object's CMs has not seen wide-spread interest in the last decade, with only one major publication in this area [65]. In [65], it was proven that the ECC between an excited antenna and a modal pattern would directly determine the percentage of a mode which contributes to an excited pattern. This is significantly different than other approaches which utilize either a single elec-

tric field quantity [16] or the excited currents to describe the amount a mode contributes to an excited antenna pattern [21].

Unlike dielectrics and modal weighting factors, theoretical research into modal quality factor has seen significant interest in recent years [72, 77, 78]. In [72], it was shown that the quality factor as determined by Vandebosch [79] matches the modal quality factor that was described in [7]. This led to a new formula for the evaluation of the modal radiation quality factor, which was calculated using eigenmodes associated with a set of CAs. With these theoretical developments in the quality factor, different CM-based Genetic Algorithms (GAs) were developed in [59], and applications which minimized the antenna quality factor using TCM were demonstrated in [36].

In contrast to these previous developments in traditional TCM concepts, [75] utilizes (in TCM) a method of isolating a specific substructure in the MoM impedance matrix. This method was developed outside the context of TCM in [80]. This substructure concept was applied in [75] to remove the dielectric component from a solution space, so that only the solution relating to the PEC object is explicitly calculated. To utilize this method, an SIE impedance matrix must be properly formulated so that the sub-structure object is located in the appropriate section of the impedance matrix.

1.3 Thesis Overview

The work contained within this thesis began in 2012, with the initial studies focused around addressing the fundamental challenges in designing multiple antennas in compact MIMO terminals. The ideas presented in [1, 3, 4] were the foundation of how to address these challenges, as these led to the initial studies of TCM at Lund University [55]. [55] exploited TCM to determine the effects of ground plane coupling on multi-antenna systems. This work proved that antennas which use cellular operating bands below 1 GHz radiated not only from the antenna structure, but also forced the entire terminal structure into resonance. This demonstrated that the idea of platform coupling developed in [23] applied to MIMO systems. Furthermore, the work in [57] developed the first TCM optimized MIMO terminal at 2.5 GHz. From these works it was apparent that TCM could be beneficial in the development of MIMO terminal systems. Moreover, these works showed that many fundamental aspects of TCM antenna theory were either

missing or incomplete. For wide-spread adoption of TCM in both academic and industrial applications these areas would need to be further developed. Therefore, the Ph.D. work contained within this thesis was completed in an effort to mature the topic of TCM through providing critical insights, development of new theoretical concepts, and improvements in practical antenna design methodologies using TCM.

In an effort to effectively overview the completed Ph.D. work, this thesis presents the mathematics, mechanics, and developments of TCM in a progressive fashion. Each chapter is carefully constructed to utilize the information contained in previous chapters. As such, the thesis is constructed in the following manner.

Chapter 1 introduces TCM as the main focus of this doctoral work, starting by describing the topic from the perspective of objects encountered in everyday life, and then moving into a more technical overview. Additionally, this chapter provides a historical introduction into TCM, and the many important research contributions which define this field.

Chapter 2 overviews the mathematics needed to solve and understand TCM. First, electromagnetic theory is introduced, as this is the building block of all computational electromagnetics. Second, a short introduction into MoM is provided, while this is not the focus of this doctoral work, the impedance matrix from MoM was utilized to solve for CMs throughout this work. Most importantly, this section provides a full derivation of TCM for both PEC and non-PEC (dielectric and magnetic) materials.

Chapter 3 introduces to the reader the eight most common Characteristic Attributes (CAs). A complete overview of each attribute, as well as several examples relating these to traditional concepts is presented. Understanding these attributes is important to fully comprehend the work completed during this doctoral study.

Chapter 4 presents the topic of characteristic eigenvalue (or modal) tracking. Within this chapter several different traditional, and novel tracking categories are overviewed, and examples into their performance are provided. A new modal tracking approach is one of the main contributions of this doctoral work.

Chapter 5 further examines the problems associated with analyzing dielectric and magnetic materials using TCM. This chapter details why it is difficult to solve for the CMs of objects which contain these materials. Some of the main contributions of this doctoral work are related to solving for the CMs of objects

containing dielectric and magnetic materials.

Chapter 6 examines how to utilize TCM for antenna design. This chapter presents several techniques for systematically designing antennas using the concepts from Chapters 3 - 5. A systematic TCM antenna design paradigm is one of the main contributions of this doctoral work.

Chapter 7 concludes the overview part of the thesis (Part I), and summarizes each of the doctoral candidate's contributions to this field of research. Possible future work is also discussed.

Chapter 2

Mathematics of Characteristic Modes

Mathematics of Characteristic Modes

THE word electromagnetic refers to the phenomenon of an electric and magnetic field's association to, and reliance on, one another. The relationship between these two fields can be defined by Maxwell's equations. These equations, and their associated boundary conditions, can be solved using the Method of Moments (MoM) for both radiation and scattering problems. This solution can then be used to define a unique set of currents for a predefined object. This is the case when directly solving for Characteristic Modes (CMs) using [3]. To fully understand how to solve for CMs of different objects, a basic understanding of Maxwell's equations (Section 2.1) and the quantities within these equations (Section 2.1.1) is required. From these equations the amount of radiated and reactive energy can be found for any object. Based on the knowledge of both the object and the amount of radiated and reactive energy, CMs can be fully defined and understood. Moreover, once the characteristic currents are found, different associated Characteristic Attributes (CAs) can be derived. Herein, the basic electromagnetic concepts of the Theory of Characteristic Modes (TCM) will be overviewed.

2.1 Maxwell's Equations

Electromagnetic theory can be described by four equations, often referred to as Maxwell's equations. These are comprised of different theoretical laws: Gauss' law for electricity, Gauss' law for magnetism, Faraday's law of induction, and generalized Ampère's law. The rotationally symmetric form of these equations are often described by (2.1) - (2.4) and referred to as the rotationally symmetric integral form of Maxwell's equations [81–83].

$$\oiint_S \mathcal{D} \cdot d\mathbf{S} = \iiint_V \rho_e dV \quad (2.1)$$

$$\oiint_S \mathcal{B} \cdot d\mathbf{S} = \iiint_V \rho_m dV \quad (2.2)$$

$$\oint_S \mathcal{E} \cdot d\mathbf{l} = -\frac{d}{dt} \iint_S \mathcal{B} \cdot d\mathbf{S} - \iint_S \mathcal{M}_f \cdot d\mathbf{S} \quad (2.3)$$

$$\oint_C \mathcal{H} \cdot d\mathbf{l} = \frac{d}{dt} \iint_S \mathcal{D} \cdot d\mathbf{S} + \iint_S \mathcal{J} \cdot d\mathbf{S} \quad (2.4)$$

However, it is possible to invoke Stokes' and Gauss' theorems on these integral equations, to derive the rotationally symmetric differential form of Maxwell's equations (2.5) - (2.8) [81–83].

$$\nabla \times D = \rho_e \quad (2.5)$$

$$\nabla \times B = \rho_m \quad (2.6)$$

$$\nabla \times \mathcal{E} = -\frac{\partial \mathcal{B}}{\partial t} - \mathcal{M} \quad (2.7)$$

$$\nabla \times \mathcal{H} = \frac{\partial \mathcal{D}}{\partial t} + \mathcal{J} \quad (2.8)$$

These equations describe the relationships between six vector field quantities, and their associated charge densities. The six vector field quantities are defined as follows:

\mathcal{E} is defined as the electric field intensity (volts per meter)

\mathcal{H} is defined as the magnetic field intensity (amperes per meter)

\mathcal{D} is defined as the electric flux density (coulombs per square meter)

\mathcal{B} is defined as the magnetic flux density (weber per square meter)

\mathcal{J} is defined as the electric current density (amperes per square meter)

and

\mathcal{M} is defined as the magnetic current density (volts per square meter).

These quantities are valid for all media, and can be related to one another through a set of constitutive relationships [84]. Additionally, these relationships define how polarization, as well as electric conduction impact electromagnetic waves within different media types. These constitutive relationships are defined by (2.9).

$$\begin{aligned} \mathcal{D} &= \mathcal{D}(\mathcal{E}, \mathcal{H}) \\ \mathcal{B} &= \mathcal{B}(\mathcal{E}, \mathcal{H}) \\ \mathcal{J} &= \mathcal{J}(\mathcal{E}, \mathcal{H}) \end{aligned} \quad (2.9)$$

The constitutive relationships are valid under every condition. However, when objects are made up of simple media, these relationships can be simplified to the constitutive relationships as defined by (2.10).

$$\begin{aligned}\mathcal{D} &= \epsilon \mathcal{E} \\ \mathcal{B} &= \mu \mathcal{H} \\ \mathcal{J} &= \sigma \mathcal{E}\end{aligned}\tag{2.10}$$

In (2.10), ϵ is the permittivity, μ is the permeability, and σ is the conductivity. With these constitutive relationships in place, both the integral and differential form of Maxwell's equations can be described in terms of free charges and currents. While the asymmetric form of (2.1) - (2.8) are often described in common texts (e.g. [85]), the presented rotationally symmetric form utilizes a set of non-existent magnetic currents [86]. These magnetic currents are a mathematical tool that simplifies the analysis of dielectric problems through forcing Maxwell's equations into rotational symmetry. In the traditional form, \mathcal{E} and \mathcal{B} are only rotationally symmetric when both $\mu = \mu_0$ and $\epsilon = \epsilon_0$. This is due to the electric charge density ρ_e , which breaks the symmetry in simple media. In an effort to force symmetry, the fictional magnetic current density was introduced. Additionally, when a magnetic current density (\mathcal{M}) is introduced a magnetic charge density ρ_m must also be introduced. With these additions, if Maxwell's equations are rotated, the resulting sources and fields are also swapped (i.e., electrons would have a fictional magnetic charge, and no longer contain an electric charge). Although, this magnetic current density is strictly fictional, it is utilized in this thesis as many of the key contributions require the analysis of simple media, and as such \mathcal{M} is required.

In addition to Maxwell's equations, the free charges and currents must satisfy two additional continuity equations [83,86]. When these are paired with Maxwell's equations, the resulting set of equations are not independent for time-varying fields. This is because Faraday's and Ampère's circuital law can be derived from Gauss' law. In these, there are more unknowns than equations, and thus a unique solution cannot be found without more information. Therefore, a specified set of boundary conditions are required to reduce the number of unknowns, thus allowing Maxwell's equations to be solved in any continuous medium.

It is often advantageous to solve these problems at a single frequency as it

greatly reduces the dimensionality of the overarching problem. Furthermore, this eliminates the time variability in these equations, and allows for three unknown spatial variables to be solved. When applied, all derivatives can be represented by a single complex number ($j\omega$), where $\omega = 2\pi f$, f is the single frequency for which the equations are solved, and $j = \sqrt{-1}$. In the time-harmonic version of Maxwell's equations \mathcal{E} , \mathcal{H} , \mathcal{D} , \mathcal{B} , \mathcal{J} , and \mathcal{M} are defined as \mathbf{E} , \mathbf{H} , \mathbf{D} , \mathbf{B} , \mathbf{J} and \mathbf{M} respectively.

Through utilization of the constitutive relationships, the time harmonic version of Maxwell's equations, continuity equations, and the different boundary conditions, Maxwell's equations can be used to solve electromagnetic problems. This includes, the current induced on an object from an incoming wave, as well as the radiation produced from a known current source.

2.1.1 Radiation and Scattering - Helmholtz Equation

If a lossless object encounters an incident electromagnetic plane wave, a set of currents will be induced across the object's surface. Correspondingly, if a set of time-varying currents are present on an object's surface, the currents will radiate electromagnetic energy into free space. If these two scenarios are combined, the total power flow across the surface must be equal to zero. This analysis can be simplified if the object is composed of only Perfect Electric Conducting (PEC) materials, as depicted by Fig. 2.1 and characterized by (2.11).

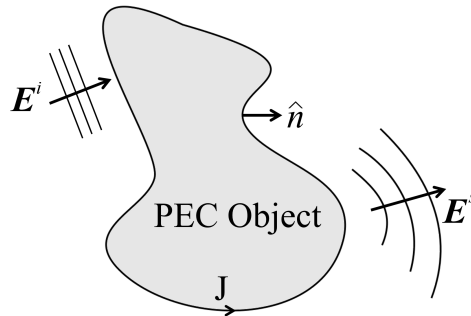


Figure 2.1: Electric-field interaction with a cross-sectional 2-D cut of an arbitrary object. An incoming electric-field will induce tangential currents on a PEC object, these currents are then radiated as a scattered electric-field.

$$\left(\mathbf{E}^i + \mathbf{E}^s \right)_{tan} = 0 \quad (2.11)$$

Using (2.11) it is possible to characterize an object's scattered electric field (\mathbf{E}^s) through knowledge of an incident electric field (\mathbf{E}^i). Additionally, it can be shown that the currents of an object can be determined using the energy radiated by the object. This problem can be solved through relating the electric and magnetic fields to the electric and magnetic currents, derived from Maxwell's equations and the boundary conditions. Through combining Faraday's law (2.7) and Ampère's law (2.8) with the proper constitutive relationships (2.10), (2.12) and (2.13) can be constructed using complex phasors in a time harmonic system.

$$\nabla \times \mathbf{E} = -j\omega\mu\mathbf{H} - \mathbf{M} \quad (2.12)$$

$$\nabla \times \mathbf{H} = j\omega\epsilon\mathbf{E} + \sigma\mathbf{E} \quad (2.13)$$

To analyze the described system, \mathbf{J} is defined as the currents which are impressed (or induced) on the object by means of an incident wave, and $\mathbf{M} = 0$ as the object is comprised of only PEC materials. This set of equations can now be used to solve for the complex wave equation, often referred to as the Helmholtz equation [81]. This is done through setting the divergence of \mathbf{H} to be zero (2.14).

$$\nabla \cdot \mathbf{H} = 0 \quad (2.14)$$

As (2.14) is now a divergenceless system, \mathbf{H} can again be redefined through the curl of the magnetic vector potential \mathbf{A} (2.15). Through substitution of (2.15) with (2.12), (2.16) can be obtained.

$$\mathbf{H} = \nabla \times \mathbf{A} \quad (2.15)$$

$$\nabla \times (\mathbf{E} + j\omega\mu\mathbf{A}) = 0 \quad (2.16)$$

Finally, any curl free vector can be defined as a gradient of a scalar, as such the electric scalar potential (Φ) can be introduced, thus solving for the Helmholtz equation (2.17).

$$\mathbf{E} = -\mathcal{L}(\mathbf{J}) = -j\omega\mu\mathbf{A}(\mathbf{J}) - \nabla\Phi(\mathbf{J}) = -j\omega\mu\mathbf{A} + \frac{1}{j\omega\epsilon}\nabla(\nabla \cdot \mathbf{A}) \quad (2.17)$$

This equation provides a link, using the linear operator (\mathcal{L}), between a defined set of currents on an object (\mathbf{J}), and a scattered field from the object (\mathbf{E}^s) [3, 81]. If the object in Fig. 2.1 is analyzed, the boundary condition $\hat{n} \times \mathbf{E}^s = \mathbf{E}_{tan}^s = 0$ shows that any tangential electric field impressed on a PEC object (\mathbf{E}_{tan}^i) must be transformed in to a current. Therefore, (2.11) and (2.17) can be combined to express an incident field as a function of a set of electric currents (2.18). In (2.18) and (2.19), the subscript *tan* denotes the tangential component of an electric field interacting with the object, and the linear operator $\mathcal{L}(\cdot)$ can be determined using (2.17).

$$\left(\mathcal{L}(\mathbf{J}) - \mathbf{E}^i \right)_{tan} = 0 \quad (2.18)$$

$$\left(\mathcal{L}(\mathbf{J}) \right)_{tan} = -\mathbf{E}_{tan}^s \quad (2.19)$$

Equation (2.17) is critical to the development of TCM as it relates a current to a scattered electric field. Whereas the Helmholtz equation can relate a set of currents to a field quantity, further knowledge into the different types of power in the electromagnetic system is necessary to fully understand the theoretical basis of TCM.

2.1.2 Complex Power - Poynting's Theorem

The entire theoretical basis for TCM is defined by an object's radiated far-field power. This is because each characteristic current has associated to it a far-field radiated pattern which is orthogonal to the other characteristic currents' far-field patterns. Moreover, the eigenvalues associated to each CM are defined by a relationship between the radiated and stored power. Both the radiated (far-field) and stored powers can be found using Maxwell's equations [83, 87], and the theoretical method for finding these is defined by Poynting's theorem. Starting from the time-harmonic differential version of Maxwell's equations, it is possible to derive the complex Poynting's theorem.

As described in [87], Poynting's theorem can be derived by taking the dot product between (2.12) and the complex conjugate of the magnetic field intensity (\mathbf{H}^*), and second taking the dot product between the complex conjugate of (2.13) and the electric field intensity (\mathbf{E}). Finally, through subtracting these two modified

equations with one another, the time-harmonic derivative form (point form) of Poynting's theorem is found as (2.20).

$$\nabla \cdot (\mathbf{E} \times \mathbf{H}^*) = -j\omega |\mathbf{H}|^2 + j\epsilon |\mathbf{E}|^2 - \sigma |\mathbf{E}|^2 - \mathbf{H}^* \cdot \mathbf{M} - \mathbf{E} \cdot \mathbf{J}^* \quad (2.20)$$

By integrating over a known volume and using Gauss' theorem, the integral form of Poynting's theorem can be found, and arranged in a manner in which TCM can be derived, as in (2.21).

$$\begin{aligned} -\frac{1}{2} \iiint_V (\mathbf{E} \cdot \mathbf{J}^* + \mathbf{H}^* \cdot \mathbf{M}) dV &= \frac{1}{2} \oint_S (\mathbf{E} \times \mathbf{H}^*) \cdot d\mathbf{S} + \\ \frac{1}{2} \iiint_V \sigma |\mathbf{E}|^2 dV + 2j\omega \left(\frac{1}{4} \iiint_V \epsilon |\mathbf{E}|^2 dV - \frac{1}{4} \iiint_V \mu |\mathbf{H}|^2 dV \right) & \end{aligned} \quad (2.21)$$

Poynting's theorem expressed as (2.21) can be broken down into five distinct quantities relating to different physical meanings (i.e., (2.22) - (2.26)).

$$P_s = -\frac{1}{2} \iiint_V (\mathbf{E} \cdot \mathbf{J}^* + \mathbf{H}^* \cdot \mathbf{M}) dV \quad (2.22)$$

$$P_e = \frac{1}{2} \oint_S (\mathbf{E} \times \mathbf{H}^*) \cdot d\mathbf{S} \quad (2.23)$$

$$\bar{P}_d = \frac{1}{2} \iiint_V \sigma |\mathbf{E}|^2 dV \quad (2.24)$$

$$\bar{W}_m = \frac{1}{4} \iiint_V \epsilon |\mathbf{E}|^2 dV \quad (2.25)$$

$$\bar{W}_e = \frac{1}{4} \iiint_V \mu |\mathbf{H}|^2 dV \quad (2.26)$$

For any power or energy to be radiated or stored by an object, first power must be supplied to the object, this quantity is defined as the supplied power, and is denoted by (P_s). When power is supplied to an object, the object can either radiate the power into free space (P_e), dissipate the power into heat (\bar{P}_d), or store magnetic (\bar{W}_m) or electric (\bar{W}_e) energy. In (2.21), stored magnetic and electric energies are quantified as reactive power through taking the time derivative ($2j\omega$) of these quantities. The reactive power is defined as the time rate of change for the difference of the two stored energy quantities.

The supplied power, radiated power, and dissipated power have convenient physical meanings. However, the physical interpretation of stored energy is not as intuitive, and its computation is not straightforward as the integrals (2.25) and (2.26) can go to infinity [88]. Based on Maxwell's equations the electric and magnetic fields have a constant phase difference and dependence on one another. When electric (magnetic) energy is maximized over a given frequency cycle, the magnetic (electric) energy must be at its minimum value, for the reactive power to be efficiently transitioned into radiated power. This transfer of energy can be directly related to the energy stored by an ideal Inductive Capacitive Resonant Circuit (LC). However, if the total reactive power is not zero (i.e. an object stores more electric (magnetic) than magnetic (electric) energy ($\bar{W}_m - \bar{W}_e \neq 0$)), some reactive power must be stored to convert between the different types of energy over time. If an object stores any reactive power, it is not considered to be in perfect resonance, as it must maintain some energy for the next radiation cycle. The TCM eigenvalue is a mathematical relationship between the imaginary part (reactive power) and the real part of Poynting's theorem (radiated and lost power).

Maxwell's equations, the Helmholtz equation, and Poynting's theorem are the only theoretical electromagnetic concepts needed to derive and understand TCM. However, to solve for the CMs of any object, a computational method of solving Maxwell's equations is necessary. TCM traditionally uses the MoM, which is a method for solving the integral form of Maxwell's equations using matrix formulations.

2.2 Solving Maxwell's Equations Using MoM

The Method of Moments (MoM) or method of weighted residuals, is a computational technique which is used to solve a set of Integral Equations (IEs), such as Maxwell's equations described by (2.1) - (2.4). These types of IEs are solved through reducing them into a set of linear equations, such as the Electric Field Integral Equation (EFIE) defined by (2.19) [82, 86]. This technique is generally applied to an EFIE or Magnetic Field Integral Equation (MFIE) in electromagnetic problems, and the EFIE and MFIE can be combined to create a Combined Field Integral Equation (CFIE) when necessary (Section 2.3.3).

The MoM for PEC can be summarized in four steps. First, an integro-differential equation (inhomogeneous equation) for the electromagnetic problem

must be defined. Second, the global currents on the object are discretized to represent local currents. This is often referred to as meshing. Throughout this thesis triangular elements will be the primary meshing element, but tetrahedrons will be used in some instances. Third, each meshed element is expanded into a set of basis functions that realize these local currents. The triangle elements, from step two, can be expanded into basis functions in many different ways, but the popular Rao-Wilton-Glisson (RWG) basis functions [89] will be applied to the problems solved in this thesis, these represent a rooftop-like current distribution. Finally, a set of linearly independent weighting functions (often referred to as testing functions) are defined for each basis. This testing function (testing current) is defined on each element and the voltage distribution throughout the object is calculated, this is then repeated for all other elements. These testing functions ensure that the boundary conditions are enforced. The summation of the induced currents is then normalized across all elements; this normalization is done through setting the sum of the induced voltage across the structure to zero. When this specific solution is found, the unique electromagnetic properties of the meshed object have been determined. Herein, these four steps will be overviewed in further detail for PEC objects.

2.2.1 The Integral Equation

All MoM problems begin with an inhomogeneous equation which must be solved. This equation takes the form of (2.27) in electromagnetic problems [82].

$$\mathcal{L}(f) = g \quad (2.27)$$

In this integro-differential equation, \mathcal{L} is the linear operator, often defined by an integral operator, g is a known function and can be defined by an incident electric-field in electromagnetic problems, and f is the unknown function to be determined, in electromagnetic problems this is the currents throughout the object. The inhomogeneous EFIE, derived in Section 2.1.1 and described by (2.19), must be rewritten to be used within a MoM problem. An example of the EFIE for a PEC object utilizing the Green's function and excited by a known incident electric-field is described by (2.28).

$$\hat{n} \times \mathbf{E}^i(\mathbf{r}) = \hat{n} \times \iint_S \left[j\omega\mu \mathbf{J}_s G(\mathbf{r}, \mathbf{r}') + \frac{1}{j\omega\epsilon} (\nabla'_s \cdot \mathbf{J}_s) \nabla' G(\mathbf{r}, \mathbf{r}') \right] dS \quad (2.28)$$

To determine the type of expansion that should be used in an integro-differential equation, either the Surface Equivalence Principle (SEP) or Volume Equivalence Principle (VEP) must be applied to the electromagnetic problem. Throughout the majority of this thesis work, the SEP will be applied to objects consisting of homogeneous media. However, a prominent issue with applying an SEP to solving Maxwell's equations using MoM, is that internal resonances can form in closed objects, these internal resonances are dependent upon how the IE solution is formed [90]. The problems associated with these internal resonances, and various solutions to the internal resonance problem in TCM, will be outlined in later sections.

The SEP transforms the electromagnetic fields ($\mathbf{E}_1, \mathbf{H}_1$) which result from an impressed field into two sets of currents. The first is a current which is induced on the outer surface (S^+) of the object from the electromagnetic field, and the second is the current induced on the inner surface (S^-) of the object from the same electromagnetic field. In SEP problems the two equivalent surface current densities are depicted in the cross-sectional cut of an arbitrary object as shown in Fig. 2.2(b) and (c), where Fig. 2.2(a) is the standard electromagnetic representation of the same cross-sectional cut of the object. The currents which are impressed on the object are dependent on the object's shape, as well as the electromagnetic permittivity and permeability characteristics outside (ϵ_1, μ_1) and inside (ϵ_2, μ_2) the object. The EFIE for PEC objects is a special case of a SEP, as no fields can be excited by an incident field inside the PEC object.

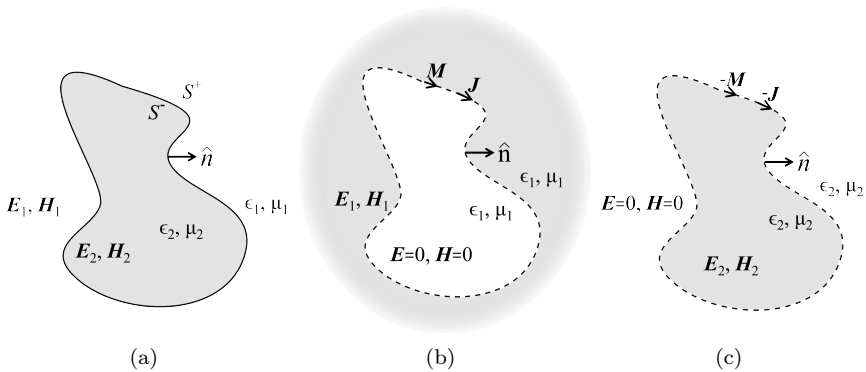


Figure 2.2: Cross-sectional view of an SIE equivalent problem: (a) standard representation of a body in a homogeneous environment, (b) external equivalent problem, (c) internal equivalent problem

The equivalent electric and magnetic surface current densities which represent the field outside (Fig. 2.2(b)) and inside (Fig. 2.2(c)) the object can be mathematically described by a Surface Integral Equation (SIE) [91]. Using the SEP, a set of equivalent currents can be found on an object which radiate the same field as the original problem in Fig. 2.2(a). However, as the currents (\mathbf{J}) now cover the continuous surface of an object in an infinite number of locations, the object must first be discretized into a finite set of currents, which allows for computational methods to be applied. In a surface problem, an object can be discretized by a set of triangular elements, as described by Fig. 2.3(a). However, when solving inhomogeneous non-PEC objects a VEP method can be applied which requires the use of a Volume Integral Equation (VIE). In this type of problem, the volume currents must pertain not to a 2-D surface mesh, but rather to a Three-Dimensional (3-D) volume mesh. When volume currents are utilized in this thesis (for objects consisting of real media), the mesh will be defined by a set of 3-D tetrahedral elements, as described by Fig. 2.3(b).

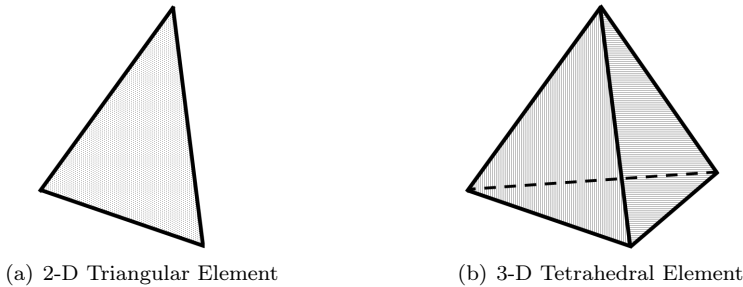


Figure 2.3: 2-D and 3-D meshing elements used to discretize objects

2.2.2 Solving $\mathcal{L}(f) = g$

The first step in solving an integro-differential equation using MoM is to expand the current (\mathbf{J}) into a finite sum of basis functions. Once the object has been split into a set of discrete mesh elements, the original unknown f from (2.27), corresponding to the current \mathbf{J} of (2.28), must be expanded into a series of basis functions. The most commonly used set of basis functions for SIE problems are the RWG basis functions [89]. RWG elements describe how two triangles which share a common edge can be defined in terms of current flow. Figure 2.4 shows a visual description of this type of basis function, and (2.29) provides a mathematical description of Fig. 2.4. In these representations, T_n^+ and T_n^- are two triangles

connected by the common edge n , where n has the length l_n . Each triangle has an area of A_n^\pm , and the position vectors (ρ_n^\pm) connect the respective centroids to the non-common vertices of the two separate triangles.

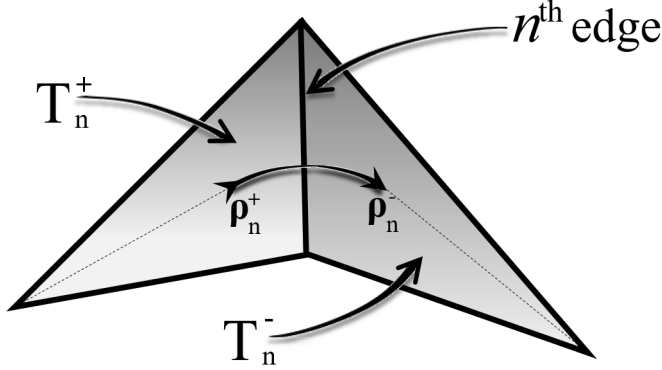


Figure 2.4: An RWG basis function defined over a set of two connected triangles.

$$f_n(\mathbf{r}) = \begin{cases} \frac{l_n^\pm}{2A_n^\pm} \rho_n^\pm, & \mathbf{r} \in T_n^\pm \\ 0, & \mathbf{r} \notin T_n^\pm \end{cases} \quad (2.29)$$

Once a type of basis functions has been determined, such as those in (2.29), the object's unknowns (currents) can be expanded as a finite sum of N weighted basis functions, as shown by (2.30).

$$f(\mathbf{r}) = \sum_{n=1}^N a_n f_n(\mathbf{r}) \quad (2.30)$$

In (2.30), $f_n(\mathbf{r})$ are the basis functions, and a_n are the unknown coefficients. As the integro-differential equation operator (\mathcal{L}) is a linear operator, the substitution of (2.30) into (2.27) results in (2.31). The difference between the approximate value of g and the actual value of g is called the weighted residual.

$$g \approx \sum_{n=1}^N a_n \mathcal{L}(f_n) \quad (2.31)$$

To solve for the unknowns of the object, boundary conditions must be enforced. This is done by defining an inner product between the basis function at the location \mathbf{r}' , and a testing function at location \mathbf{r} . The moment (or inner product) of the basis function and the testing function is defined by (2.32). The residual is integrated

into the testing function resulting in (2.33).

$$\langle w_m, f_n \rangle = \iint_S w_m(\mathbf{r}) \cdot f_n(\mathbf{r}') d\mathbf{S} \quad (2.32)$$

$$\sum_{n=1}^N a_n \langle w_m, \mathcal{L}(f_n) \rangle = \langle w_m, g \rangle \quad (2.33)$$

Applying this method directly to the EFIE in (2.28) results in the linear matrix equation described by (2.34).

$$[Z][J] = [E^s] \quad (2.34)$$

When solving for surface currents of a PEC object using the EFIE and proper boundary conditions, the impedance matrix ($[Z]$) can be found using (2.35), where $G(\mathbf{r}, \mathbf{r}')$ is the free space Green's function defined by (2.36), and λ is the free space wavelength. The voltage ($[E^s]$) on each basis function is defined by (2.37).

$$[Z]_{m,n} = \left(\frac{j\omega\mu}{4\pi} \right) \iint_S (f_m(\mathbf{r}) \cdot f_n(\mathbf{r}') G(\mathbf{r}, \mathbf{r}')) d\mathbf{S} d\mathbf{S}' - \left(\frac{j}{4\pi\omega\epsilon} \right) \iint_S ((\nabla \cdot f_m(\mathbf{r})) (\nabla' \cdot f_n(\mathbf{r}')) G(\mathbf{r}, \mathbf{r}')) d\mathbf{S} d\mathbf{S}' \quad (2.35)$$

$$G(\mathbf{r}, \mathbf{r}') = \frac{\exp\left(-j\frac{2\pi}{\lambda} |\mathbf{r} - \mathbf{r}'|\right)}{|\mathbf{r} - \mathbf{r}'|} \quad (2.36)$$

$$[E^s]_m = \left\langle f_m(\mathbf{r}), \mathbf{E}^i(\mathbf{r}) \right\rangle = \iint_S f_m(\mathbf{r}) \cdot \mathbf{E}^i(\mathbf{r}) d\mathbf{S} \quad (2.37)$$

This solution, which utilizes MoM, makes it possible to find an impedance matrix ($[Z]$) for any discretized PEC object. Through the use of different sets of IEs, the impedance matrix of any object can be found, not just PEC objects as previously described. As will be shown in Section 2.3, finding the impedance matrix of an object is a critical first step in solving for the CMs of any object.

2.3 The Theory of Characteristic Modes

The most traditional method for deriving TCM builds upon the concepts presented in Section 2.1 and 2.2. This TCM derivation was first described by Harrington *et al.* in [3] and [4]. These articles describe how the electric field of the EFIE in (2.19) can solve for the impedance matrix and currents, as shown in (2.34). This insight allows for a weighted eigenvalue equation to be found, relating the unknown characteristic currents to a previously-solved impedance matrix. Furthermore, Harrington *et al.* describe how Poynting's theorem can be used to define how the currents relate to a set of orthogonal far-field patterns, and how the eigenvalues relate to an object's reactive power. This is done through the use of a weighted inner product, where the currents are weighted by the complex impedance matrix. This derivation is only applicable to PEC objects, whereas the derivation for objects consisting of simple media are presented [33, 34]. However, none of these works fully detail the underlying theoretical concepts behind these derivations. A more complete coverage of the PEC TCM derivation is given in [86], but the information is spread over several chapters. In the following sections, these insights will be condensed and explained in a simple and logical manner.

2.3.1 Solving for TCM in PEC Objects (EFIE)

TCM is a unique amalgamation of three separate theories: Poynting's theorem, the Helmholtz equation, and the Sturm-Liouville theory. Without understanding these three theoretical concepts it is difficult to fully understand why TCM provides a comprehensive understanding of an object's electromagnetic properties. As described in Section 2.1.2, Poynting's theorem (2.21) has fundamental importance in electromagnetic problems, as it establishes the total amount of power stored, lost, and radiated by an object. Furthermore, the Helmholtz equation (2.17) relates an incident (2.18) or scattered (2.19) electric-field to an integro-differential linear operator which operates on the currents of the structure (2.28). It is apparent that these equations cannot be unified into a single equation. However, as (2.19) takes the form of a second-order differential equation, this equation can be related to the well-known Sturm-Liouville problem [5, 86, 92]. This theory has many unique sub-theorems, but the main theorem states that any second-order differential equation can be described by a weighted eigenvalue problem, and the first sub-theorem states that for any second-order operator, "*it is always possi-*

ble to define a weighted inner product for which \mathcal{L} is formally self-adjoint" [86]. Additionally, the weighting variable in the first sub-theorem must be Hermitian, i.e. $\boldsymbol{\xi}(x)^* = \boldsymbol{\xi}(x)$, where $(\cdot)^*$ is the Hermitian transpose operator. The classical Sturm-Liouville equation is described by (2.38), and the weighted inner product is defined by (2.39)

$$\mathcal{L}_1(f_n) = -\frac{1}{w} \frac{d}{dx} \left(p(x) \frac{df_n}{dx} \right) - q(x) f_n = \nu_n \boldsymbol{\xi}(x) f_n \quad (2.38)$$

$$\langle f_1, \boldsymbol{\xi} f_2 \rangle = \int \boldsymbol{\xi}(x) f_1(x) f_2(x) dx = \delta \quad (2.39)$$

Through applying the Sturm-Liouville problem to (2.19), the eigenvalue problem (2.40) is obtained.

$$\mathcal{L}_1(\mathbf{J}_n) = \mathcal{L}(\mathbf{J}_n)_{tan} = \mathbf{E}_{tan}^i = -j\omega\mu\mathbf{A} + \frac{1}{j\omega\epsilon} \nabla(\nabla \cdot \mathbf{A}) = \nu_n \boldsymbol{\xi}(\mathbf{J}_n) \quad (2.40)$$

Additionally, as \mathcal{L}_1 operates on the currents (\mathbf{J}_n) , \mathcal{L}_1 must transform the surface current density \mathbf{J} ($\frac{A}{m}$) into an electric-field \mathbf{E} ($\frac{V}{m}$), and as such \mathcal{L}_1 is required to maintain the unit of ohms (Ω), and can be defined to be the impedance operator \mathbf{Z} (Ω); this substitution is shown by (2.41).

$$\mathbf{Z}(\mathbf{J}_n) = \mathbf{E}_{tan}^i = \nu_n \boldsymbol{\xi}(\mathbf{J}_n) \quad (2.41)$$

Although any Hermitian weighted variable can be used to find a set of orthogonal currents with respect to the chosen weighting variable ($\boldsymbol{\xi}$), the appropriate weighting factor matters as it defines the orthogonality of the eigenvalue problem. When the problem space is limited to PEC objects, where $\bar{P}_d = 0$ and no magnetic currents exist, Poynting's theorem can be related to the first sub-theorem of the Sturm-Liouville problem (2.39), providing insight into the proper weighting variable. For PEC, the magnetic current density (\mathbf{M}) must be zero for Maxwell's equations to remain symmetric, and as such Poynting's theorem (2.21) can be re-defined as (2.42).

$$\begin{aligned} -\frac{1}{2} \langle \mathbf{J}_n^*, \mathbf{Z}(\mathbf{J}_n) \rangle &= -\frac{1}{2} \iiint_V (\mathbf{E} \cdot \mathbf{J}^*) dV = \frac{1}{2} \iint_S (\mathbf{E} \times \mathbf{H}^*) \cdot d\mathbf{S} + \\ &0 + 2j\omega \left(\frac{1}{4} \iiint_V \epsilon |\mathbf{E}|^2 dV - \frac{1}{4} \iiint_V \mu |\mathbf{H}|^2 dV \right) \end{aligned} \quad (2.42)$$

Equation (2.42) takes the same form as (2.39), with two major differences. First, while \mathbf{Z} is symmetric for EFIE problems, it is not Hermitian-symmetric, whereas $\boldsymbol{\xi}$ must be. Second (2.42) applies the complex conjugate operator to one of the two \mathbf{J} 's, but this operation will not have any effect if a proper weighting is found for (2.41). This is because the second sub-theorem of a Sturm-Liouville problem (described by Theorem 1.2 of [93]) states that when f_n is solved through an eigenvalue decomposition of (2.38), the f_n 's are required to be real valued (i.e. $f_n = f_n^*$). As such \mathbf{J} must be real valued (i.e., $\langle \mathbf{Z}(\mathbf{J}_n), \mathbf{J}_n^* \rangle = \langle \mathbf{Z}(\mathbf{J}_n), \mathbf{J}_n \rangle$).

Due to the non-Hermitian properties of the complex impedance operator, the left-hand-side of (2.42) cannot be directly substituted into (2.39). However, it can be shown that the power radiated by the scalar wave equation can be expressed in Hermitian form when the field satisfies the Helmholtz equation, as is the case with (2.17) [81]. Furthermore, if a boundary condition is defined by the radiated-field over the sphere at infinity, the radiated power is described by (2.43). This equation is identical to the real part of Poynting's theorem (2.42) [86].

$$\mathbf{P} = \text{Re} \iiint_V (\mathbf{E} \cdot \mathbf{J}^*) dV = \text{Re} \langle \mathbf{Z}(\mathbf{J}_n), \mathbf{J}_n^* \rangle = \langle \text{Re}(\mathbf{Z})\mathbf{J}_n, \mathbf{J}_n^* \rangle \quad (2.43)$$

As \mathbf{Z} is a symmetric complex operator, it can be expressed by its real and imaginary parts (2.44), where \mathbf{R} and \mathbf{X} are both Hermitian-symmetric operators. As such (2.43) can be equated to (2.39), and \mathbf{R} can be used as the Sturm-Liouville weighting operator. This is an advantageous choice for a weighting operator, as (2.43) is the radiated power of the object. Furthermore, (2.39) states the currents must be orthogonal to the weighted inner product. This means that the set of currents found through an eigenvalue decomposition of (2.41) using \mathbf{R} as the weighting variable, will correspond to an orthogonal set of radiated far-field patterns.

$$\mathbf{Z} = \mathbf{R} + j\mathbf{X} \quad (2.44)$$

When \mathbf{R} is utilized as the weighting variable, (2.41) can be re-written as (2.45).

$$\mathbf{Z}(\mathbf{J}_n) = \nu_n \mathbf{R}(\mathbf{J}_n) \quad (2.45)$$

In this representation the left-hand-side of (2.45) is composed of the complex operator (\mathbf{Z}). The right-hand-side is composed of an eigenvalue (ν_n) and the real operator \mathbf{R} . For this reason, the eigenvalue must be composed of both a real part

and an imaginary part as described by (2.46).

$$\boldsymbol{\nu}_n = 1 + j\lambda_n \quad (2.46)$$

When (2.46) is used as the eigenvalue in (2.45), the combined Sturm-Liouville problem is simplified to (2.47), which is the base equation for TCM.

$$\mathbf{X}(\mathbf{J}_n) = \lambda_n \mathbf{R}(\mathbf{J}_n) \quad (2.47)$$

Furthermore, as the real part of $\boldsymbol{\nu}_n$ is a constant, it only affects the \mathbf{R} operator, as such λ_n is directly linked to the imaginary part of the eigenvalue equation, and therefore the eigenvalue pertains to the imaginary part of Poynting's theorem, i.e., the object's reactive power. The TCM eigenvalue can now be defined mathematically by (2.48), using the definitions of \bar{W}_m and \bar{W}_e given in (2.25) and (2.26).

$$\lambda_n = 2\omega (\bar{W}_m - \bar{W}_e) \quad (2.48)$$

The TCM eigenvalue equation in (2.47) is unique in the sense that both \mathbf{X} and \mathbf{R} are real and symmetric operators. This allows for all of the Sturm-Liouville sub-theorems to remain true, and as such the following properties are guaranteed for the generalized PEC TCM problem:

- (a) The orthogonality relationships (2.49) - (2.51) must apply to the characteristic currents for $m \neq n$.

$$\langle \mathbf{J}_m, \mathbf{R}(\mathbf{J}_n) \rangle = 0 \quad (2.49)$$

$$\langle \mathbf{J}_m, \mathbf{X}(\mathbf{J}_n) \rangle = 0 \quad (2.50)$$

$$\langle \mathbf{J}_m, \mathbf{Z}(\mathbf{J}_n) \rangle = 0 \quad (2.51)$$

- (b) The radiated power orthogonality relationships (2.52) - (2.54) must apply to the characteristic currents for $m \neq n$ as \mathbf{J}_n is a real value.

$$\langle \mathbf{J}_m^*, \mathbf{R}(\mathbf{J}_n) \rangle = 0 \quad (2.52)$$

$$\langle \mathbf{J}_m^*, \mathbf{X}(\mathbf{J}_n) \rangle = 0 \quad (2.53)$$

$$\langle \mathbf{J}_m^*, \mathbf{Z}(\mathbf{J}_n) \rangle = 0 \quad (2.54)$$

- (c) The characteristic currents of all external resonances can be normalized according to the Sturm-Liouville normalization function (2.55).

$$\langle \mathbf{J}_n^*, \mathbf{R}(\mathbf{J}_n) \rangle = 1 \quad (2.55)$$

- (d) The orthogonality relationships (2.49) - (2.54) can be combined with the normalization function (2.55) to produce (2.56) - (2.58).

$$\langle \mathbf{J}_m^*, \mathbf{R}(\mathbf{J}_n) \rangle = \langle \mathbf{J}_m, \mathbf{R}(\mathbf{J}_n) \rangle = \delta_{mn} \quad (2.56)$$

$$\langle \mathbf{J}_m^*, \mathbf{X}(\mathbf{J}_n) \rangle = \langle \mathbf{J}_m, \mathbf{X}(\mathbf{J}_n) \rangle = \lambda_n \delta_{mn} \quad (2.57)$$

$$\langle \mathbf{J}_m^*, \mathbf{Z}(\mathbf{J}_n) \rangle = \langle \mathbf{J}_m, \mathbf{Z}(\mathbf{J}_n) \rangle = (1 + j\lambda_n) \delta_{mn} \quad (2.58)$$

When applying properties (a) and (b) to the normalization function (2.55), the solution to both inner products of (2.47) can be defined by (2.56) and (2.57). Furthermore, (2.57) is equal to the reactive power of the object [3]. Therefore, as the real part of Poynting's theorem is equal to P_e , and the imaginary part is equal to $2\omega(\bar{W}_m - \bar{W}_e)$, the characteristic eigenvalue can be found using (2.59).

$$\lambda_n = \frac{\langle \mathbf{J}_m^*, \mathbf{X}(\mathbf{J}_n) \rangle}{\langle \mathbf{J}_m^*, \mathbf{R}(\mathbf{J}_n) \rangle} = \frac{2\omega(\bar{W}_m - \bar{W}_e)}{P_e} \quad (2.59)$$

The base eigenvalue equation for TCM as shown by (2.47) can be solved through discretization of the operators using MoM, as described in Section 2.2, where \mathbf{Z} is decomposed into a discrete set of RWG basis functions and (2.35) defines the matrix elements. When properly carried out the MoM reduces the operators \mathbf{Z} , \mathbf{R} , and \mathbf{X} into a set of $N \times N$ matrices defined by $[Z]$, $[R]$, and $[X]$. Additionally, the eigenvector \mathbf{J}_n is transformed into the $N \times 1$ matrix $[J_n]$. This transforms the TCM operator equation (2.47) into the TCM matrix equation (2.60). Throughout the remainder of this thesis the discretized version of the TCM base equation will be applied.

$$[X][J_n] = \lambda_n [R][J_n] \quad (2.60)$$

The derivation of TCM throughout this section is only applicable for PEC objects. Moreover, (2.60) is only valid for the EFIE SIE formulation of MoM. However, an object consisting of real materials also has a set of CMs which describe the object's resonant and scattering properties. To determine these CMs other

matrix solutions must be applied, and as such some of the theoretical concepts described in this section are no longer valid.

2.3.2 Solving for TCM in Real Media (VIE)

The VIE uses the VEP to transform a standard representation of a body in an electromagnetic environment, as described by Fig. 2.5(a), into an equivalent problem which makes use of volume polarization currents to represent the field in and around the object, as described by Fig. 2.5(b).

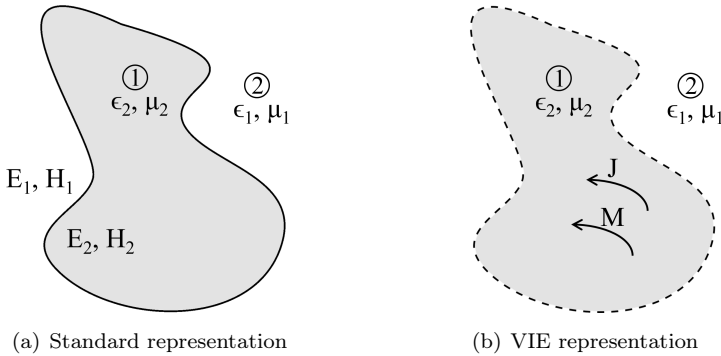


Figure 2.5: Representations of the cross-sectional cut of an object in an electromagnetic field: (a) the standard representation of this problem, and (b) the VIE equivalent model.

As this current is continuous throughout the object, the object must first be discretized into a set of 3-D volumetric tetrahedrons, such as the one shown in Fig. 2.3(b). The MoM unknown currents can be found from the scattered electric or magnetic field induced by an incident field. When this is applied to volumetric currents the electric or magnetic field must be represented by the sum of both an incident field (\mathbf{E}^i or \mathbf{M}^i) on a volumetric element, as well as the scattered fields from other volumetric elements (\mathbf{E}^s or \mathbf{M}^s). This constitutive relationship is defined by (2.61) for dielectric structures and (2.62) for magnetic structures.

$$\mathbf{J} = \left(\omega (\epsilon_2'' - \epsilon_1'') + j\omega (\epsilon_2' - \epsilon_1') \right) \left(\mathbf{E}^i + \mathbf{E}^s \right) \quad (2.61)$$

$$\mathbf{M} = \left(\omega (\mu_2'' - \mu_1'') + j\omega (\mu_2' - \mu_1') \right) \left(\mathbf{H}^i + \mathbf{H}^s \right) \quad (2.62)$$

In (2.61) and (2.62), ϵ_1 and μ_1 are the permittivity and permeability outside a given basis tetrahedral, and ϵ_2 and μ_2 are respectively the permittivity and permeability of a basis tetrahedral. The real part of the permittivity (ϵ') and permeability (μ') are associated with the stored energy within the medium, and the imaginary part of the permittivity (ϵ'') and permeability (μ'') are associated to the energy lost within the medium. These equations can be expressed in terms of the impedance operators \mathbf{Z}_v and \mathbf{Z}_m , as described by (2.63) and (2.64). It can be seen that these relationships are different than those in the traditional MoM SIE formulation.

$$\mathbf{Z}_v(\mathbf{J}) = -\mathbf{E}^s \quad (2.63)$$

$$\mathbf{Z}_m(\mathbf{J}) = (\omega(\epsilon_2'' - \epsilon_1'') + j\omega(\epsilon_2' - \epsilon_1'))^{-1}(\mathbf{J}) \quad (2.64)$$

From the theoretical concepts presented in Section 2.3.1, the induced current from a given incident field which interacts with the volume of an object can be described by (2.65).

$$(\mathbf{Z}_v + \mathbf{Z}_m)(\mathbf{J}) = \mathbf{Z}(\mathbf{J}) = \mathbf{E}^i \quad (2.65)$$

In (2.65), the matrix representation of the impedance operator (\mathbf{Z}) is different for dielectric, magnetic, and mixed material objects. In dielectric and magnetic structures, the impedance matrix is a linear operator which operates on only electric or magnetic currents. However, in mixed material objects the matrix is formed using both electric and magnetic currents, this system of equations (in operator form) can be represented by (2.66) - (2.69) as defined in [33, 81].

$$\mathbf{J} = (\omega(\epsilon_2'' - \epsilon_1'') + j\omega(\epsilon_2' - \epsilon_1'))(\mathbf{E}^i + \mathbf{E}^s) \quad (2.66)$$

$$\mathbf{M} = (\omega(\mu_2'' - \mu_1'') + j\omega(\mu_2' - \mu_1'))(\mathbf{H}^i + \mathbf{H}^s) \quad (2.67)$$

$$\mathbf{E}^s = -j\omega\mathbf{A}(\mathbf{J}) - \nabla\phi(\mathbf{J}) - \frac{1}{\epsilon_0}\nabla \times \mathbf{A}(\mathbf{M}) \quad (2.68)$$

$$\mathbf{H}^s = -j\omega\mathbf{A}(\mathbf{M}) - \nabla\phi(\mathbf{M}) + \frac{1}{\mu_0}\nabla \times \mathbf{A}(\mathbf{J}) \quad (2.69)$$

In these equations ϕ is the scalar potential integral, and \mathbf{A} is the potential integral. When these equations are linked together they form a single operator matrix equation. The impedance operator matrix in this equation is not symmetric as shown by (2.70), where \mathbf{Y} and \mathbf{N} are defined in [33].

$$\begin{bmatrix} \mathbf{Z} & -\mathbf{N} \\ \mathbf{N} & \mathbf{Y} \end{bmatrix} \begin{bmatrix} \mathbf{J} \\ \mathbf{M} \end{bmatrix} = \begin{bmatrix} \mathbf{E}^i \\ \mathbf{H}^i \end{bmatrix} \quad (2.70)$$

This implies that the Sturm-Liouville problem cannot be effectively utilized. To allow for mixed material to be applied to the Sturm-Liouville problem, Harrington *et al.* found that it was possible to force this matrix into symmetry in the method shown by (2.71) [33].

$$\begin{bmatrix} \mathbf{Z} & -j(-\mathbf{N}) \\ j\mathbf{N} & \mathbf{Y} \end{bmatrix} \begin{bmatrix} \mathbf{J} \\ j\mathbf{M} \end{bmatrix} = \begin{bmatrix} \mathbf{E}^i \\ j\mathbf{H}^i \end{bmatrix} \quad (2.71)$$

Using (2.65) and the symmetric forms of the impedance operator matrix, the same concepts which were applied in Section 2.3.1 for solving the Sturm-Liouville problem can again be implemented. This is because the weighted inner product of the system of equations remains related to the radiated power of the object. For lossless materials, this operation will perfectly diagonalize the impedance matrix, but for lossy objects this is not the case. The Sturm-Liouville problem for the VIE matrix for lossy objects can be mathematically described by (2.72), where the common terms are canceled in (2.73).

$$(\mathbf{Z}_v + \mathbf{Z}_m)(\mathbf{J}_n) = (1 + j\lambda_n) \text{Re}(\mathbf{Z}_v)(\mathbf{J}_n) \quad (2.72)$$

$$(\text{Im}(\mathbf{Z}_v) - j\mathbf{Z}_m)(\mathbf{J}_n) = (1 + j\lambda_n) \text{Re}(\mathbf{Z}_v)(\mathbf{J}_n) \quad (2.73)$$

There are two issues pertaining to the eigenvalue that arise when using this system of equations. The first issue pertains to the eigenvalue solution when analyzing lossy structures, and the second pertains to the direct interpretation of the eigenvalue when a non-zero magnetic current is introduced. When (2.73) is used to solve for the eigenvalue and characteristic currents of lossless objects, the non-zero magnetic current forces the left-hand side of (2.73) to utilize a non-Hermitian-symmetric operator, introducing several problems into the original theory. One such problem is the eigenvalue solution will be complex as the first sub-theorem of the Sturm-Liouville problem is not satisfied. Second, mathematically obtaining the impedance matrix for a VIE problem can be found in many different ways, but the method used throughout this thesis does not allow for the matrix to be split into the separate sub-matrices: \mathbf{Z}_v and \mathbf{Z}_m [90, 91]. In this type of solution $\mathbf{Z} = \mathbf{Z}_v + \mathbf{Z}_m$, and as such only a single matrix is obtained. This matrix

relates the objects individual basis elements to both the incident field as well as the scattered fields from other volumetric basis elements. However, it is possible to utilize this single linked VIE impedance matrix to obtain a set of non-complex eigenvalues. This is done by utilizing only the real values and the imaginary values of the obtainable single impedance matrix in the eigenvalue equation, as described by (2.74). This equation is equal to (2.73) for lossless objects.

$$(\text{Im}(\mathbf{Z}_v) + \text{Im}(\mathbf{Z}_m))(\mathbf{J}) = \lambda_n(\text{Re}(\mathbf{Z}_v) + \text{Re}(\mathbf{Z}_m))(\mathbf{J}_n) \quad (2.74)$$

While this solves the issue pertaining to complex eigenvalues, the single linked impedance matrix introduces a new problem, which again only pertains to lossy objects. This problem stems from eigenvalue decomposition of (2.74). Equation (2.74) maintains mode-to-mode current orthogonality as described by (2.49) - (2.51), but the radiated far-field energy (scattering matrix) is not perfectly diagonalized for all objects. As such, the far-fields are not guaranteed to be orthogonal to one another. This new VIE orthogonality relationship is described by (2.75), where the orthogonality offset between different CMs is determined by the size of $\langle \mathbf{J}_m^*, \text{Re}(\mathbf{Z}_m)(\mathbf{J}_n) \rangle$, and as (2.76) shows, this offset is directly related to the dissipated power of the object. However, as described by (2.73) a lossless structure will maintain perfect far-field orthogonality.

$$\langle \mathbf{J}_m^*, \text{Re}(\mathbf{Z}_v)(\mathbf{J}_n) \rangle + \langle \mathbf{J}_m^*, \text{Re}(\mathbf{Z}_m)(\mathbf{J}_n) \rangle = \delta_{mn} \quad (2.75)$$

$$\bar{P}_d = \text{Re} \langle \mathbf{J}^*, \mathbf{E}^i + \mathbf{E}^s \rangle = \text{Re} \langle \mathbf{J}^*, \mathbf{Z}_m(\mathbf{J}) \rangle \quad (2.76)$$

The second issue concerns how the eigenvalue associated with (2.72) and (2.73) is related to Poynting's theorem. As seen in PEC problems, an object's eigenvalue is directly related to the reactive power as defined by Poynting's theorem. This allows the eigenvalue to provide insights into what type of energy is stored by an object, and defines when that object is in resonance. This is not the case with the VIE CM decomposition. In the described VIE CM problem, the eigenvalue has no apparent relationship to the resonant properties of the structure and is defined by (2.77). As can be seen, (2.77) is not related to the imaginary part of Poynting's theorem as described by (2.21).

$$\begin{aligned} \lambda_n = \text{Im} \langle \mathbf{J}_m^*, (\mathbf{Z}) \mathbf{J}_n \rangle &= 2j\omega \left(\frac{1}{4} \iiint_V \epsilon |\mathbf{E}|^2 dV \right) - \\ &2j\omega \left(\frac{1}{4} \iiint_V \mu |\mathbf{H}|^2 dV \right) - \frac{1}{\omega} \iiint_V \mathbf{J}^* (\mathbf{Z}_m)^{-1} \mathbf{J} dV \end{aligned} \quad (2.77)$$

Although there are many problems associated with the original theoretical derivation of TCM in VIE MoM solutions, as is fully described in [33], there are many ways that the VIE TCM solution can be effectively utilized. Further insights and a more in-depth analysis of VIE CMs will be further explored in Chapter 5.

2.3.3 Solving for TCM in Real Media (SIE)

If the problem depicted in Fig. 2.5(a) is analyzed not by a set of volumetric currents, but rather through the use of equivalent surface currents, the eigenvalue problem must be redefined. This can be accomplished through solving a set of SIEs. There are three main types of SIE formulations: EFIE, MFIE, and CFIE. The standard EFIE and MFIE MoM solutions do not allow for an operator equation to be found that can be utilized on objects containing a homogeneous mixture of materials. However, CFIE does allow for this type of operator to be found. In a CFIE, both the electric and magnetic operators are utilized, unlike a EFIE or a MFIE. This allows for the electromagnetic properties of a variety of different materials to be analyzed. Whereas there are several different CFIE formulations, the Poggio-Miller-Chang-Harrington-Wu-Tsai (PMCHWT) formulation described in [94] will be applied throughout this thesis.

This particular SIE, like the EFIE in Section 2.2.2, uses the SEP to transform a standard representation of a body in an electromagnetic environment into a surface equivalent representation of that body, as described by Fig. 2.2(a). This equivalent problem makes use of surface currents which represent the field in and around the object, as depicted by Fig. 2.2(b) and (c). To allow for proper field interaction between an object and the surrounding media, equivalent electric and magnetic surface current densities \mathbf{J}_s and \mathbf{M}_s must be fully integrated into the SIE. This can be accomplished by properly applying SEP to the homogeneous body, since SEP allows for an object to be depicted by two different spaces, the space inside and outside the object. The inside media and the outside media must be composed of real materials, with the material's electromagnetic properties being

described by (2.78) and (2.79).

$$\epsilon_i = \epsilon_0 \epsilon_{r,i} - j \frac{\sigma_i}{\omega} = \epsilon_0 \epsilon_{r,i} (1 - j \tan \delta_i) \quad (2.78)$$

$$\mu_i = \mu_0 \mu_{r,i} - j \frac{\sigma_i}{\omega} = \mu_0 \mu_{r,i} (1 - j \tan \delta_i) \quad (2.79)$$

In these equations $(\cdot)_i$ defines the material, ϵ_i is the materials complex permittivity, μ_i is the materials complex permeability, ϵ_0 is the free-space permittivity, μ_0 is the free-space permeability, $\epsilon_{r,i}$ is the relative permittivity, $\mu_{r,i}$ is the relative permeability, σ_i is the conductivity, and $\tan \delta_i$ is the loss angle or dissipation factor.

When an exterior field interacts with either a single or a combination of materials, the SEP states that the electric and magnetic fields scattered by the object must be replaced by an equivalent electric and magnetic surface current, which can be described by (2.80) and (2.81). These equivalent electric and magnetic surface currents are utilized to account for the discontinuities between the different field components of the interacting exterior field on the object.

$$\mathbf{J}_s = \hat{n} \times \mathbf{H}_1(S^+) = \hat{n} \times \mathbf{H}_2(S^-) \quad (2.80)$$

$$\mathbf{M}_s = -\hat{n} \times \mathbf{E}_1(S^+) = -\hat{n} \times \mathbf{E}_2(S^-) \quad (2.81)$$

The SEP has two distinct field conditions. The first states that the sum of the fields incident on the exterior of the object create a set of currents which force the field in the volume of S^- to be zero. This allows a representation of the system where the exterior field and currents are not extended into the interior. Therefore, the objects interior electromagnetic properties will not disturb the exterior field or current. The second condition is similar. As the currents on S^+ produce a null-field inside the volume of S^- , the negative currents of S^+ will produce a null-field in the volume outside the object, and as such the interior medium parameters may be extended to the exterior. These two conditions can be visualized in Fig. 2.2(b) and (c).

Applying these two separate conditions allows for the medium parameters to be extended into the null-field regions. This is possible as materials cannot create a field without a source, and as such the null-field region will not be effected by any real material placed therein. This allows the interior and exterior surface currents

to reside in a homogeneous media. With this realization the entire system can be comprised of the same media, allowing for the homogeneous medium Green's function to be used when representing the corresponding field [95]. Through the application of these conditions (equivalence principle and extinction theorem) the null field conditions can be written in terms of the incident and scattered fields produced by the equivalent electric and magnetic currents, as described mathematically by (2.82) - (2.85) [96].

$$\mathbf{E}^s(\mathbf{J}, \mathbf{M}) + \mathbf{E}^i = 0, \quad \mathbf{r} \in V^- \quad (2.82)$$

$$\mathbf{H}^s(\mathbf{J}, \mathbf{M}) + \mathbf{H}^i = 0, \quad \mathbf{r} \in V^- \quad (2.83)$$

$$\mathbf{E}^s(-\mathbf{J}, -\mathbf{M}) = 0, \quad \mathbf{r} \in V^+ \quad (2.84)$$

$$\mathbf{H}^s(-\mathbf{J}, -\mathbf{M}) = 0, \quad \mathbf{r} \in V^+ \quad (2.85)$$

Any weighted combination of (2.82) and (2.83) to (2.84) and (2.85) will form a valid set of integral equations for the unknowns \mathbf{J} and \mathbf{M} . However, it should be noted that not all combinations of these equations form a unique solution at all frequencies, but the PMCHWT is one particular formulation which forms a unique and well-conditioned solution. The PMCHWT produces two equations from these four by weighting all the equations by a unitary value, and setting (2.82) to be equal to (2.84) and (2.83) to be equal to (2.85). This equation set can now be utilized to determine the fields using: the homogeneous Green's function, a proper set of integral equations, boundary conditions, and bases.

As the surface currents, described by (2.82) - (2.85), are continuous across the object, the object's surface must be discretized into a set of 2D surface triangles, as shown in Fig. 2.3(a), before MoM can be used to solve for the unknown currents. Using this discretization and the set of basis described by (2.86) and (2.87), the coupled system can be described by (2.88).

$$\mathbf{J}(\mathbf{r}) = \hat{\mathbf{n}} \times \mathbf{H} = \sum_{n=1}^N \mathbf{I}_n f_n(\mathbf{r}) \quad (2.86)$$

$$\mathbf{M}(\mathbf{r}) = \mathbf{E} \times \hat{\mathbf{n}} = \sum_{n=1}^N \mathbf{V}_n f_n(\mathbf{r}) \quad (2.87)$$

$$\underbrace{\begin{bmatrix} [Z^+ + Z^-] & [-\beta^+ - \beta^-] \\ [\beta^+ + \beta^-] & [Y^+ + Y^-] \end{bmatrix}}_{[Z]} \begin{bmatrix} [J_n] \\ [M_n] \end{bmatrix} = \begin{bmatrix} [E_n^i] \\ [H_n^i] \end{bmatrix} \quad (2.88)$$

In (2.88), the elements of the impedance ($[Z^\pm]$), admittance ($[Y^\pm]$), and linking ($[\beta^\pm]$) sub-matrices are defined by (2.89), (2.90), and (2.91).

$$[Z^\pm]_{mn} = j\omega [L^\pm]_{mn} + \frac{1}{j\omega} [S^\pm]_{mn} \quad (2.89)$$

$$[Y^\pm]_{mn} = \frac{[Z^\pm]_{mn}}{(\eta^\pm)^2} \quad (2.90)$$

$$[\beta^\pm]_{mn} = \int_S \int_{S'} f_m(\mathbf{r}) \cdot (f_n(\mathbf{r}') \times \nabla G^\pm(\mathbf{r}, \mathbf{r}')) d\mathbf{S}' d\mathbf{S} \quad (2.91)$$

In these equations $[L^\pm]_{mn}$ and $[S^\pm]_{mn}$ is defined by (2.92) and (2.93), with the homogeneous Green's function ($G^\pm(\mathbf{r}, \mathbf{r}')$) defined by (2.94).

$$[L^\pm]_{mn} = \mu^\pm \langle f_m; G^\pm; f_n \rangle \quad (2.92)$$

$$[S^\pm]_{mn} = \frac{1}{\epsilon^\pm} \langle \nabla \cdot f_m, G^\pm, \nabla \cdot f_n \rangle \quad (2.93)$$

$$G^\pm(\mathbf{r}, \mathbf{r}') = \frac{e^{(-jk^\pm |\mathbf{r} - \mathbf{r}'|)}}{4\pi |\mathbf{r} - \mathbf{r}'|} \quad (2.94)$$

It can be shown that each of the individual sub-matrices of the impedance matrix in (2.88) is symmetric for this specific SIE MoM problem. However, due to the sign difference between the two linking matrices, the full impedance matrix of (2.88) is not symmetric. As such, the Sturm-Liouville theory used to derive TCM for PEC materials in Section 2.3 cannot be applied. To allow for any material to be analyzed using TCM through the application of a PMCHWT SIE impedance matrix, the weighting factor of the SIEs (2.82) - (2.85) must be altered to force the operator matrix into symmetry. This is accomplished through a complex weighting of these equations, as described by Harrington in [34]. The complex weighting results in the new matrix equation (2.95), which presents a symmetric impedance matrix.

$$\underbrace{\begin{bmatrix} [(Z^+ + Z^-)/\eta_0] & -j[-\beta^+ - \beta^-] \\ j[\beta^+ + \beta^-] & [\eta_0(Y^+ + Y^-)] \end{bmatrix}}_{[Z]} \begin{bmatrix} \eta_0[J_n] \\ j[M_n] \end{bmatrix} = \begin{bmatrix} [E_n^i] \\ j\eta_0[H_n^i] \end{bmatrix} \quad (2.95)$$

As with the VIE TCM analysis, several problems associated with the eigenvector and eigenvalue solutions arise when the SIE impedance matrix ($[Z]$) of (2.95) is applied to the Sturm-Liouville theory. As the original derivation for TCM, described in Section 2.3, was developed using an impedance operator which operated only on the electric current density, the derivation is not perfectly suited for use on an SIE impedance operator which operates on both the electric and magnetic current densities. As such, the theoretical concepts of Section 2.3 are not perfectly suited for this specific problem. However, as the PMCHWT MoM problem is computationally efficient, and can be utilized for all real media, significant research into solving the problems associated with this method have ensued. These problems and their associated solutions will be further discussed in Chapter 5.

2.3.4 Solving for TCM in Mixed Media (SIE)

Solving for the CMs of an object composed of multiple media types is nearly identical to solving for the CMs of an object composed of a single media type as described in Section 2.3.3. As previously outlined, the PMCHWT SIE utilizes an asymmetric impedance operator. This type of operator does not form a suitably weighted Sturm-Liouville eigenvalue equation. Therefore, a method of forcing this specific SIE solution into symmetry was described in (2.95).

When the PMCHWT MoM solution is applied to solve an object comprised of separate homogeneous media types, an individual MoM matrix is created for all basis functions of each media type (i.e., two objects would create two individual PMCHWT matrices). Additionally, a new set of linking matrices must be created to describe the interactions between these media types. The simplest example of such a system can be describe by a single object comprised of PEC $(\cdot)_{m1}$, and a real material $(\cdot)_{m2}$. The PMCHWT impedance matrix for these two interacting media can be described by (2.96). In (2.96), $[Z^+ + Z^-]$, $[Y^+ + Y^-]$, and $[\beta^+ + \beta^-]$ are removed and replaced by the single sub-matrices $[Z]$, $[Y]$, and $[C]$ respectively, with relevant indices.

$$\underbrace{\begin{bmatrix} [Z_{m1}] & [C_{m1,1}] & [C_{m1,2}] \\ [-C_{m1,1}] & [Z_{m2}] & [C_{m2,2}] \\ [-C_{m1,2}] & [-C_{m2,2}] & [Y_{m2}] \end{bmatrix}}_{[Z]} \begin{bmatrix} [J_{m1,n}] \\ [J_{m2,n}] \\ [J_{m2,n}] \end{bmatrix} = \begin{bmatrix} [E_{m1,n}^i] \\ [E_{m2,n}^i] \\ [H_{m2,n}^i] \end{bmatrix} \quad (2.96)$$

As was shown with the single material analysis, the weighting factor of the SIEs (2.82) - (2.85) can be altered to force the impedance matrix into symmetry. Using the same complex weighting of these equations, as described in Section 2.3.3, the multiple media object's impedance matrix is also forced into symmetry. When applied to (2.96), the resulting symmetric system of equations is described by (2.97).

$$\underbrace{\begin{bmatrix} [(Z_{m1})/\eta_0] & -j [C_{m1,1}] & -j [C_{m1,2}] \\ j [-C_{m1,1}] & [(Z_{m2})/\eta_0] & -j [C_{m2,2}] \\ j [-C_{m1,2}] & j [-C_{m2,2}] & [\eta_0(Y_{m2})] \end{bmatrix}}_{[Z]} \begin{bmatrix} \eta_0 [J_{m1,n}] \\ \eta_0 [J_{m2,n}] \\ j [M_{m2,n}] \end{bmatrix} = \begin{bmatrix} [E_{m1,n}^i] \\ [E_{m2,n}^i] \\ \eta_0 j [H_{m2,n}^i] \end{bmatrix} \quad (2.97)$$

2.4 Summary

Within this chapter, the mathematical foundations required to solve for the CMs of an object were overviewed. Although a full understanding of each topic within this chapter is not necessary to apply TCM to complex antenna problems, the theoretical foundations are crucial to fully understand how to solve for the CMs of an object. Furthermore, the practical methods which are applied to form some of these theoretical formulations are not perfect, and as such the resulting CMs of some media types do not adhere to all the original TCM requirements for CMs. Therefore, some knowledge into these practical implementations is introduced to provide an understanding into the weaknesses that exist in different TCM solution types.

To provide the necessary insights into the foundations of TCM, this chapter began by providing an overview of the important theoretical concepts which are used, these include: Maxwell's equations and their associated quantities (Section 2.1), electromagnetic radiation and scattering (Section 2.1.1), and complex electromagnetic power flow (Section 2.1.2). The equations within these sections are

often solved using MoM, which is a computationally efficient approximation to Maxwell's equations. The EFIE MoM is detailed in Section 2.2. The MoM equations solve for the electromagnetic characteristics of an object, where part of the MoM solution solves for a matrix which approximates the impedance of an object. This impedance matrix can then be used to solve for the CMs of any PEC object, as described by Section 2.3. Finally, this chapter concludes by detailing how the impedance operator changes when solving for dielectric and magnetic media. This change is caused by the introduction of magnetic currents in the MoM solution, changing the mathematical and physical nature of TCM .

The mathematical concepts presented do not only solve for the CMs of an object, but also allow many CAs to be obtained. These CAs provide a physical understanding of the electromagnetic properties of an object. To fully utilize these CAs for antenna design, they must first be understood. Chapter 3 details the eight most important CAs, and provides examples of how they can be used to design or understand basic antenna structures.

Chapter 3

Characteristic Attributes

Characteristic Attributes

THE Theory of Characteristic Modes (TCM) weighted eigenvalue equation (2.47) solves for two distinct physical quantities, the characteristic currents (\mathbf{J}_n) and the characteristic eigenvalues (λ_n). Whereas these are the only two quantities solved in the base equation, many more physical insights into the electromagnetic properties of an object can be obtained through applying these quantities to different formulations. Collectively, these insights may be referred to as an object's Characteristic Attributes (CAs). A good understanding of these CAs is important to fully utilize all the benefits provided by Characteristic Mode Analysis (CMA). While there are many different CAs, the eight main attributes are defined as the characteristic eigenvalue, modal significance, characteristic current, characteristic angle, modal scattering angle, modal Quality Factor (Q-factor), characteristic near-field, and characteristic far-field. In this chapter, these eight attributes will be overviewed. Additionally, illustrations of these attributes will be given with respect to a long thin ($\lambda/50$) Two-Dimensional (2-D) Perfect Electric Conducting (PEC) wire strip.

3.1 Characteristic Eigenvalues

As overviewed in Section 2.3.1, the characteristic eigenvalue (λ_n) is directly obtained in the process of solving the TCM weighted eigenvalue equation (2.47). When relating this solution to Poynting's theorem (2.21), it was shown that the eigenvalue is equal to the imaginary part, i.e. the reactive power.

The characteristic eigenvalue is one of the most important quantities of TCM, and is as important as the characteristic current. This is due to the eigenvalue's relationship to the stored energies \bar{W}_m and \bar{W}_e . The information provided by these quantities is essential for proper analysis of different objects. The difference between the stored energies defines when an object is in a resonant, capacitive, or inductive state. These energy states are akin to a simple Resistive, Inductive, Capacitive (RLC) circuit where the electric and magnetic energies are stored by a

capacitor or inductor, and power is dissipated in the circuit by means of a resistor. When analyzing a lossless object using TCM, the resistor represents the power dissipated by the antenna through far-field radiation.

Electromagnetic theory indicates that a radiated field is composed of equal amounts of electric and magnetic energy, this allows for a time-space transformation between the two quantities (Section 2.1). As such, if a Characteristic Mode (CM) is made up of more magnetic than electric energy, the total amount of supplied power cannot be transformed into radiated power, and some energy must be stored. When $\lambda_n = 0$, the stored energies are equal, as defined by (3.1), and thus the mode is in resonance (i.e. no energy is stored by the object over a full frequency cycle). When $\lambda_n < 0$, there is more electric energy than magnetic energy stored over any given frequency cycle (3.2), and the CM is defined to be capacitive. Finally, when $\lambda_n > 0$, more magnetic energy than electric energy is stored as defined by (3.3), and the CM is inductive.

$$\iiint_V \epsilon |\mathbf{E}_n|^2 dV = \iiint_V \mu |\mathbf{H}_n|^2 dV \quad (3.1)$$

$$\iiint_V \epsilon |\mathbf{E}_n|^2 dV > \iiint_V \mu |\mathbf{H}_n|^2 dV \quad (3.2)$$

$$\iiint_V \epsilon |\mathbf{E}_n|^2 dV < \iiint_V \mu |\mathbf{H}_n|^2 dV \quad (3.3)$$

When characteristic eigenvalues are plotted, the eigenvalues are traditionally ordered with respect to the frequency at which each eigenvalue crosses resonance. However, as some eigenvalues never become resonant the ordering of non-resonant eigenvalues depends on their importance to the problem being solved. Furthermore, as the impedance matrix changes across frequency, the ordering of the eigenvalues does not remain constant. To combat the randomness of plotting eigenvalues across frequency, many different eigenvalue tracking algorithms have been developed, and these will be detailed in Chapter 4.

3.1.1 CM Eigenvalue Example

The usefulness of characteristic eigenvalues can be effectively demonstrated by analyzing the CMs of a thin wire object. The first three eigenvalues of this object are plotted in Fig. 3.1.

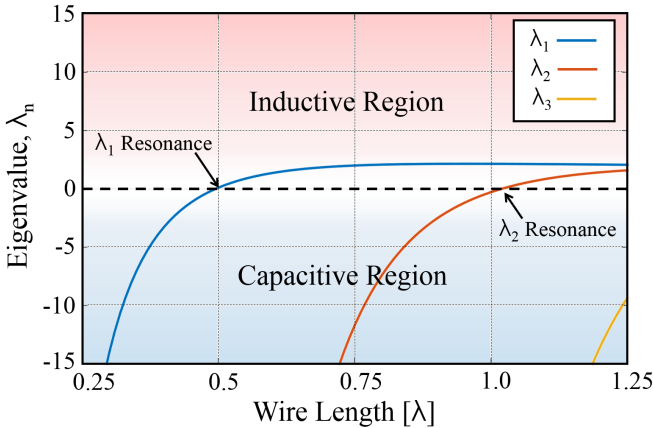


Figure 3.1: Characteristic eigenvalues of a 2-D PEC object with variable length and $\lambda/50$ width.

In general, an eigenvalue plot provides a significant amount of information into the resonant and scattering properties of an object. For this specific object, the plotted CMs are capacitive at frequencies below the respective resonances (e.g., below $\approx 0.5\lambda$ for λ_1). In this region the CM will store more electric than magnetic energy. At the point of resonance, a CM stores equal amounts of energy, and the object is a perfect radiator. Above the resonance point, a CM will store more magnetic than electric energy, and is considered to be an inductive mode.

The properties of these modes allow for significant insights to be obtained without applying excitation sources to the object. For example, if the 2-D wire object's first two resonant locations, as defined by the zero crossings of the eigenvalue, are compared to the resonant properties of a $\lambda/2$ and λ dipole, the resonances closely align. Additionally, it is well known that a dipole antenna stores electric energy below resonance (capacitive antenna), and magnetic energy above resonance (inductive antenna) [97], as do the first two CMs λ_1 and λ_2 .

The insights obtained through knowledge of the CM eigenvalues allow for a fundamental understanding of an object's electromagnetic properties, without analyzing the object's shape, currents, or fields. However, the eigenvalues can provide other insights beyond the type of energy stored.

3.2 Modal Significance (Modal Solutions)

As described in Section 3.3 and 2.3.1, the characteristic far-fields and the characteristic weighted currents are orthogonal. This implies that each characteristic current radiates power independently of the other characteristic currents. These unique features allow for a modal solution to be formed for any induced current (\mathbf{J}) on the object. This is accomplished through expanding the set of weighted characteristic currents (with weighting coefficients α_n), as is described by (3.4).

$$\mathbf{J} = \sum_{n=1}^N \alpha_n \mathbf{J}_n \quad (3.4)$$

The weighting coefficients can be found through substituting (3.4) into the linear operator (\mathcal{L}) of the incident field equation (2.18) and obtaining a weighted set of currents that correspond to an incident electric field (3.5) [3].

$$\left[\sum_{n=1}^N \alpha_n \mathcal{L}(\mathbf{J}_n) - \mathbf{E}^i \right]_{tan} = 0 \quad (3.5)$$

As overviewed in Section 2.3.1, \mathcal{L}_1 can be equated to the impedance operator (\mathbf{Z}). Through taking the inner product of (3.5) with respect to the characteristic current (\mathbf{J}_n), the characteristic far-fields can be related to the characteristic eigenvalue as shown in (3.6), where V_n^i is defined by (3.7) [86].

$$\alpha_n (1 + j\lambda_n) = V_n^i \quad (3.6)$$

$$V_n^i = \langle \mathbf{J}_n, \mathbf{E}^i \rangle = \iint_S \mathbf{J}_n \cdot \mathbf{E}^i d\mathbf{S} \quad (3.7)$$

Equation (3.7), is referred to as the modal excitation coefficient, and defines a characteristic current's relationship to the position, magnitude, phase, and polarization of an applied excitation. Furthermore, this relationship can be used to define a modal solution for any induced currents on an object using (3.8).

$$\mathbf{J} = \sum_{n=1}^N \frac{V_n^i \mathbf{J}_n}{1 + j\lambda_n} \quad (3.8)$$

Formulation (3.8) shows the key factors influencing the significance each CM has to a radiated field. Apart from the modal excitation coefficients (V_n^i) which represent the influence of an excitation source, the weighting factor of (3.8) is inversely related to the CM eigenvalues. This inverse dependence is defined as the Modal Significance (MS), as it represents the amplitude each characteristic current contributes to the total radiated field. The MS_n can be mathematically defined by (3.9).

$$MS_n = \left| \frac{1}{1 + j\lambda_n} \right| \quad (3.9)$$

The MS is able to determine both the modal resonance (when $\lambda_n = 0$), as well as the modal radiation bandwidth, i.e., the modal bandwidth (BW_n). When a mode is in resonance the $MS_n = 1$, and modes which do not contribute to the radiated field are defined by $MS_n = 0$. The most significant CM, at any given frequency, is defined by the CM with the maximum valued modal significance (MS_n). Moreover, as the MS is defined by the weighting factor of a radiated field, the half-power radiating bandwidth can be approximated using (3.10).

$$BW_n \approx \frac{f_H(MS_n = 1/\sqrt{2}) - f_L(MS_n = 1/\sqrt{2})}{f_{res}(MS_n = 1)} \quad (3.10)$$

In (3.10), f_H and f_L are the high and low frequency band edges of any local maximum, at which the MS is equal to or greater than $1/\sqrt{2}$. f_{res} is the resonant frequency where $MS_n = 1$ or the location of maximum MS. The modal bandwidth is often an important Figure of Merit (FoM) in many TCM antenna and scattering problems, as it helps to determine the radiating performance of a specific CM. However, it is important to understand that the modal bandwidth corresponds to the radiated pattern's half-power bandwidth (for single mode excitation), and not the impedance bandwidth of an excited structure.

The MS and modal bandwidth is often utilized as a metric to determine what modes are relevant in CM problems. Often these problems are presented using the MS rather than the characteristic eigenvalue. This is due to the MS being more intuitive, and easier to plot than the eigenvalue, as the eigenvalue ranges from $[-\infty, +\infty]$, whereas the MS has a range between $[0, 1]$. Nevertheless, MS suffers from the drawback that, in presenting an absolute value, it does not indicate if a mode is capacitive or inductive, and the MS does not provide characteristic current phase information.

3.2.1 Modal Significance Example

When the 2-D thin wire object is analyzed using MS, other insights beyond those found in the eigenvalue solution can be obtained. The first three MS curves and the first two modal bandwidths (highlighted in red) are plotted in Fig. 3.2. The resonant frequencies are determined by $MS = 1$ (for this specific example), and the larger the MS value the more significant is the mode. As such, the most significant modes of a 0.25λ to 1.25λ 2-D thin wire object are found to be λ_1 and λ_2 (λ is the free space wavelength, and λ_n is the characteristic eigenvalue), which have the corresponding resonant frequencies of $\approx 0.5\lambda$ and $\approx 1\lambda$. Furthermore, these MS curves provide evidence that within the modal bandwidth of each significant CM, no other CMs substantially contribute to the radiated or scattered fields.

As described, MS is able to define the radiating bandwidth of a CM. This is important, as it can help determine feed positions when designing excitation structures. Using the thin wire example, it is apparent from Fig. 3.2 that the radiation bandwidths of the two modes do not overlap. Therefore, any designed excitation source cannot substantially excite both radiation modes over a continuous bandwidth.

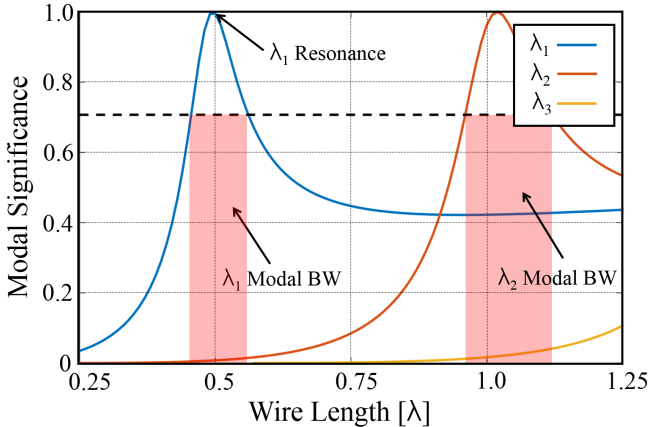


Figure 3.2: Modal Significance of a 2-D PEC object with variable length and a fixed width of $\lambda/50$.

3.3 Characteristic Currents

Section 2.3.1 described how the characteristic current (\mathbf{J}_n) is directly obtained in the process of solving the TCM weighted eigenvalue equation (2.47). However, as this problem is designed to guarantee that the radiated current maintains far-field orthogonality, it is not obvious that the characteristic currents are also orthogonal to one another. The first sub-theorem of the Sturm-Liouville problem states the weighted inner product must be self-adjoint, as this applies to the currents \mathbf{J} the orthogonality properties described by (2.56) - (2.58) are guaranteed.

The characteristic currents are unique because they provide many view-points in understanding the radiation properties of an object. Through analysis of these currents, an object can be transformed into an antenna with known characteristics, through applying a proper excitation source in a location of significant characteristic currents. Furthermore, as each CM maintains polarization orthogonality, any given CMs can be excited or dampened through applying specific excitation structures, allowing for the design of excitation sources which are able to control the polarization purity of an object.

3.3.1 CM Currents Example

The first two characteristic currents and their corresponding eigenvalues of the previous long and thin 2-D PEC object are plotted in Fig. 3.3. As the currents on the object are real, they can be utilized in many different ways. First, at the location of highest current, an excitation source can be placed to transform this object into an antenna. Often this is realistically implemented through splitting the object and placing a voltage source between the two sections. If this is applied to the λ_1 currents in Fig. 3.3, the object will turn into a $\lambda/2$ dipole antenna. Second, if the object is modified in areas of high current, there will be a greater impact on the resonant properties of the CM than if areas of low current density are modified. Finally, currents corresponding to different CMs can be analyzed to determine if feeding one mode will excite a different mode.

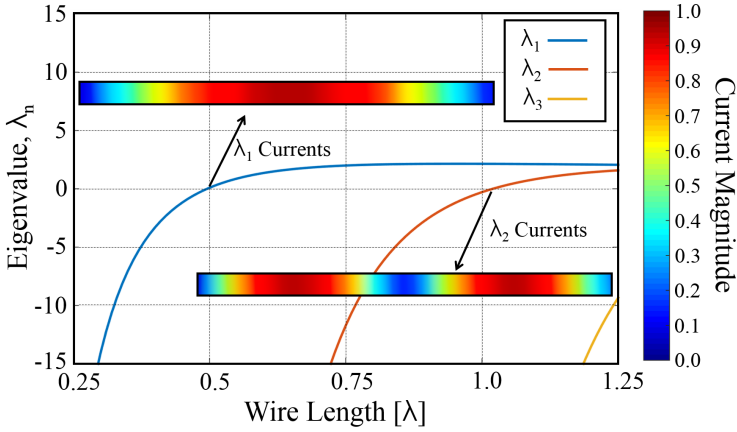


Figure 3.3: Characteristic currents of a 2-D PEC object of variable length (in λ) and a fixed width of $\lambda/50$. The currents are normalized to the maximum value in each case. The aspect ratio of the presented currents is skewed, allowing for better visualization.

3.4 Characteristic Phase

The CAs overviewed in Sections 3.1 - 3.3 provide evidence that the eigenvalues and the characteristic currents are able to yield insights into the phase characteristics of an object. There are three unique properties which allow for phase information to be obtained from a CM solution:

1. The characteristic eigenvalues are directly related to the amount and type of stored energy in a given CM. This excess stored energy will produce a time lag between an incident and scattered, or excited and radiated field.
2. The MS derivation (3.8) relates any current to a set of characteristic currents, with the significance of each current directly related to the characteristic eigenvalue.
3. The characteristic currents are defined to be equiphase across the object, i.e. $(\mathbf{J}_n = \mathbf{J}_n^*)$.

Using these insights Garbacz *et al.* in [2] and Harrington *et al.* in [3] were able to relate the eigenvalue to a perturbation (3.11) and scattering (3.12) matrices. The perturbation matrix provides the phase information of individual CMs,

whereas the scattering matrix describes the scattered field's phase lag relative to the incident field for each CM.

$$[P] = \begin{bmatrix} \frac{-1}{1+j\lambda_1} & 0 & 0 & \dots \\ 0 & \frac{-1}{1+j\lambda_2} & 0 & \dots \\ \dots & \dots & \dots & \dots \end{bmatrix} \quad (3.11)$$

$$[S] = \begin{bmatrix} -\frac{1-j\lambda_1}{1+j\lambda_1} & 0 & 0 & \dots \\ 0 & -\frac{1-j\lambda_2}{1+j\lambda_2} & 0 & \dots \\ \dots & \dots & \dots & \dots \end{bmatrix} \quad (3.12)$$

Furthermore, these matrix elements are linked to individual characteristic currents, and as such Garbacz discovered that any single perturbation matrix element must be contained within the half unit circle, due to the equiphase response of the incident wave [2]. This allows for a phase response to be attributed to each CM.

The angle of a (diagonal) perturbation matrix element (the angle of the complex number in the half-unit circle) is determined by the negative angle of (3.11) and an additional phase offset defined by the boundary condition associated with the incident field ($(\mathbf{E}^i)_{tan}$). This angle is often referred to as the characteristic angle (α_n), and can be mathematically described by (3.13). The difference between α_n and α_m accounts for the phase difference, or phase lag, between two characteristic currents.

$$\alpha_n = 180^\circ - \text{angle}(P_n) = 180^\circ - \arctan(\lambda_n) \quad (3.13)$$

The angle of a (diagonal) scattering matrix element defines the phase relationship between an incident wave and the scattered wave produced by a CM. This relationship is determined by the angle of each diagonal element (S_n) in the scattering matrix (3.12), referred to as the modal scattering angle (ϕ_n), and is determined using (3.14).

$$\phi_n = \text{angle}(S_n) = \arctan\left(\frac{\text{Im}(S_n)}{\text{Re}(S_n)}\right) \quad (3.14)$$

3.4.1 Characteristic Phase Example

The characteristic angle and the modal scattering angle can be effectively utilized in many antenna problems, including the analysis of the $\lambda/50$ 2-D PEC wire strip. The characteristic angle provides values ranging from 90° to 270° and is often used to describe the CMs of an object; as all the modes lie on a well-defined scale. The first three characteristic angles of the example wire strip are plotted in Fig. 3.4. In this figure λ_1 is in resonance at nearly 0.5λ , when the characteristic angle is 180° .

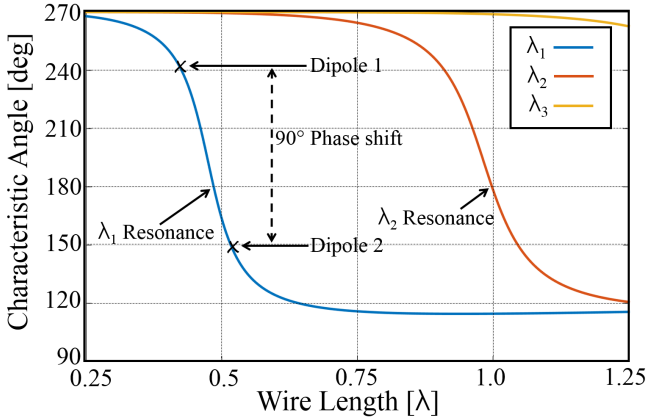


Figure 3.4: Characteristic angle of a $\lambda/50$ 2-D PEC wire strip.

Figure 3.4 shows how the phase of each characteristic current is different from the other characteristic currents and also describes how the phase of a single current changes over frequency. This unique perspective of each mode can be utilized to design antennas which require specific phase characteristics, such as Circularly Polarized (CP) antennas. When designing a CP antenna using vertically and horizontally polarized currents, a phase lag of 90° between the two currents is required. As is shown in this figure, a phase difference can be found and attributed to different wire lengths. If a phase shift of 90° is needed, the lengths which are attributed to these phase shifts can be found. By analyzing the CAs of the different wire lengths, a high CP axial ratio with a single feed cross dipole antenna can be designed. The currents, feed position, and lengths for this CP antenna are described in Fig. 3.5(a). Additionally, this antenna maintains the typical cross dipole bidirectional pattern (Fig. 3.5(b)), and an axial ratio of better than $-0.5dB$ for both the Right Hand Circular Polarized (RHCP) (Fig. 3.5(c)) and Left Hand

Circular Polarized (LHCP) patterns.

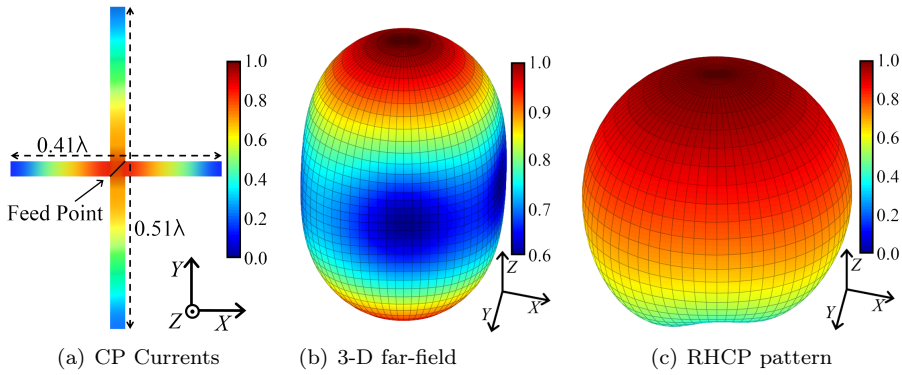


Figure 3.5: CP antenna designed using the 2-D thin wire object. The length of the object is determined using the characteristic angle. Normalized (a) currents of the single cross wire object, (b) 3-D far-field pattern, and (c) 3-D RHCP pattern.

It appears that the modal scattering angle has not been utilized in designing antennas for specific applications, since no previous publication in this area could be found. However, this unique attribute provides insights into the phase characteristics of scattering objects; thus defining how a CM re-radiates an incident wave. This attribute can be effectively utilized in many scattering applications ranging from RADAR systems to reflector/director antenna designs. The modal scattering angle ranges from -180° to $+180^\circ$, corresponding to the phase lag between an incident wave and a CM produced scattered wave. The first three modal scattering angles for the $\lambda/50$ thin wire are plotted in Fig. 3.6.

Figure 3.6 describes the phase lag of each mode relative to the field which excited the mode. While there are many uses of the reflected phase characteristics, one obvious advantage is reducing the number of unknowns for a director antenna system. When designing these types of coupled systems, many unknowns must be solved; such as coupling characteristics, resonances, phase relationships, and the distances between the director and exciter elements. Using the previously described CAs and the modal scattering angle, these unknowns can be reduced to one. For example, the phase can be defined and the wire length determined, or vice-versa. If a phase shift of 49° is required for the director, this can be found from the modal scattering angle (Fig. 3.6) corresponding to a wire length of 0.4λ . From this information, a separation length between the exciter and the director is

found to be 0.31λ . This results in constructive interference in the forward direction and destructive interference in the reverse direction (Fig. 3.7(a)). It should be noted, that this phase relationship only predicts far-field phase differences, and as such the front-to-back ratio is only 4.1dB (Fig. 3.7(b)). This is because near-field coupling has an impact on the phase and coupling relationships of this specific example.

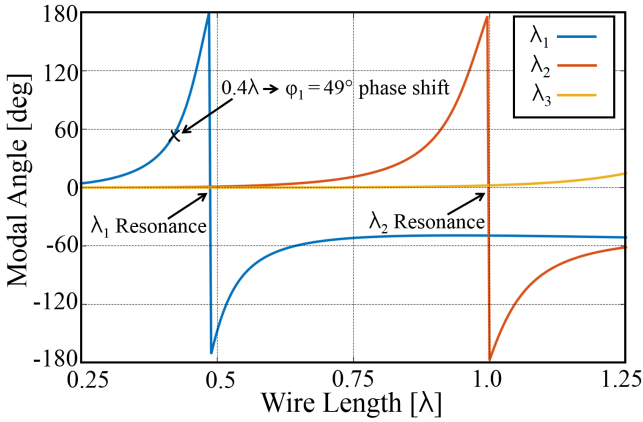


Figure 3.6: Characteristic modal scattering angles of a $\lambda/50$ 2-D PEC wire strip.

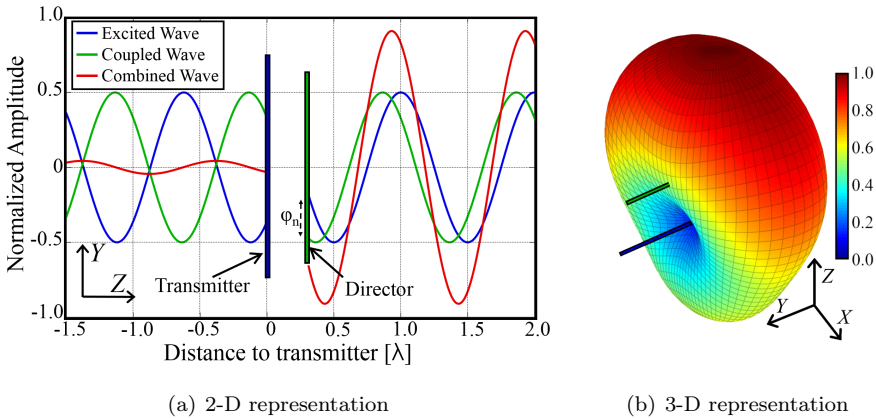


Figure 3.7: 2-element director antenna system (Yagi): (a) 2-D time domain representation of the single coupled element system, and (b) the 3-D radiation pattern of the designed antenna system evaluated using a single excitation and a MoM solver.

3.5 Modal Quality Factor

The concept of Q-factor is important in most electromagnetic problems, as this dimensionless parameter relates the amount of energy lost (i.e., radiated and dissipated energy) to the amount of energy stored within any object. As such, the larger the Q-factor the less energy lost per frequency cycle. Often this concept is utilized in antenna problems, as this quantity is inversely proportional to an antenna's bandwidth. Antennas with low Q-factors either have low bandwidths or high losses. Likewise, high Q-factor antennas have either narrow bandwidths or low losses [98, 99].

The Q-factor for an object is defined by the maximum amount of energy stored by an object, and the efficiency at which the object radiates or loses energy (by means of radiation or heat dissipation), as represented by (3.15). Furthermore, this quantity can be used to define a set of physical bounds for a known object [100], thus determining the maximum antenna performance of that object.

$$Q = \frac{2\omega \max\{\bar{W}_e, \bar{W}_m\}}{P_e + \bar{P}_d} \quad (3.15)$$

In TCM problems, (3.15) is not useful in determining the Q-factor of a given CM, as the individual quantities \bar{W}_e and \bar{W}_m are not known. However, there are multiple other methods of determining the Q-factor of a CM, some of which are described in [77, 101]. The most traditional approach to determining the modal Q-factor is through the use of the characteristic eigenvalue. As the eigenvalue is defined as 2ω times the difference in stored energy of a CM ($\omega = 2\pi f$, f is the frequency), it was shown in [7] that it can be used to approximate the Q-factor using (3.16).

$$Q_n \approx \omega \frac{\partial \lambda_n}{\partial \omega} \quad (3.16)$$

One caveat to this approximation is that it is only valid at resonance, and thus should not be used at any frequency, or for all CMs. This is also true when the modal bandwidth, as described by (3.10), is utilized to define the modal Q-factor.

Traditionally non-resonant modes are difficult to analyze as the modal bandwidth is only defined in resonance. However, many solutions to this problem have been investigated, such as the approach outlined in [102]. In [102], a useful approx-

imation of the Q-factor is defined through forcing a set of currents into resonance using a single circuit element. This is done using an object's impedance matrix to determine the proper circuit element which will force the mode into resonance. This theoretical concept uses the partial derivative with respect to the angular frequency (ω) of the imaginary part of the MoM impedance matrix, the real part of the impedance matrix, and the object's surface currents. When applied to TCM, the Q-factor for any CM can be defined for any frequency using (3.17).

$$Q_n = \frac{\omega[J_n]^* (\partial[Z]/\partial\omega) [J_n] + |[J_n]^* X [J_n]|}{2[J_n]^* [R] [J_n]} \quad (3.17)$$

The Q-factor of individual CMs is important in TCM analysis, as the information provided by this quantity allows insights into any CM's maximum obtainable bandwidth, thus providing knowledge into the radiation performance of the object.

3.5.1 Modal Quality Factor Example

The modal Q-factor can be effectively utilized in many antenna problems including the analysis of the thin wire strip. The first three modal Q-factors for the two separate formulations, as defined in Section 3.5, are plotted in Fig. 3.2. In this figure the solid lines were calculated using (3.17), and the dotted lines calculated using (3.16). It is apparent that these two calculations are significantly different, and as discussed (3.17) should be more accurate than (3.16). However, in many situations, e.g., when using commercially available TCM software packages, the more accurate solution is not possible to obtain, as access to the TCM currents at two different but closely related frequencies, as well as the full impedance matrices at those frequencies are required.

As the modal bandwidth can be determined by the modal Q-factor, it is possible to plot the maximum obtainable modal bandwidth which corresponds to each of the CMs. The bandwidths of the first three CMs are presented in Fig. 3.9. This figure shows that the resonant bandwidth of a $\lambda/2$ thin wire is approximately 20% (when calculated using either the MS or the currents), this is closely related to the ideal half-power radiation bandwidth of a $\lambda/2$ dipole. As can be expected, the bandwidth, as predicted from the inverse of the eigenvalue slope obtained from (3.16), does not agree well with that obtained from the other two methods.

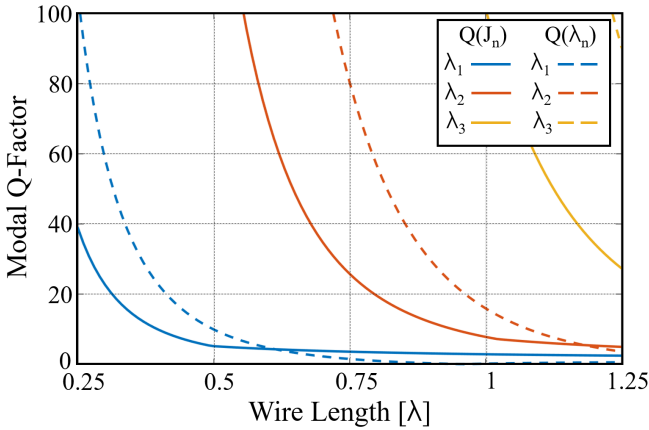


Figure 3.8: Modal Q-factor of a $\lambda/50$ 2-D PEC wire strip.

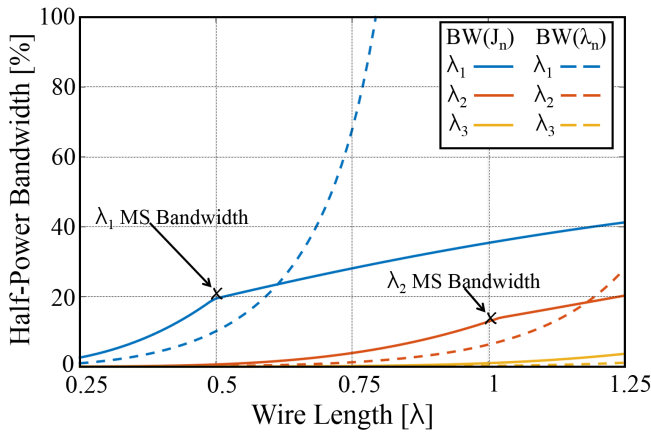


Figure 3.9: Modal half-power bandwidth of a 2-D PEC wire strip with a width of $\lambda/50$. Calculated using the MS bandwidth obtained using (3.10), and the inverse of the quality factors (3.16) and (3.17).

3.6 Characteristic Fields

The Theory of Characteristic Modes is designed to create a set of orthogonal far-fields (i.e., when evaluated over a closed surface at infinity). While these fields are known to be orthogonal, they are not directly available from the solution to the TCM eigenvalue problem. In many practical situations it may be important to determine the near-fields (i.e. the field close to the object) or far-fields of

an object's characteristic currents. Unlike the far-fields, the near-fields are not guaranteed to be orthogonal, but can be helpful in describing the electromagnetic characteristics of an object. Additionally, the near-fields can be used for coupling applications such as Radio-Frequency Identification (RFID) or when exciting an object. Furthermore, the exact far-field solution is also useful in applications including modal decomposition, modal tracking, Multiple-Input Multiple-Output (MIMO) antenna design, and scattering problems.

There are several different ways to calculate the fields radiated by a set of currents. The most traditional approach directly uses the currents to determine the radiated fields, this is often referred to as the direct approach [83, 103]. More details on how to utilize this method to solve for the near-fields or far-fields defined by a set of currents can be found in Sections 6.8.1 and 6.8.2 of [83], respectively.

However, it is also possible to calculate the near- or far-fields of a set of currents on an object using the dipole method as specified in [103–105]. This method is more easily implemented, and is used in many commercial electromagnetic MoM solvers. The dipole method for calculating the fields produced by the currents of an object uses the individual currents of each basis function, and places Hertzian dipoles with the corresponding current at these locations. This dipole is located at the center of the mesh element, with the dipole oriented along the dotted line in Fig. 2.4. This is a unique way of determining the fields, as the analytical expression for the fields, both \mathbf{E} and \mathbf{H} , are known for a Hertzian dipole. Once the fields of each current element are calculated, the total fields at any location can be computed by summing the contributions of all the individual dipoles (one dipole for each mesh element). This method is fully outlined in Section 3 of [106].

3.6.1 Near- and Far-Field Example

Calculation and visualization of the characteristic fields is important in many applications, as these computations provide significant insights into the electromagnetic characteristics of an object. The first three electric characteristic near-fields for λ_1 , λ_2 , and λ_3 of the thin wire at resonance are plotted in Fig. 3.10. The plotted fields are calculated over the same 2-D dimensions as the wire, but at a distance of $\lambda/15$ away in the 3rd dimension. Such an offset is required for field calculations using the dipole method, as the fields of each Hertzian dipole are only valid at a distance greater than the length of the Hertzian dipole. For

a Rao-Wilton-Glisson (RWG) meshed object, the Hertzian dipoles are made up of individual meshing elements, and this specific object is meshed with triangles $\approx \lambda/40$ in length at the λ_1 resonance point. Therefore, an offset of greater than $\lambda/40$ is required to analyze this object with this mesh [105, 106].

The near-fields of Fig. 3.10 provide information into the strength of the electric field (in volts per meter) over the calculated dimensions. For the first CM (λ_1) the amplitude is smallest in the center and largest on the two edges. This produces a half-wave near-field distribution across the object, nearly identical to that of a $\lambda/2$ dipole. The second CM (λ_2), produces a full-wave near-field distribution nearly identical to that of a full wave dipole. In areas of strong electric (magnetic) field, a Capacitive Coupling Element (CCE) (Inductive Coupling Element (ICE)) can be used to efficiently couple energy into the object, providing insights into alternative methods of exciting the object.

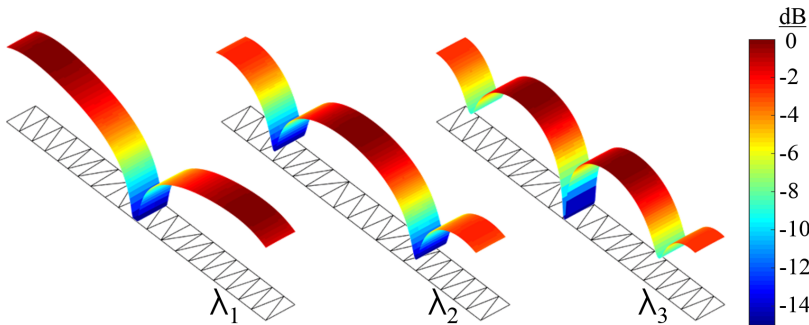


Figure 3.10: Normalized electric near-fields and the corresponding triangular mesh for a 2-D PEC wire strip of width of $\lambda/50$. The near-fields are computed at $\lambda/15$ away from the object's 2-D axis. The width of each figure is skewed to allow for better visualization.

The normalized far-fields for the first three CMs of the object at their respective resonant frequencies are plotted in Fig. 3.11. These far-fields are orthogonal to one another. One unique characteristic of this property, is that the far-fields of an antenna (such as a dipole), can be compared to the characteristic far-fields of a similar object, providing knowledge into which characteristic modes are excited [65]. This property provides evidence that if the modes of a $\lambda/2$ dipole are reconstructed using the characteristic far-fields, the dipole's far-fields can be almost completely reconstructed from the far-fields of the first CM (λ_1). Additionally, the far-fields of a λ and $3\lambda/2$ dipole antenna can be almost fully reconstructed using

the far-fields of the second and third CMs, respectively. Furthermore, far-field analysis can be used for far-field coupling calculation, and modal tracking.

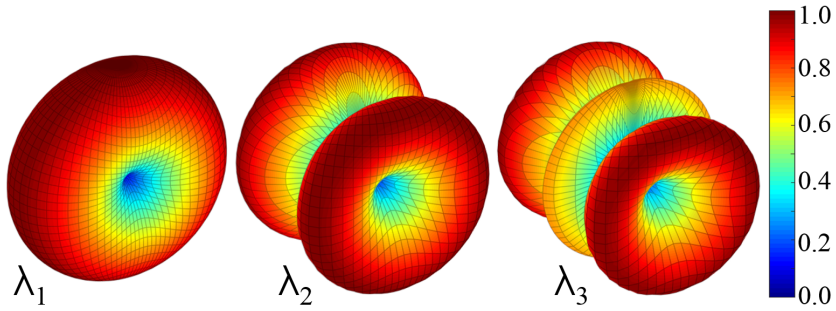


Figure 3.11: Normalized far-fields of the first three CMs at resonance for a 2-D PEC wire strip with a width of $\lambda/50$.

Chapter 4

Eigenvalue Tracking

Eigenvalue Tracking

THE Theory of Characteristic Modes (TCM) provides insights into the electromagnetic characteristics of an object when calculated at a single frequency. However, it is often useful to analyze these Characteristic Modes (CMs) over a wide frequency range in an effort to determine resonance characteristics, phase variations, modal bandwidths, and mode-to-mode interactions. As outlined in Section 2.3, the eigenvalues are determined from the decomposition of the Method of Moments (MoM) impedance matrix. This impedance matrix is numerically calculated in the frequency domain, and as such varies across frequency. This causes the solution to the Sturm-Liouville problem to change, resulting in the eigenvalues not maintaining a constant order across frequency. These disordered characteristic solutions are a significant problem, as many of the insights and Characteristic Attributes (CAs) that can be obtained from a TCM solution require the eigenvalues to be accurately tracked.

To combat this problem, many different eigenvalue tracking methods have been developed. These are often designed in an effort to link the eigenvalues together across frequency in a meaningful manner. Often this is done through utilizing a variety of different CAs, e.g., attempting to guarantee the current does not vary significantly over frequency for a single CM. While there are many benefits to correctly tracking the CMs, accurate tracking can be extremely difficult to apply in practice. One classic problem is that different tracking methods can provide conflicting solutions to the same object, and it can be difficult to determine which of these solutions is correct.

Most eigenvalue tracking methods consist of an algorithm that can be described by a flowchart, with the centerpiece being the calculation of a correlation quantity. A generalized form of a flowchart for eigenvalue tracking is outlined in Fig. 4.1. In this chart the impedance matrix of an object is solved at two different frequencies (f_a and f_b). These impedance matrices are then used to solve the TCM eigenvalue equation for the corresponding frequencies, and the resulting eigenvalues are preconditioned to reduce the problem space. Finally, a correlation matrix is built and reordered until the correlation for each diagonal element is above a required

threshold. This reorder matrix, or linking matrix, is then saved and subsequent frequencies are solved in the same manner.

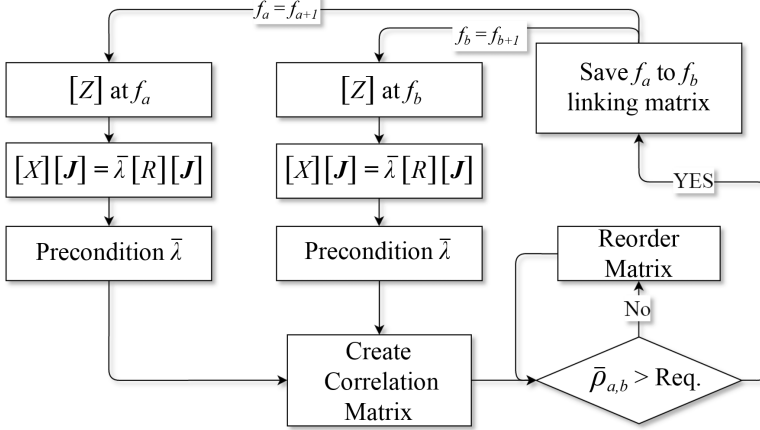


Figure 4.1: A generalized TCM tracking flowchart.

To demonstrate the difficulties of tracking TCM eigenvalues across frequency, a simple two-part structure (Fig. 4.2) can be analyzed using TCM [107]. This unique object has many special characteristics that make tracking its modes difficult. These difficulties arise from the object being symmetric, as well as having multiple resonant modes that intersect one another, high modal Quality Factors (Q-factors), high currents limited to small regions of the object, anti-resonant modes [108], and degenerated modes [74]. Each one of these issues provides a degree of difficulty for existing tracking methods.

When solving the TCM eigenvalue equation, the modes are typically sorted during the solution process, with the order determined by the smallest $|\lambda_n|$ at each frequency. Often, there is limited value to this simple type of sorting, as the modes are not electromagnetically related. This is evident when the characteristic angles are plotted for the first 30 CMs of the two-part chassis (Fig. 4.3).

Whereas many different tracking approaches exist, four distinct tracking categories will be briefly overviewed in the following sections in an effort to represent the more significant research publications in this field. There are often many different algorithms in each tracking category, but they operate with similar principles. In fact, many of the main theoretical concepts are similar even across different categories. In particular, all four categories attempt to link the modes across frequency through electromagnetically associating each mode at a given frequency

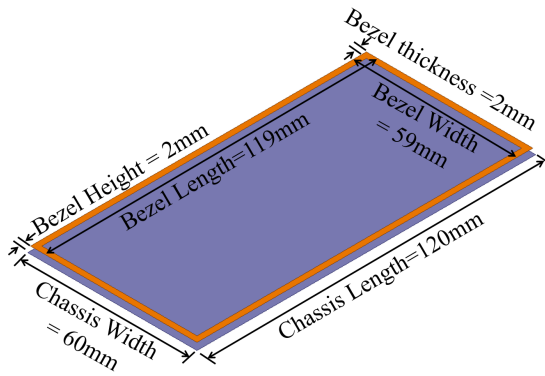


Figure 4.2: Two-part chassis comprised of a thin metal bezel and a flat plate. The CMs of this object are difficult to track due to its unique resonant properties around 2.6 GHz. ©2015 IEEE

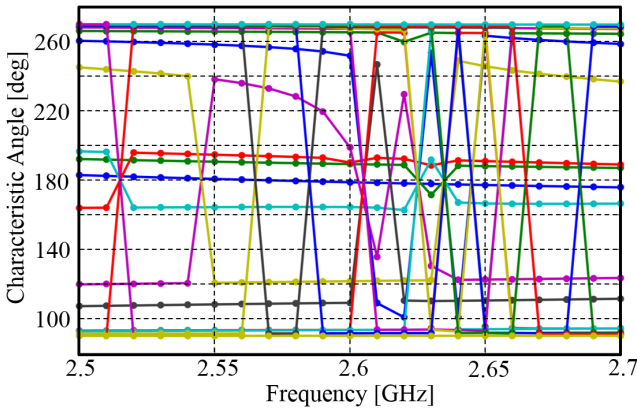


Figure 4.3: Characteristic angle of the first 30 modes of the two-part chassis tracked by eigenvalue sorting.

to a corresponding mode at a different frequency. Therefore, some amount of electromagnetic insights can be obtained from the linked modes. However, as orthogonality relationships do not strictly hold across frequency, none of the four tracking categories works perfectly and further analyses may be needed to determine if the modes are properly linked when using any type of tracking.

4.1 Eigenvector Correlation Tracking

Eigenvector tracking is one of the most computationally efficient methods for tracking the CMs of an object, and it was one of the first CM tracking categories developed [109]. This type of tracking is easily computed as it only requires access to the eigenvectors (i.e., discretized characteristic current distributions, $[J_n]$) over the frequencies of interest. The most basic form of this tracking method builds a correlation matrix using the matrix elements described by (4.1).

$$\rho_{n,m}(f_a, f_b) = \frac{[J_m(f_b)]^T [J_n(f_a)]^*}{|[J_n(f_a)]| |[J_m(f_b)]|} \quad (4.1)$$

In (4.1), $\rho_{n,m}$ is the correlation of CM n to CM m , where CMs n and m are evaluated at frequencies f_a and f_b , respectively. The matrix will then be reordered as depicted in the generic tracking flowchart of Fig. 4.1. Whereas the exact reordering of the correlation matrix is dependent on the specific algorithm and object used, the most closely related modes will maintain a value of $\rho_{n,m} \approx 1$, and modes which do not have a strong eigenvector correlation will produce values of $\rho_{n,m} < 1$.

Often this method requires the difference between f_a and f_b to be very small, as the eigenvectors will most likely not vary significantly between two different impedance matrices that contain only small differences between them. Moreover, as the eigenvectors are not guaranteed to be mathematically orthogonal at the same frequency, unlike the weighted characteristic currents and characteristic far-fields, this tracking method is more susceptible to errors than other tracking methods.

These problems become apparent when the eigenvalues of the two-part chassis (Fig. 4.2) are tracked using an eigenvector correlation algorithm. This algorithm reorders the correlation matrix by determining the $\lambda_m(f_b)$ which has the highest correlation to $\lambda_n(f_a)$. The tracked solution for the first 30 eigenvalues is shown in Fig. 4.4.

Eigenvector correlation based tracking is always superior to unconditioned and unsorted modes, as the eigenvector of each mode is, to some degree, related to the eigenvector at a subsequent frequency. However, as the eigenvectors are not mathematically orthogonal, this method does not resolve many of the outlined

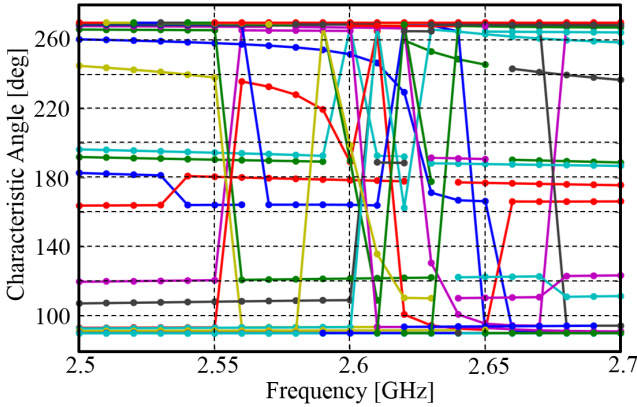


Figure 4.4: Characteristic angle of the first 30 modes of the two-part chassis tracked by eigenvector correlation.

tracking issues. Therefore, other tracking categories have been developed which rely on orthogonal CAs.

4.2 Weighted Current Correlation Tracking

Weighted current tracking is considered to be an exceptionally robust tracking method, when compared to the previously overviewed categories [74,110]. This is because the characteristic currents are perfectly orthogonal at any single frequency when properly weighted, according to the orthogonality relationships (2.56)-(2.58) as outlined in Section 2.3.1. Therefore, it would be reasonable to assume that the orthogonality relationship will be preserved to a large extent at a nearby frequency, since the impedance matrix is expected to vary only slightly between closely-spaced frequencies.

The weighted current correlation is determined using (4.2), where $\rho_{n,m}(f_a, f_b)$ is used to determine the correct reordering of the correlation matrix. If $\rho_{n,m}(f_a, f_b) \approx 1$ then the modes are highly correlated, but if $\rho_{n,m}(f_a, f_b)$ does not meet a predefined threshold the modes are not tracked to one another.

$$\rho_{n,m}(f_a, f_b) = \left\langle [J_m(f_b)], [R(f_a)] [J_n(f_a)] \right\rangle \quad (4.2)$$

The current vectors and the real impedance matrix in (4.2) are calculated when the TCM eigenvalue equation is solved. Therefore, most algorithms within this category are not significantly more computationally complex than eigenvector tracking. However, problems within this category often arise as weighted currents are only orthogonal at a single frequency, and often vary significantly across frequency. Therefore, this method requires the difference between f_a and f_b to remain small for it to work well.

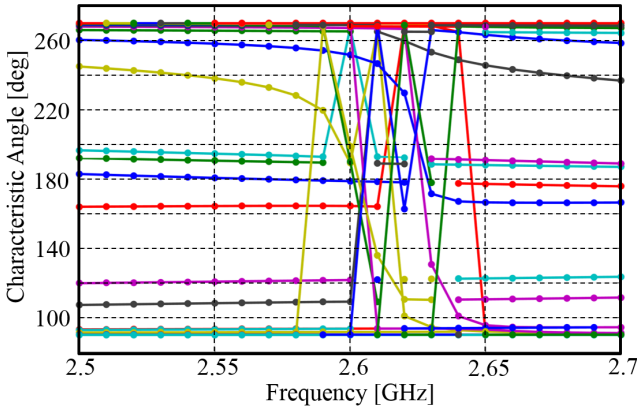


Figure 4.5: Characteristic angle of the first 30 modes of the two-part chassis tracked by weighted current correlation. ©2015 IEEE

In general, this method is extremely robust in electrically compact objects, or when an object maintains slowly varying characteristic currents. However, this category often fails in objects which have areas of high current density, intersecting resonant modes, anti-resonant modes, modes of high Q-factor, and degenerated modes. Although there are disadvantages, this category is superior to many others for most objects. The advantages of this method are obvious when it is used to track the modes of the two-part chassis shown in Fig. 4.2, with the results illustrated in Fig. 4.5.

4.3 Far-Field Correlation Tracking

Far-field correlation is able to track an object's CMs through analyzing the characteristic far-fields, rather than relying on any precomputed CAs. As outlined in Section 2.3.1, the characteristic electric (and magnetic) far-field patterns, are

mutually orthogonal to one another at a given frequency. This tracking method exploits an almost identical set of tracking concepts as are used in weighted current tracking, but far-field tracking has the distinct advantage of not relying on the discretization of the object. Although the variability in characteristic current distributions increases with structural complexity, these large variations in currents are often confined to only a few discretization (mesh) elements. However, these localized variations can significantly affect current-based tracking. On the other hand, far-field discretization is not done over the discretization elements, but rather post-processing of the characteristic currents is applied to determine the characteristic far-field at any defined point in space (Section 3.6). As each computed far-field point is composed of the radiation from every individual current element, small shifts between currents across frequency tend to be averaged out. Consequently, far-fields remain more orthogonal between frequencies and objects than current-based methods [111–113].

The first step in the algorithm for far-field tracking is to sort the eigenvalues in ascending order from the lowest to the highest $|\lambda_n|$. Second, the far-field patterns must be individually cross-correlated with the far-field patterns at subsequent frequency steps, using (4.3).

$$ECC_{n,m}(f_a, f_b) \approx \frac{\left| \oint_{4\pi} [E_{\phi,m}(f_b, \Omega) E_{\phi,n}^*(f_a, \Omega) + E_{\theta,m}(f_b, \Omega) E_{\theta,n}^*(f_a, \Omega)] d\Omega \right|^2}{\left| \oint_{4\pi} [E_{\phi,m}(f_b, \Omega) + E_{\theta,m}(f_b, \Omega)] \right| \left| \oint_{4\pi} [E_{\phi,n}(f_a, \Omega) + E_{\theta,n}(f_a, \Omega)] \right|} \quad (4.3)$$

In (4.3), $d\Omega = \sin(\theta)d\phi d\theta$, and $E_{\theta,m}(f_b, \Omega)$, $E_{\phi,m}(f_b, \Omega)$, $E_{\theta,n}(f_a, \Omega)$, $E_{\phi,n}(f_a, \Omega)$ are the θ - and ϕ - polarized electric far-fields of CMs n and m evaluated at frequencies f_a and f_b . Modes which are highly correlated have $ECC_{n,m}(f_a, f_b) \approx 1$, while uncorrelated modes have $ECC_{n,m}(f_a, f_b) \approx 0$. When $ECC_{n,m}(f_a, f_b)$ is larger than any other mode combination and meets a predetermined threshold criterion, the correlation matrix (linking matrix) is reordered to track those two modes across frequency.

The far-field patterns are not calculated in the process of solving the TCM eigenvalue equation. As such, this correlation method adds some computational complexity, beyond that of other tracking methods. The main advantage of this tracking category is due to the slow evolution of far-field patterns over frequency, when compared to the much faster localized evolution of characteristic currents.

This allows for larger frequency step sizes to be taken while reducing the tracking errors caused by current changes in localized mesh elements. Additionally, this method is able to average out the small variations caused by mirrored image currents of symmetric structures, and some intersecting resonant modes. These advantages are obvious when calculating the modes of the two-part chassis, as described by Fig. 4.6.

The far-field tracking category is fundamentally different from current based categories, and as such it is often able to produce fewer degenerated modes and mode swapping. However, far-field tracking requires that the fields be computed at a discretization that is much less than the 3dB beam-width of the pattern with the highest directivity, which can significantly increase the computational time. Additionally, problems can arise in a far-field tracking algorithm when the CMs contain anti-resonances, high Q-factors, and degenerated modes [111].

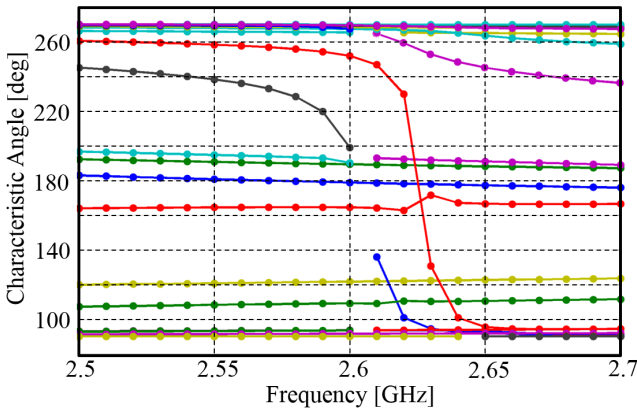


Figure 4.6: Characteristic angle of the first 30 modes of the two-part chassis tracked by far-field correlation. ©2015 IEEE

4.4 Hybrid Tracking

At the time of writing this thesis, there is no tracking category or algorithm that completely solves the CM tracking problem. However, recently many hybrid solutions have been developed which often significantly improve the CM tracking results. Many of these methods utilize image processing algorithms to effectively sort the eigenvalues, and this is then paired with one or more of the correlation

tracking types previously overviewed. Often, the threshold of $\rho_{n,m}(f_a, f_b)$ is significantly increased in hybrid algorithms in an effort to limit mode swapping. Using both image processing and the combined correlation results, the linking matrix is reordered to achieve better tracking results than using any individual method.

A nearly unlimited number of hybrid methods can be developed to aid in CM tracking. However, when a simple two-part hybrid solution, which consists of a bounded linear weighted current correlation function and the extrapolation of eigenvalues using Pearson's correlation function [107] is created; the results are superior to those of the original weighted current correlation tracking, as was presented in Section 4.2. This hybrid tracking solution for the two-part chassis example, is given in Fig. 4.7.

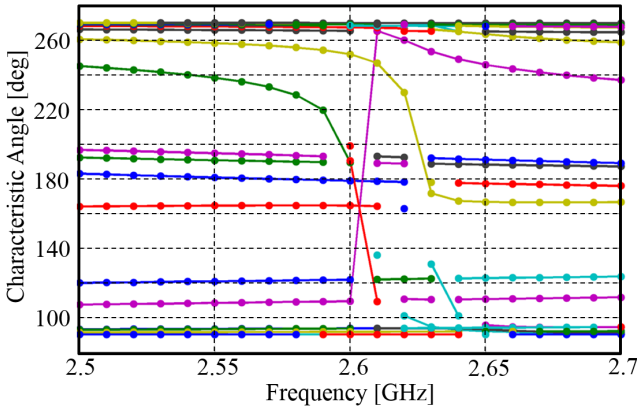


Figure 4.7: Characteristic angle of the first 30 modes of the two-part chassis tracked by weighted current correlation and Pearson's correlation function [107]. ©2015 IEEE

Chapter 5

TCM in Real Media

TCM in Real Media

IN [33] and [34], Harrington *et al.* proposed two methods for solving the Characteristic Modes (CMs) of objects consisting of real materials, which includes dielectric and magnetic materials as well as materials with losses. These methods are based on the eigenvalue decomposition of an object's Volume Integral Equation (VIE) [33] or Surface Integral Equation (SIE) [34] Method of Moments (MoM) impedance matrix. The mathematics of solving for the CMs of real objects using these impedance matrices was overviewed in Section 2.3.2 - 2.3.4. However, there are many problems associated with these methods, such as:

- Computational complexity of solving the VIE Theory of Characteristic Modes (TCM) eigenvalue problem
- Significant tetrahedral mesh density required for obtaining an accurate VIE TCM solution.
- Possible non-orthogonal characteristic far-fields when analyzing lossy structures using a VIE or SIE impedance matrix.
- Incorrect eigenvalues which may not be equal to the reactive power, for either a VIE or SIE TCM solution.
- Internal resonant modes found in SIE TCM solutions.

In this chapter, these problems will be further examined, and some existing solutions will be briefly overviewed. Furthermore, computational examples will be introduced to better explain the problems.

5.1 Analyzing VIE TCM Solutions

In [33], it was shown that the eigenvalue decomposition of a VIE MoM impedance matrix provides a complete set of CMs for an object composed of any real media. However, this method is rarely applied for a number of different reasons. Most often, it is avoided due to the computational complexity required to solve for the impedance matrix and the associated Sturm-Liouville problem.

However, as it is now possible (although not efficient) to solve for this impedance matrix and the TCM problem using modern computers, many other issues exist which deter the use of this method. The most prevailing issue is that the eigenvalues do not have a clear relationship with the object's reactive energy, as was detailed in Section 2.3.2. However, if the eigenvalues are not needed for the specific problem, another problem exists which contradicts the foundational mathematics of TCM, i.e. non-orthogonal characteristic far-fields exist in the CM solution of lossy objects.

5.1.1 Computational Limitations of VIE

Computing CMs using the VIE is computationally prohibitive due to the large number of basis functions required. The number of unknowns in this method are proportional to the square of that required for a well-conditioned SIE [90]. When applying the VIE impedance matrix to solve the CMs of an object, the total solution time increases relative to the cube of the computational time required for calculating the same object using an SIE formulation [114]. This increase in time is mainly due to matrix inversions which are required when solving for both the impedance matrix and the associated Sturm-Liouville problem.

To combat this significant increase in computational time, solutions are often critically under-meshed (e.g., sparse meshing was required in [115]). This reduces the total number of basis functions and allows for the CMs of electrically compact simple geometric objects to be solved on a high-end desktop computer. However, sparse meshing should be avoided as the accuracy of the VIE solution depends significantly on the quality of the tetrahedral mesh used. If the system is under-meshed, the solution accuracy degrades significantly. This type of inaccuracy produces surface singularities throughout the object [90], caused by large edge elements in the tetrahedral expansion functions. These surface singularities result in the impedance matrix overestimating the amount of stored energy within a given tetrahedron. This causes the calculated eigenvectors to be different from a correctly meshed solution. A sufficient tetrahedral density depends on the shape and material of the object, but the maximum edge length of a basis tetrahedron (of a dielectric object) can, to some degree, be estimated using (5.1) for VIE TCM problems [90, 91, 116].

$$l_n < \frac{(c/f_{max})}{10 \epsilon_r} \quad (5.1)$$

The effect of inaccuracies in poorly-meshed VIE objects can be observed through solving the CMs over a variety of different mesh densities. This is effectively demonstrated by solving for the CMs of a dielectric cube measuring $2.54\text{cm} \times 2.54\text{cm} \times 2.54\text{cm}$, made of a lossless dielectric with a relative permittivity of 9.4 ($\epsilon_r = 9.4$). The CMs of this object are solved over three different mesh densities consisting of 928, 1640, and 6256 basis elements (Fig. 5.1). As the number of mesh elements increase, the values converge in a nearly exponential fashion (by observation). These discrepancies are discernible in Fig. 5.1, where the maximum mesh density has an edge length approximately equal to the upper limit of (5.1) at $f = 2.5$ GHz.

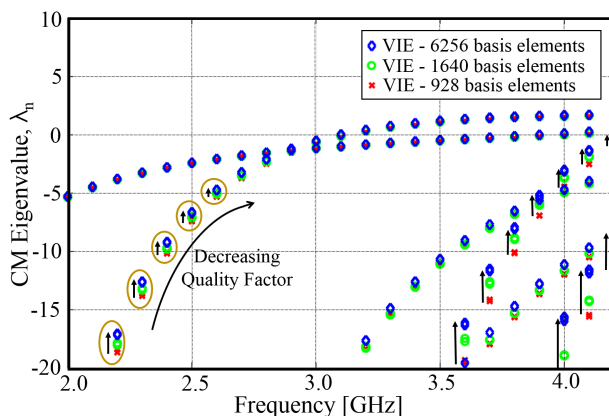


Figure 5.1: Eigenvalues of a dielectric cube with different mesh densities. ©2015 IEEE

5.1.2 Non-Orthogonal Far-Fields

Harrington *et al.* proved in [33] that, when losses are added to the VIE CM formulation, the scattering and perturbation matrices will not be perfectly diagonalized. If an eigenvalue decomposition is applied to a symmetric VIE impedance matrix, a set of characteristic currents with the orthogonal relationships of (2.49) - (2.54), will be computed, but the far-fields which are defined by those currents, will not correspond to an orthogonal set of far-field patterns.

As was detailed in Section 2.3.2, if TCM is applied to volumetric objects, the electric field must be represented as the sum of both an incident electric field (\mathbf{E}^i) on a volumetric element, as well as the scattered fields from other elements (\mathbf{E}^s). However, as the impedance operator (\mathbf{Z}) cannot be easily split into the two separate operators \mathbf{Z}_v and \mathbf{Z}_m , the VIE TCM equation must be defined by (2.74), and not by (2.73). This additional operator forces the TCM far-fields to no longer be directly related to the real part of Poynting's theorem, but rather equal to the real part of Poynting's theorem plus an unknown quantity. This quantity is equal to $\langle \mathbf{J}_m^*, \text{Re}(\mathbf{Z}_m) \mathbf{J}_n \rangle$, which disturbs the orthogonality between the characteristic far-fields. Furthermore, (2.64) shows that $\text{Re}(\mathbf{Z}_m)$ is related to the losses of the structure, and thus the offset from perfect far-field orthogonality will increase at a rate proportional to the currents and losses in each tetrahedral element. However, because \mathbf{Z}_m is not easily separable from the VIE impedance matrix, this quantity cannot be directly evaluated. It is possible to numerically solve for this quantity by determining the Envelope Correlation Coefficient (ECC) between all the characteristic far-field patterns for the object. However, as the characteristic currents are unique to the shape of an object, it is not possible to determine how much a known loss will affect this quantity across objects of different shapes.

To demonstrate these problems, the characteristic far-fields of two different objects were analyzed across different losses. The first object characterized is a dielectric sphere with a radius of 150 cm and a dielectric constant of $\epsilon_r = 10$. The characteristic far-fields were computed at 250 MHz. The second object is a dielectric cylinder with a radius of 135 cm, height of 300 cm, and a dielectric constant of $\epsilon_r = 10$. The characteristic far-fields of this object were computed at 350 MHz. Both objects have a complex natural resonance near their respective evaluation frequencies. The first twelve CMs of each structure were analyzed, across four different loss values, and the mode-to-mode far-field ECCs were computed. These results are displayed in Fig. 5.2.

These figures show that the modal correlation is zero for lossless objects, and as such $\langle \mathbf{J}_m^*, \text{Re}(\mathbf{Z}_m) \mathbf{J}_n \rangle$ must also equal zero. However, two problems exist when losses are introduced into the objects. The first problem is that objects of different shape, but with the same loss behave very differently, thus no generalization can be made. The second problem is that many modes are correlated. Additionally, as the loss of an object increases, the non-orthogonality in the characteristic far-fields becomes more apparent. These results demonstrate that lossy VIE objects do not

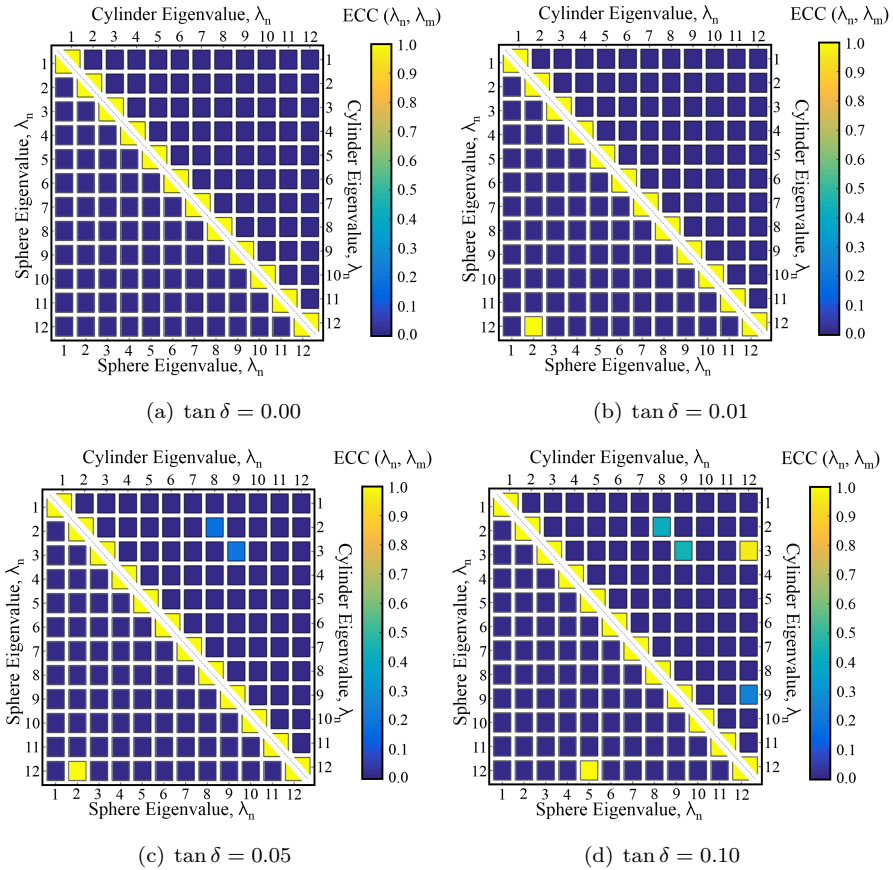


Figure 5.2: Far-field ECC of four different VIE objects, with different losses (a), (b), (c), and (d). The dielectric sphere is represented by the left-lower triangle in each plot, while the dielectric cylinder is represented by the right-upper triangle in each plot.

adhere to the TCM theoretical foundations, and as such VIE CMs should only be used in lossless objects where the correct eigenvalues are not required.

5.2 Analyzing SIE TCM Solutions

In [34], it was shown that the eigenvalue decomposition of an SIE MoM impedance matrix can be used to solve for the CMs of objects composed of real

materials. When compared to VIE methods, the SIE TCM solution is computationally efficient, and thus it is preferred when solving complex TCM problems. However, as was discovered in VIE TCM, an SIE eigenvalue decomposition also leads to some significant issues in the TCM solution [76, 117]. However, recently methods have been developed which solve many of the problems associated with some SIE TCM methods.

5.2.1 Problems with SIE TCM Solutions

As was overviewed in Section 2.3.3, the Poggio-Miller-Chang-Harrington-Wu-Tsai (PMCHWT) impedance matrix must be forced into symmetry, in order for it to be used in a Sturm-Liouville problem. However, when this is done the weighting factors of the SIEs (2.82) - (2.85) must be altered. The resulting impedance matrix is often referred to as the forced symmetric PMCHWT impedance matrix. However, the forced symmetry is problematic, since the weighting factors associated to (2.82) - (2.85) are no longer identical to the PMCHWT SIE weightings. Furthermore, as with the VIE solution, it can be shown that the eigenvalues of the forced-symmetric PMCHWT SIE TCM are not related to the reactive power of the object's characteristic currents.

Internal Resonances Due to Forced Symmetry

As previously overviewed, there are three main types of SIE formulations: Electric Field Integral Equation (EFIE), Magnetic Field Integral Equation (MFIE), and Combined Field Integral Equation (CFIE). The standard EFIE and MFIE suffer from what is known as the internal resonance problem [90]. The existence of these internal resonances can be easily understood in some cases (objects made of Perfect Electric Conductors (PEC) and Perfect Magnetic Conductors (PMC)), whereas it is less understood in other cases (dielectric and magnetic objects). For a closed PEC object, the internal resonances can be related to non-radiating resonant cavity modes. However, this is not as easily explained for dielectric objects, but can be proved, or observed, through different Gedanken experiments (thought experiments) [118]. These internal resonances can be eliminated through proper combination of the EFIE, MFIE, Electric Combined Integral Equation (ECIE), and Magnetic Combined Integral Equation (MCIE).

Equations (2.82) - (2.85) provide four equations and two unknowns. In order

to reduce the equation space so that there are the same number of equations as unknowns, the number must be reduced to two. This is done through a linear combination of these equations as shown by (5.2) and (5.3), where a_i , b_i , c_i , and d_i are the weighting coefficients within the full domain described by Fig. 2.2(a) [119].

$$\text{Combined Equation 1: } a_i ECIE + b_i EFIE \quad (5.2)$$

$$\text{Combined Equation 2: } c_i MCIE + d_i MFIE \quad (5.3)$$

There are several ways of combining (2.82) - (2.85) using (5.2) and (5.3) to obtain a unique solution free from internal resonances. A computationally efficient way is to use a linear combination which forces two of the integral equations to zero; this can be done by setting $a_i = c_i = 0$ or $b_i = d_i = 0$. The two most used SIE formulations utilize this method, and are referred to as the NMüller and PMCHWT MoM SIE formulations [90]. The NMüller formulation, the most popular variant of the Müller formulation, sets $a_i = \mu_i$ and $c_i = \epsilon_i$. The PMCHWT formulation is the most widely implemented SIE solution and sets $a_i = c_i = 0$ and $b_i = d_i = 1$. The method in which the weighting coefficients are chosen is important, as the choice of these weighting coefficients will determine if a solution is free from internal resonances. A simple method for determining if a particular solution is free of internal resonances can be found by calculating $a_i c_i^*$ and $b_i d_i^*$; if both these terms yield real and positive numbers, the solution is unique (i.e., free of the internal resonance problem). However, these expressions no longer result in a real number for the forced symmetric PMCHWT equation, described by (2.95). Therefore, the SIE TCM solution is not guaranteed to be free of internal resonances.

It was proven in [34] that the external resonant modes of an SIE TCM solution will form an orthogonal set of far-fields. However, as internal resonances do not radiate far-field energy, they are not required to be contained within this orthogonal set. Furthermore, as (2.95) is not guaranteed to be free from internal resonances, if any are found in a solved object using (2.95), this specific SIE solution can be determined as not being free from the internal resonance problem, i.e. through a Gedanken experiment. This theoretical concept can be confirmed by analyzing an object, and calculating the ECC between the individual characteristic far-fields. Furthermore, if any two CMs are not-orthogonal to one another (excluding rounding errors), and additionally one or more of these modes do not radiate unity far-field energy, each non-radiating mode must correspond to an internal resonance. For lossless objects, the internal resonances within the SIE

solution will not be present in the VIE solution. However, as the eigenvalues of both the VIE and SIE solutions do not directly reflect the reactive power, this comparison does not necessarily prove the existence of internal resonant modes, contradictory to [119].

If the CMs of the cube structure from Section 5.1.1 are computed using the impedance matrix as defined by (2.95), a set of orthogonal CMs would be expected. However, the computed far-field ECCs among these CMs indicate that some modes are significantly correlated with each other. This is not the case with the characteristic weighted currents, as these remain orthogonal in the sense of (2.49) due to them being solved directly by the Sturm-Liouville problem. Furthermore, when the characteristic far-fields, ECC are computed for the VIE CMs, no correlated modes can be found. These characteristic far-field ECC results for the two different methods are depicted by Fig. 5.3. Moreover, the number of low valued eigenvalues in the SIE solution significantly outnumbers those in the VIE solution (Fig. 5.4).

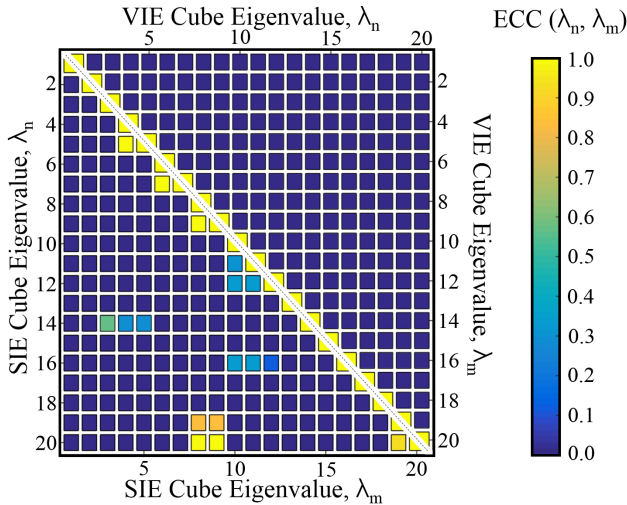


Figure 5.3: ECC of characteristic far-fields obtained from the VIE and forced symmetric PMCHWT SIE solutions for a lossless dielectric cube of dimensions $2.54\text{cm} \times 2.54\text{cm} \times 2.54\text{cm}$ and relative permittivity of 9.4.

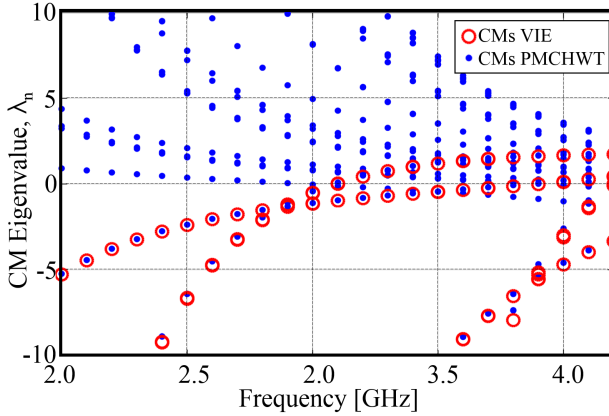


Figure 5.4: Eigenvalues of the VIE TCM and the forced symmetric PMCHWT SIE TCM for a lossless dielectric cube of dimensions $2.54\text{cm} \times 2.54\text{cm} \times 2.54\text{cm}$ and relative permittivity of 9.4.

Eigenvalue's Relationship to Poynting's Theorem

In [33] it was proved that the eigenvalues of a VIE impedance matrix do not directly correspond to the reactive power of the solved object. Additionally, a similar problem can be found with the eigenvalues' relationship to an object's reactive power in SIE problems, but this was not conveyed in the original SIE TCM proof [34]. In SIE MoM formulations which solve for the CMs of objects consisting of complex media, the Sturm-Liouville theorem states that the inner product must be orthonormal with respect to the weighting vector (Section 2.3.1). As was overviewed in Section 2.1.2, this orthonormal relationship can be used to relate the real part of the SIE TCM solution to the radiated and dissipated power as described by the Poynting's theorem derivation. Although this remains true for SIE formulations, the imaginary part of Poynting's theorem can no longer be related to the imaginary part of the TCM solution (the eigenvalue). This can be proven by applying the second sub-theorem of the Sturm-Liouville problem to Poynting's theorem. This sub-theorem states that the eigenvector solution must be composed of only real values, i.e., the characteristic currents must be real. Using (2.95) as the SIE formulation for TCM, the electric currents (\mathbf{J}) for this specific formulation must be real, whereas the magnetic currents (\mathbf{M}) must be imaginary, as indicated in Poynting's theorem given by (5.4). Equation (5.4) can be expanded into its real and imaginary parts as described in (5.5), where $(\cdot)_R$ indicates real-valued variables, and $(\cdot)_I$ indicates imaginary-valued variables. This specific form of Poynting's theorem can be split up into its real and imaginary components

which can be associated to the radiated / dissipated and reactive power (5.6).

$$P_s = \iint_S \left(\underbrace{\mathbf{J}^*}_{\text{Im}\{\}=0} \cdot \mathbf{E} + \underbrace{\mathbf{M}}_{\text{Re}\{\}=0} \cdot \mathbf{H}^* \right) dS \quad (5.4)$$

$$P_s = \iint_S \left(\mathbf{J}_R \cdot (\mathbf{E}_R + j\mathbf{E}_I) + (-j\mathbf{M}_I) \cdot (\mathbf{H}_I + j\mathbf{H}_R) \right) dS \quad (5.5)$$

$$P_s = \underbrace{\iint_S (\mathbf{J}_R \cdot \mathbf{E}_R + \mathbf{M}_I \cdot \mathbf{H}_I) dS}_{P_e + \bar{P}_d} + j \underbrace{\iint_S (\mathbf{J}_R \cdot \mathbf{E}_I + \mathbf{M}_I \cdot \mathbf{H}_R) dS}_{\Delta P_{\text{stored}} = 2\omega(\bar{W}_m - \bar{W}_e)} \quad (5.6)$$

Using the original TCM (Section 2.3.1), it is possible to link Poynting's theorem, as described by (5.6), to the SIE TCM solution using the Sturm-Liouville relationships (2.54). When this is applied to the SIE solution, which requires the use of magnetic currents, the Sturm-Liouville relationship is defined by (5.7). When the right hand side of (5.7) is expanded into its real and imaginary components (5.8), it can be seen that the real part of (5.9) is equivalent to the real part of Poynting's theorem, whereas the imaginary part is no longer equivalent. Therefore, the SIE TCM derived eigenvalues are not directly related to the reactive power, and as such cannot be used to directly obtain information pertaining to an object's stored energy, or resonance behavior.

$$\left\langle [\mathbf{J}_n, \mathbf{M}_n]^*, \mathbf{Z}[\mathbf{J}_n, \mathbf{M}_n] \right\rangle = \iint_S \left(\underbrace{\mathbf{J}_n^*}_{\text{Im}\{\}=0} \cdot \mathbf{E}_n + \underbrace{\mathbf{M}_n^*}_{\text{Re}\{\}=0} \cdot \mathbf{H}_n \right) dS \quad (5.7)$$

$$P_s \neq \iint_S \left(\mathbf{J}_{n,R} \cdot (\mathbf{E}_{n,R} + j\mathbf{E}_{n,I}) + (-j\mathbf{M}_{n,I}) \cdot (\mathbf{H}_{n,R} + j\mathbf{H}_{n,I}) \right) dS \quad (5.8)$$

$$P_s \neq \underbrace{\iint_S (\mathbf{J}_{n,R} \cdot \mathbf{E}_{n,R} + \mathbf{M}_{n,I} \cdot \mathbf{H}_{n,I}) dS}_{P_e + \bar{P}_d} + j \underbrace{\iint_S (\mathbf{J}_{n,R} \cdot \mathbf{E}_{n,I} + \mathbf{M}_{n,I} \cdot \mathbf{H}_{n,R}) dS}_{\text{Unknown}} \quad (5.9)$$

5.2.2 Removal of SIE TCM Internal Resonances

Solutions to many of the problems related to SIE TCM can be solved using the unique properties of TCM. Unlike other MoM solutions, TCM is able to pro-

vide an independent solution to each current an object is capable of supporting (both internal and external currents). As these different currents are separated in the TCM solution, if the internal resonant modes can be identified, they can be removed. Furthermore, it can be argued that as internal resonances should radiate no far-field power, if the total far-field power is calculated for each characteristic current (Section 3.6), the modes which radiate no far-field power can be attributed to internal resonant modes, and removed [76]. However, due to the use of approximate expansion functions and characteristic current normalization, the radiated power of internal resonances can be greater than zero. Furthermore, when losses are included in the SIE solution, through the introduction of complex permeability and permittivity, some external resonances will radiate less power than some normalized internal resonances.

Another simple, and intuitive, solution for removing these internal resonances is through the use of a MoM mesh perturbation, thus altering the individual basis functions [120]. When the MoM mesh is varied, the expansion functions must also change. This will relate to a change in the amount of far-field power radiated by the internal resonant modes. If the same mode under two different mesh perturbations radiate different amounts of far-field power, the mode can be associated with an internal resonance. However, it is not yet understood how much the mesh should be perturbed to guarantee that every internal resonant mode provides significant enough radiated power difference to be detected and identified.

A more robust solution for determining which CMs correspond to internal resonant modes of an object containing lossy real media is to define the maximum amount of loss which a mode can incur [119]. This maximum loss can be calculated through determining the Quality Factor (Q-factor) associated to individual CMs, and utilizing the information to bound the object's losses. The Q-factor relates the energy stored by an object to the power loss of that object, which can be used to lower bound the radiation efficiency [121, 122]. This theoretical concept can be applied to the CMs of an object. Any CMs found with a radiation efficiency (calculated from the characteristic far-field pattern) less than the lower radiation efficiency bound of that mode can be associated to an internal resonance. This concept can be applied through calculating the minimum efficiency of a mode using (5.10) - (5.14) [122–124]. In these equations, $(\cdot)_{tot}$, $(\cdot)_{rad}$, $(\cdot)_{sw}$, $(\cdot)_d$, and $(\cdot)_c$ are, respectively, the quality factors and radiated power associated with the total structure, radiation, surface wave, dielectric, and conductor.

$$\frac{1}{Q_{tot}} = \frac{1}{Q_{rad}} + \frac{1}{Q_{sw}} + \frac{1}{Q_d} + \frac{1}{Q_c} \quad (5.10)$$

$$\eta_{tot} = \frac{P_{rad}}{P_{rad} + P_c + \bar{P}_d + P_{sw}} \quad (5.11)$$

$$\eta_{rad} \geq \frac{Q_{com}}{Q_{com} + Q_{rad}} \quad (5.12)$$

$$Q_{com} = Q_{sw} + Q_d + Q_c \quad (5.13)$$

$$\frac{1}{Q_d} = \tan \delta_d + \tan \delta_m = \frac{\epsilon''}{\epsilon'} + \frac{\mu''}{\mu'} \quad (5.14)$$

Using (5.12) and the associated Q-factors, computed using (3.17) for Q_{rad} and (5.14) for Q_d (in most objects Q_c and Q_{sw} can be neglected [119]), it is possible to determine if a mode is related to an internal or external resonance. The modes which do not adhere to (5.12) can be associated to internal resonances, whereas all other modes can be associated to external resonances. This method is referred to as the physical bounds method [119], and it can be applied to SIE TCM solutions to remove internal resonances. However, the physical bounds method is not perfect; this is due, in part, to the required Q-factor calculation. Calculating the Q-factor of a set of SIE currents is not fully characterized, and as such the Q-factor may not correctly compute the stored energy of the object [80, 125]. Furthermore, as the SIE TCM eigenvalue is not related to the stored energy, in its current form it cannot be used to calculate the Q-factor. Even though this problem exists, the physical bounds method is the most robust of the three internal resonance removal methods overviewed in this subsection.

5.2.3 Deriving the Correct TCM Eigenvalue

As stated in Section 3.1, TCM eigenvalues are one of the most important Characteristic Attributes (CAs), and in many circumstances the eigenvalues are critical for a principal understanding of an object. However, this fundamental TCM quantity is not valid for objects solved using an SIE MoM impedance matrix (Section 5.2.1). However, through the relationship between the real and imaginary parts of the simplified version of Poynting's theorem (5.6), the valid SIE TCM eigenvalues

can be derived. This is possible as the eigenvalues are defined as the difference in the time rate of change of the stored magnetic and electric energy quantities, divided by the sum of radiated and dissipated powers. This eigenvalue solution is described for PEC objects by (2.59). Using this information, the eigenvalues can be derived from Poynting's theorem in (2.59) for PEC problems where no magnetic currents exist; additionally, this can be applied to TCM problems which require magnetic currents. Using these insights, (5.15) and (5.16) can be used to determine the correct eigenvalues for symmetric and forced-symmetric MoM impedance matrices, respectively.

$$\lambda_{n,M_R}^{PEC} = \frac{\iint_S (\mathbf{J}_{n,R} \cdot \mathbf{E}_{n,I} - \mathbf{M}_{n,R} \cdot \mathbf{H}_{n,I}) dS}{\iint_S (\mathbf{J}_{n,R} \cdot \mathbf{E}_{n,R} - \mathbf{M}_{n,R} \cdot \mathbf{H}_{n,R}) dS} = \frac{2\omega (\bar{W}_m - \bar{W}_e)}{P_{rad} + \bar{P}_d} \quad (5.15)$$

$$\lambda_{n,M_I}^{PEC} = \frac{\iint_S (\mathbf{J}_{n,R} \cdot \mathbf{E}_{n,I} + \mathbf{M}_{n,I} \cdot \mathbf{H}_{n,R}) dS}{\iint_S (\mathbf{J}_{n,R} \cdot \mathbf{E}_{n,R} + \mathbf{M}_{n,I} \cdot \mathbf{H}_{n,I}) dS} = \frac{2\omega (\bar{W}_m - \bar{W}_e)}{P_{rad} + \bar{P}_d} \quad (5.16)$$

Equations (5.15) and (5.16) are equivalent to the PEC definition of the eigenvalue, as described by Harrington *et al.* in [4]. Additionally, these eigenvalues can be used to determine modal resonances as well as the Q-factor of real objects.

Chapter 6

Correlation Based TCM Antenna Design

Systematic TCM Antenna Design

THE Theory of Characteristic Modes (TCM) is different from other computational electromagnetic methods. Finite-Difference Time-Domain (FDTD) [126], Finite Element Method (FEM) [127], and traditional Method of Moments (MoM) [86] solvers require a predefined excitation to simulate the electromagnetic properties of an object; this is not required when analyzing an object using TCM [23]. When TCM analysis is used to develop an integrated antenna, it is not burdened by the need for an optimized excitation as is the case with classical methods. For this reason, TCM analysis methods can effectively quantify an object's electromagnetic properties, and using the insights gained, the object can be adapted to meet a set of radiation requirements.

Typically, when an engineer designs an antenna, the antenna must be enclosed within, mounted on, or developed around a preexisting object. In this type of design, the object's electromagnetic properties will greatly affect the final antenna structure. As such, the electromagnetic characteristics of the object should be fully understood before the implementation of excitation elements. However, this is not often done in practice. For example, the design of a mobile phone typically starts with a general size or outline, and components are then added (screens, batteries, microphones, etc.). Finally, the antenna structures are implemented without taking into account the electromagnetic properties of the object (e.g., the components in the mobile phone). This same development procedure is often applied to cars, ships, planes, and many other objects. The problem with this approach is that once an object is built, it is difficult to determine the best way to adapt it to meet a set of antenna related goals. Unlike other electromagnetic solvers, TCM can be utilized to understand the radiation properties of an object before, during, or after any geometrical or material alterations are made. As such, extensive antenna optimization and semi-random excitation placement is not required. Instead, the insights gained from TCM analysis provide an engineer with the knowledge necessary to correctly optimize an object before implementing the excitation for each antenna.

6.1 Characteristic Attribute Analysis

The first step in understanding the radiation properties of an object is to calculate and analyze the Characteristic Mode (CM) eigenvalues. If the required number of modes are resonant in the band of interest (as defined by the eigenvalues' zero crossings), the maximum obtainable bandwidth of each mode should be calculated. However, if the required number of modes is not met, additional non-resonant modes should be analyzed. Traditionally, these modes are difficult to directly analyze (Section 3.5), but it is possible to determine the Quality Factor (Q-factor) and modal bandwidth using (3.17). Through the use of this equation, it is computationally possible to determine the maximum obtainable bandwidth for a given reflection coefficient (Γ) [102] of a CM. If the required bandwidth is not met by any single CM, this means that the structure may not support the intended application or multiple mode excitations may be required. However, if any near-resonant mode (e.g., $|\lambda| < 15$) supports the requirements, the resonant properties of that mode should be further analyzed to determine if the structure can be optimized to force that mode into resonance.

Understanding the mechanics of forcing a CM into resonance is only possible if insights beyond those provided by the characteristic eigenvalue or modal Q-factor are obtained. There are several methods of utilizing Characteristic Attributes (CAs) to determine what acceptable structural modifications will force a CM into resonance, with some being less trivial than others [128, 129]. One of the most intuitive methods of understanding an object's CMs is to link a CM to a well-understood antenna. This can be accomplished through identifying a CM's far-field pattern and correlating this pattern to a set of known fundamental sources (antennas) with orthogonal far-fields. When these fundamental source far-fields are used to describe a characteristic far-field, the relationship a specific CM has to a fundamental source can be used to better understand the object. This can be accomplished through discretization of the far-field patterns for both the fundamental source and the CM. These discretized far-fields can then be correlated against one another using (6.1), providing the percentage contribution each fundamental source has to the CM's radiated far-field (using the same method as [65], although in [65] the intention is to decompose an antenna's far-field into orthogonal characteristic far-fields).

$$ECC_{n,a} \approx \frac{\left| \oint_{4\pi} [E_{\phi,n}(\Omega)E_{\phi,a}^*(\Omega) + E_{\theta,n}(\Omega)E_{\theta,a}^*(\Omega)] d\Omega \right|^2}{\left| \oint_{4\pi} [E_{\phi,n}(\Omega) + E_{\theta,n}(\Omega)] d\Omega \right| \left| \oint_{4\pi} [E_{\phi,a}(\Omega) + E_{\theta,a}(\Omega)] d\Omega \right|} \quad (6.1)$$

In (6.1), $(\cdot)_a$ corresponds to the fundamental source pattern, and $(\cdot)_n$ corresponds to the CM of interest. This equation is best applied using closed-form orthogonal fundamental sources, namely, x , y , and z oriented dipole and loop elements across multiple resonances ($\lambda/2$, λ , $3\lambda/2$, etc.). Once a specific CM is broken down into its fundamental source types, generalized antenna theory can be effectively applied, and the insights gained can be used to optimize the object's currents, forcing a mode into resonance.

This method of forcing a mode into resonance, with the help of expressing the mode in terms of fundamental sources, can be effectively demonstrated through analyzing the fundamental mode (λ_1) of a thin wire with an electrical length of $\approx \lambda/4$. This object's CMs are described in Fig. 3.1, where λ_1 is not near a resonance point at this electrical length. When this $\lambda/4$ thin wire object is broken down into its fundamental source elements, it can be found that the radiated field matches that of a fundamental dipole element with a correlation of 0.98 (i.e., 98% similarity to the object's fundamental mode λ_1). As a dipole is a well-known antenna element, antenna theory defines how the currents should behave for this structure to support the calculated far-field pattern. Additionally, it is well understood that a small dipole can be forced into resonance through capacitively loading the ends of the dipole, or adding series inductance to the areas of high current density [97]. Therefore, the resonant frequency of this mode can be reduced through the addition of parallel capacitance or series inductance to the object.

This method requires an elevated understanding of basic antenna theory, and how to adapt these fundamental antenna types. However, with this knowledge, most CMs can be better understood. This approach to understanding a specific object's CMs works best for small objects. This is because, as the electrical size of the object becomes large, the number and types of source elements required to decompose the object will rapidly increase and array elements may be required, thus complicating the analysis. If the required number of CMs can be optimized for a given application over a specific frequency range, the bandwidth as defined by

the Q-factor of the CMs should be re-calculated. If the maximum obtainable modal bandwidth is lower than the required bandwidth for a specified application, the CM may need to be adjusted or should not be used for the application. However, if the mode is capable of supporting the required bandwidth, or multiple mode excitation can be implemented, then proper excitation of the CM must be determined.

6.2 CM Excitation Analysis and Optimization

In traditional antenna design, excitation types and positions are found through visual analysis of excited currents of similar antennas, or by means of trial-and-error excitation placement. However, as the currents are predefined prior to source excitation in Characteristic Mode Analysis (CMA), the placement and type of excitation can be determined through either visual analysis of the individual CAs [129], or through computational analysis of various CAs (i.e. characteristic currents, near-fields and far-fields). Visual analysis is simple and effective for most applications, and is widely utilized for single-mode excitation characterization. However, to achieve a full understanding into region-specific differences, a computational method should be implemented, which also allows for multi-mode excitation analysis.

6.2.1 Visual Analysis

Visual analysis is quick, intuitive, and can be used to design excitation structures for most applications. Multiple CAs can be used to visually determine the most effective type of excitation. For simple single-purpose antenna systems, current feed implementations are often applied, as regions of high current density can be exploited to excite an object. This is often implemented through introducing a discontinuity (e.g. a slot) in the region of high current density, and inserting an excitation source (often a voltage source) across the discontinuity. For example, at resonance, the fundamental mode (λ_1) of a thin Two-Dimensional (2-D) wire object has high currents in the middle of the wire, as shown by Fig. 3.3. If a discontinuity is introduced in the middle of the wire, and a voltage source is placed at this location, a dipole antenna is created. However, many integrated objects do not allow for such discontinuities due to application requirements. Additionally, some objects have areas of high current where it is not possible to introduce a

discontinuity. In these types of objects and applications, the characteristic near-fields can be exploited to determine if a Capacitive Coupling Element (CCE) or Inductive Coupling Element (ICE) can be implemented to excite the structure. The magnetic and electric near-fields provide the x , y , and z spatial components of the electric or magnetic fields at any point in space outside the structure (Section 3.6). These fields can be used to determine the location and type of Coupling Element (CE) which will effectively excite the structure. In areas of high electric (magnetic) field density a CCE (ICE) can be used to excite the structure. When the CE method of object excitation is applied to the fundamental mode (λ_1) of the thin wire object, a CCE can be used to excite the structure if it is placed at either end of the object where high fields exist (Fig. 3.10). However, in general, it is not easy to determine near-field excitation through visual analysis, examples include: single-mode excitation with limited to no coupling into other CMs, multi-mode excitation for extended bandwidth, and single excitation of multiple resonances. As such, computational tools exist which can be applied to determine a feasible excitation for a specific application.

6.2.2 Computation of CM Interdependence

The ability to uniquely excite a single CM, or a specific set of CMs, is important in many applications. Single-mode excitation is a sufficient requirement to maintain far-field orthogonality relationships, which is vital for many applications, including Multiple-Input Multiple-Output (MIMO). If more than one CM is excited the orthogonality between different excitations is no longer guaranteed. In order to excite one mode without coupling into another, the location where a voltage source or CE should be placed can be determined through the analysis of different CAs. CM interdependence calculates the dependencies between two different characteristic currents or near-fields over a surface (region) of interest [130]. In the case of characteristic near-fields, the CM interdependence matrix for a given component (x , y , or z) is defined by (6.2).

$$[\mathbb{I}_r] = \left(\left| \frac{[F_m]}{\max (|[F_{x,m}]|, |[F_{y,m}]|, |[F_{z,m}]|)} \right| \circ \left| \frac{[F_n]}{\max (|[F_{x,n}]|, |[F_{y,n}]|, |[F_{z,n}]|)} \right| \right)^{\frac{1}{2}} \quad (6.2)$$

In (6.2), F_m and F_n are the CA matrices of the CMs m and n for the given component over the surface being analyzed, and normalized by the maximum near-

field value over the surface and over all components (x , y , and z), and (\circ) is the Hadamard product. The CM interdependence of the characteristic current can be defined as in (6.2), with the exception that the normalization is performed with respect to the maximum current over the surface (i.e., only one current component exists). If the interdependence of two CMs at the same frequency ($f_1 = f_2$) are calculated, the dependence of the currents or near-fields is obtained. For example, the λ_1 and λ_2 of the thin wire object have current distributions matching those of a half-wave dipole and a full-wave dipole, respectively. When the interdependence of these two CMs is calculated, there is significant dependence in the areas around a quarter of the length from each end of the wire, corresponding to the high current areas of a full wave dipole (Fig. 6.1(a)). On the other hand, the interdependence of the electric fields of these first two modes (Fig. 6.1(b)) shows that the dependence is maximum at the two edges of the thin wire. It should be noted that the CM interdependence concept can be extended to more than two modes, by adding to (6.1) more terms relating to additional CMs.

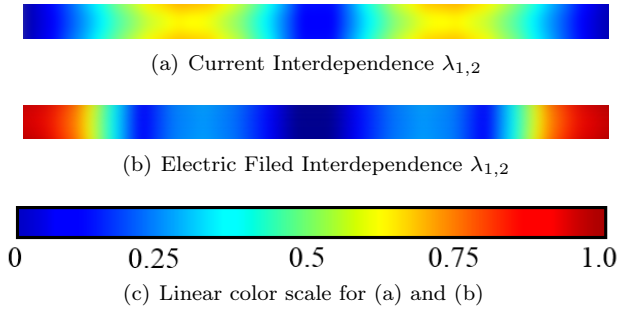


Figure 6.1: Calculated interdependence of the 2-D thin wire object for the length corresponding to the resonance of λ_1 and width of $\lambda/50$. (a) λ_1 current to λ_2 current interdependence, (b) λ_1 electric near-field to λ_2 electric near-field interdependence. The thin wire sizes are skewed for visualization purposes.

6.2.3 Point Excitation Analysis

The interdependence information can be used to determine which excitation locations can be exploited to excite a single CM. Mathematically, this can be determined in many ways, but the simplest version is through defining a thresholding inverse function (using an if-else statement) applied to the interdependence of the CM to be excited. This analysis will provide the optimal locations for placing a

single-source. In equation form, the matrix function providing the optimal source locations to excite mode n is described by (6.3).

$$[\perp_{F,n}] = \left(\left(\left[\text{if } ([\perp_r] > \beta, [\perp_r] = 0), \text{else } ([\perp_r] = 1) \right] \right) \circ \left| \frac{[F]_n}{\max(|[F]_{x,n}|, |[F]_{y,n}|, |[F]_{z,n}|)} \right| \right) \quad (6.3)$$

To excite one mode with zero coupling into another, β should be equal to zero. However, it has been found through experimentation, that any $\beta < 0.15$ yields low enough coupling for most practical purposes. When (6.3) is used to compare λ_1 to the interdependence of $\lambda_{1,2}$ for the thin wire object, a potential voltage excitation placement can be found in the center of the thin wire, where the half wave dipole mode (λ_1) has the highest currents, and the full-wave dipole (λ_2) has zero current. If an excitation source is placed at this location, as described by the center of Fig. 6.2(a), λ_2 will not be excited. If only specific bandwidths must maintain low coupling to another CM, the Modal Significance (MS) can be used to weight this equation. When the reverse comparison is applied (excitation of λ_2 without exciting λ_1), there is no single excitation location which can solve this problem, as illustrated in Fig. 6.2(b). However, this equation can be further extended through the use of near-field phase information, and applied to provide possible locations which can be used to excite modes using two separate excitation points. For example, it is possible to excite λ_2 of the thin wire without exciting λ_1 , through the placement of two excitation sources with a 180° phase difference at two locations a quarter of the length from each end of the wire.

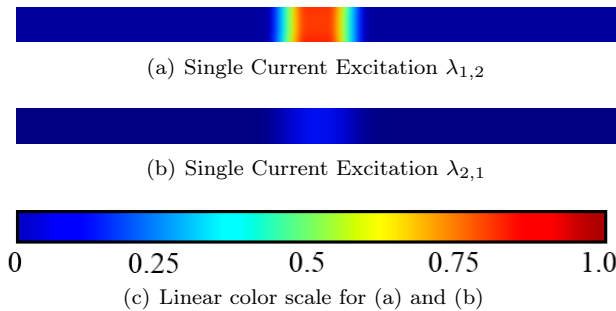


Figure 6.2: Visualization of possible excitation location(s) based on (6.3) for single-mode excitation for: (a) excitation of λ_1 , (b) excitation of λ_2 .

It is often necessary to excite multiple CMs either to extend an object's bandwidth, or to allow the object to obtain a multi-resonant behavior. In these cases, the previously described excitation analysis cannot be directly applied. However, (6.2) can be applied to two different modes at two separate frequencies. When this is effectively applied, locations of large $\perp\!\!\!\perp_r$ describe which modes (at two frequencies) have common high current or field densities. These specific locations can be exploited to allow for a single excitation source to excite multiple CMs at separate frequencies.

6.2.4 CM Regional Frequency Evolution

In their basic forms, visual and computational based excitation analysis only apply to the specific frequency for which the CMs were calculated. However, as Chapter 4 overviewed, characteristic currents, near-fields, and far-fields constantly evolve over frequency, and thus the performance of a chosen excitation type and location will be influenced due to CA variation over frequency. Therefore, it is often necessary to determine how the effect of an excitation will change over the bandwidth to which it will be applied. To achieve a more complete understanding into region-specific differences of an object's CAs over frequency, an analysis technique was developed to effectively quantify the frequency evolution of region-specific changes in the CAs [130]. This is referred to as CM regional frequency evolution, and it mathematically describes the locations where two CAs differ from one another, as defined by the matrix quantity in (6.4).

$$[F_\alpha] = \left| \frac{[F_n(f_1)]}{\max\left(\left[|[F_{x,n}(f_1)]|, |[F_{y,n}(f_1)]|, |[F_{z,n}(f_1)]|\right]\right)} - \frac{[F_n(f_2)]}{\max\left(\left[|[F_{x,n}(f_2)]|, |[F_{y,n}(f_2)]|, |[F_{z,n}(f_2)]|\right]\right)} \right| \quad (6.4)$$

When (6.4) was used to compare the CMs of the thin wire object, relatively little changes were found in any single CM across its usable bandwidth (e.g., as defined by the modal bandwidth). This is in part due to the small bandwidth which this object's CMs are able to support. However, if the CMs of an object have wider bandwidths, the frequency evolution often becomes more relevant. For

example, if a bow-tie type object's CMs are computed across the full bandwidth of the fundamental resonance, the advantages of (6.4) become apparent. The bow-tie object is made of Perfect Electric Conductors (PEC), and its dimensions are $100 \text{ mm} \times 40 \text{ mm}$. The characteristic currents for the fundamental mode at resonance are illustrated in Fig. 6.3 (a). The electric near-fields at the lower and upper edges of the modal bandwidth as calculated by the MS Q-factor are presented in Fig. 6.3 (b) and (c). If (6.4) is applied to this object's near-fields (at 10mm above the bow-tie) and currents, the near-fields change significantly (Fig. 6.3 (d)), whereas the location of maximum currents do not change. This indicates that the object can be more effectively excited across the entire modal bandwidth if it is fed using a voltage source rather than a CCE.

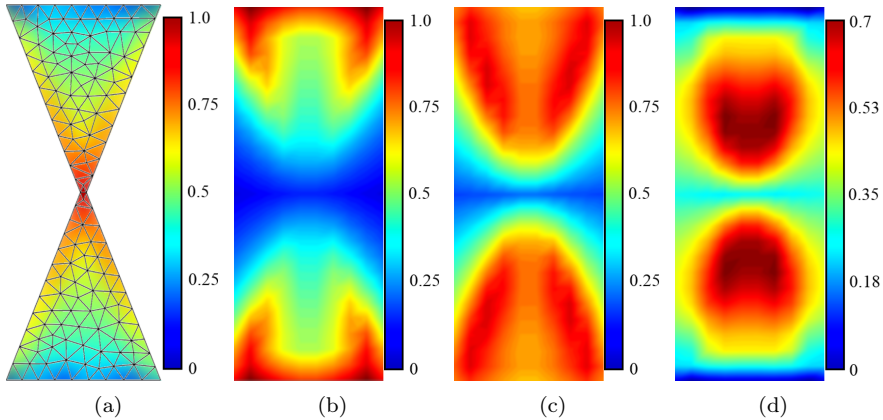


Figure 6.3: (a) Currents and structure mesh, (b) near-fields of the lowest bandwidth frequency, (c) near-fields of the highest bandwidth frequency, and (d) the calculated near-field CM frequency evolution between the two separate near-fields, for the fundamental mode λ_1 .

Chapter 7

Contributions, Conclusions,
and Future Work

Contributions, Conclusions, and Future Work

DURING the time period of this doctoral research, over twenty new works were published in the field of Characteristic Modes. Some of the main contributions from these publications will be overviewed in this chapter. The six papers included in this thesis (found in Part II) will be summarized, and my contributions to these works will be detailed. Additionally, a carefully selected set of non-included publications will be outlined in this chapter. The non-included papers were selected from those considered as they are significant to both the field and this thesis. Furthermore, an overall conclusion and a discussion on the possible direction and future work in the area of Characteristic Modes (CMs) will be provided.

7.1 Overview of Included Papers

The included papers in this thesis were chosen as they represent the doctoral work's most significant contributions. In addition, the publications complement the thesis structure by providing further insights, and additional theoretical concepts.

7.1.1 Paper I: Wide Band Characteristic Mode Tracking Utilizing Far-Field Patterns

I (Zachary Thomas Miers) was the main contributing author, and the lead researcher for the entirety of this scientific work. I was the main researcher involved in all parts of the scientific process, including but not limited to: implementation of all analysis codes (Matlab, C, and Python), numerical analysis, figure creation, as well as the manuscript writing. This manuscript was edited by both Buon Kiong Lau and myself.

In this letter, a method for tracking the CMs of complex objects through

characteristic far-field pattern analysis is presented. As overviewed in Chapter 4, the tracking of characteristic modes over frequency remains a challenge, especially for materials containing both perfect electric conductors and dielectrics. This work provides a new approach to tracking characteristic modes by means of cross-correlating far-field patterns, this method effectively eliminates many of the mode mapping ambiguities found in other CM tracking algorithms. In this context, the significant contributions of this work are:

- The first research publication providing a CM tracking solution which is based on characteristic far-field patterns.
- The first analysis of CMs with anti-resonances, and how these unique modes effect CM tracking algorithms.
- The first tracking algorithm which helps to prevent mode swapping and false mode detection.
- The first study into the effect that mirrored currents of symmetric structures have on CM tracking.

7.1.2 Paper II: Computational Analysis and Verifications of Characteristic Modes in Real Materials

I (Zachary Thomas Miers) was the main contributing author, and the lead researcher for the entirety of this scientific work. I was the main researcher involved in all parts of the scientific process, including but not limited to: implementation of all analysis codes (Matlab, C, and Python), numerical analysis, prototype creation, measurements, figure creation, as well as manuscript writing. This manuscript was edited by both Buon Kiong Lau and myself.

This transaction proposes a new and practical post-processing method that yields the correct CMs in real materials. This paper utilizes the Poggio-Miller-Chang-Harrington-Wu-Tsai (PMCHWT) Surface Integral Equation (SIE) formulation of Method of Moments (MoM) to analyze an object, showing that when this solution is forced into symmetry, the CM solution is susceptible to the MoM internal resonance problem. Furthermore, this transaction provides a proof that the internal resonances do not correspond to radiating structural resonances, and can be found in any object which uses the forced symmetric PMCHWT formulation. Additionally, a radiation efficiency threshold derived from the object's physical bounds was used to isolate the internal resonances in the CM solution. In an

effort to demonstrate the effectiveness of this method, the SIE CMs of different homogeneous dielectric and magnetic composite objects were compared against the Volume Integral Equation (VIE) CMs for these same objects. The results show that the proposed method correctly removes all the internal resonances. The main contributions of this work are:

- An explanation of the appearance of internal resonant modes when the CMs of an object are computed by means of the forced symmetric PMCHWT SIE MoM formulation.
- An effective method for isolating and removing the non-real CMs of an object that are found using a MoM SIE formulation.
- CMs are verified to be real through multiple means: VIE formulation, full-wave time-domain analysis, and measured physical prototypes.

7.1.3 Paper III: On Characteristic Eigenvalues of Complex Media in Surface Integral Formulations

I (Zachary Thomas Miers) was the main contributing author, and the lead researcher for the entirety of this scientific work. I was the main researcher involved in all parts of the scientific process, including but not limited to: implementation of all analysis codes (Matlab, C, and Python), numerical analysis, simulation, figure creation, as well as manuscript writing. This manuscript was edited by both Buon Kiong Lau and myself.

This letter provides details on how and why all SIE implementations, symmetric and asymmetric, improperly solved for the Theory of Characteristic Modes (TCM) characteristic eigenvalues. It is shown that the resulting eigenvalues do not pertain to any physical quantity, and cannot be related to the traditional definition of CM eigenvalues. Additionally, this letter provides a method of solving for the correct eigenvalues of both symmetric and forced symmetric MoM impedance matrices. Throughout this letter, no simplification was made on the method used to solve for the MoM impedance matrix, thus allowing the paper to be generalized for use across all TCM implementations. Furthermore, it is shown that once the correct eigenvalues are solved, they can be used to approximate the quality factor for any CM of a given object. The main contributions of this work are:

- Insight into why the solved eigenvalues of SIE TCMs problems, which utilize magnetic currents, are not directly related to the objects reactive power, and

hence do not have a clear physical meaning.

- An effective solution proposed to solve for the correct eigenvalues of any object based on SIE formulations.
- The resonances of the corrected eigenvalues are verified to be nearly the same as to the complex natural resonances of the specific object analyzed.

7.1.4 Paper IV: Antenna Analysis and Design Using Characteristic Modes

I (Zachary Thomas Miers) was the main contributing author, and the lead researcher for the entirety of this scientific work. I was the main researcher involved in all parts of the scientific process, including but not limited to: implementation of all analysis codes (Matlab, C, and Python), numerical analysis, prototype creation, measurements, figure creation, as well as manuscript writing. This manuscript was edited by both Buon Kiong Lau and myself.

In this transaction, a set of equations were developed which allow for a systematic method to design antennas with different features (including narrow-band, wide-band, multi-band, and Multiple-Input Multiple-Output (MIMO)) in a fully integrated system. This technique does not solely rely on the initial intuition of an engineer, but rather it decomposes the CMs into fundamental sources to enable the engineer to better understand the fundamental physical properties of the object. This understanding provides valuable information on achievable performance for a given object and how to adapt the object to improve performance. Furthermore, to design the antenna feed, the method provides an effective way to analyze the characteristic near-fields and currents, identifying a suitable excitation location and type. In this context, the main contributions of this work are:

- The development of an easy-to-follow CM antenna design methodology allowing for the creation of one or more antennas in an integrated system.
- A method was developed to decompose CMs into their fundamental source types, allowing for insight into appropriate structural adaptations.
- An equation developed to analyze the mutual reliance of individual orthogonal CMs (interdependence) in the near-fields and currents, allowing for antenna feed design as well as wide-band and multi-band performance to be obtained.

- A numerical approach was derived to quantify the change of various characteristic attributes over frequency, which can impact the final excitation performance.
- A modal tracking algorithm is applied to track the CMs across different structures, allowing for an in-depth understanding of the differences between the structures from an electromagnetic viewpoint.
- The first fully integrated antenna system designed using TCM, with the performance verified in simulations and measurements.

7.1.5 Paper V: Orthogonal Multi-band Antennas Designed Using Characteristic Modes

I (Zachary Thomas Miers) was the main contributing author, and the lead researcher for the entirety of this scientific work. I was the main researcher involved in all parts of the scientific process, including but not limited to: implementation of all analysis codes (Matlab, C, and Python), numerical analysis, prototype creation, measurements, figure creation, as well as manuscript writing. This manuscript was edited by Buon Kiong Lau, Hui Li, and myself.

In this letter, a novel procedure for exploiting TCM for the analysis and synthesis of objects is proposed. The procedure enables the CMs to be used in the design of dual-band, multi-element antennas which require high isolation and sufficient bandwidth. This was accomplished through manipulating the object (i.e., a mobile terminal) in an industry-acceptable manner, thus demonstrating that it is possible to perturb the characteristic currents of an object in such a way that multiple orthogonal modes are excitable, even when an object is electrically compact. Furthermore, this letter showed that once low frequency modes are realized and excited with suitable antenna feeds, it is possible to track the CMs across frequency, and through further object modification excite additional modes at higher frequencies using the same feeds. The main contributions of this work are:

- The first multi-band MIMO chassis antenna which was implemented using a clearly defined CM design methodology.
- A method for designing terminal antennas with wide-band and multi-band resonances was developed through tracking characteristic near-fields and currents over frequency.

7.1.6 Paper VI: Design of MIMO Terminal Antennas with User Proximity Using Characteristic Modes

I (Zachary Thomas Miers) was the main contributing author, and the lead researcher for the entirety of this scientific work. I was the main researcher involved in all parts of the scientific process, including but not limited to: implementation of all analysis codes (Matlab, C, and Python), numerical analysis, prototype creation, measurements, figure creation, as well as manuscript writing. This manuscript was edited by both Buon Kiong Lau and myself.

In this paper, the SIE TCM formulations of Paper II and III were used to design a MIMO terminal antenna in the presence of human tissue (i.e. lossy dielectrics). Using the described methods, it is possible to analyze a terminal chassis for optimal excitation design and feed implementation in the presence of lossy dielectrics prior to designing and implementing the excitation structures. This design technique presents optimal locations to excite specific CMs of the terminal chassis, which can be chosen based on the total amount of current that is excited within a lossy dielectric. This technique minimizes the effect of human body tissue when it is in close proximity to a terminal antenna structure, allowing for decreased Envelope Correlation Coefficient (ECC) while maintaining high total efficiencies. The main contributions of this work are:

- The Theory of Characteristic Modes utilized to design efficient antennas in the presence of user effects.
- The design procedure in Paper II optimized to allow for the analysis of current density in objects which should not be excited.

7.2 Not-Included, Notable Publications

Although many different contributions were published in the time frame of this doctoral work, only six papers were chosen to be included in this thesis. Here, other publications that are considered to contain significant contributions are briefly overviewed.

Design of Orthogonal MIMO Handset Antennas Based on Characteristic Mode Manipulation at Frequency Bands below 1 GHz

Hui Li, Zachary T. Miers, and Buon Kiong Lau

In *IEEE Transactions on Antennas and Propagation*, Vol. 62, no.5, pp. 2756-2766, May. 2014.

In this transaction, a novel and practical approach to design dual antennas for MIMO mobile handset with very low correlation was proposed for frequencies where the antenna is electrically compact. Through manipulating the chassis in a reasonable manner, two orthogonal resonant modes of the chassis can be created. This was demonstrated using two example modifications of a chassis, in the forms of a bezel loaded chassis and a T-strip loaded chassis. Due to its larger bandwidth, the T-strip loaded chassis was chosen for dual-antenna design, where a coupling feed is used to excite the new mode attributed to the T-strip loading. On the other hand, a coupled monopole is used to excite the chassis' fundamental dipole mode. The T-strip antenna covers Long Term Evolution (LTE) Band 8, whereas the coupled monopole covers both LTE Band 8 and LTE Band 5. The envelope correlation coefficient between the two antennas in free space was below 0.1 over the common operating band. The influence of the user on the performance of the proposed dual-antenna system was studied with respect to a one-hand scenario and a two-hand scenario. The results show that the S parameters and the envelope correlations were only marginally influenced by the hands. However, the efficiencies were more notably decreased by the absorption loss in the hand tissue. Moreover, it was found the capacity of the proposed design is higher than that of a conventional dual-monopole design by 1 - 1.7 bits/s/Hz at a reference Signal to Noise Ratio (SNR) of 20 dB, depending on the user scenario.

Design of Bezel Antennas for Multi-band MIMO Terminals Using Characteristic Modes

Zachary T. Miers, Hui Li, and Buon Kiong Lau

In *Proceedings of the 8th European Conference on Antennas and Propagation*, The Hague, The Netherlands, 2014, pp. 2556-2560.

In this article, the framework as described in Paper V was used to design a multi-band MIMO antenna for a bezel-loaded mobile phone chassis with low antenna correlation and sufficient bandwidth for LTE operation. Through examining the characteristic currents and near-fields of the initial bezel structure, minor ad-

adjustments to the position and size of the ground plane were found to facilitate simultaneous excitation of multiple CMs at frequencies below 1 GHz. Characteristic Mode Analysis (CMA) at the high frequency band provided insights into creating a slot antenna in the structure to support multi-band operation at higher frequencies. The final chassis was capable of supporting multiple efficient and uncorrelated antennas that can simultaneously cover LTE bands 2, 5, 6, 7, 15, 16, 19, and 25.

Effects of Dielectrics and Internal Resonances on Modal Analysis of Terminal Chassis

Zachary T. Miers, and Buon Kiong Lau

In *Proceedings of the 10th European Conference on Antennas and Propagation*, Davos, Switzerland, 2016, pp. 1-5.

In this article, the CMs of a structure are shown to be highly dependent on the materials used to form the structure. Dielectric and magnetic materials load resonant Perfect Electric Conductors (PEC) structures differently, and dielectric objects have the ability to become self-resonant. To determine the influence of mixed-material objects on the inherent CMs symmetry must be forced on the SIE impedance matrix utilized to solve the problem. As described in Section 2.3.4, the symmetric PMCHWT mixed-material SIE impedance matrix is not free from the internal resonance problem, and as such non-real CMs (internal resonances) are found in the solution set. When the CMs of a mixed-material objects were analyzed the modes attributed to non-real CMs, as determined by post-processing, could not be excited or reconstructed using full-wave analysis. These non-excitable modes were thus considered to be non-real CMs and they should be removed before performing traditional CM analysis.

Effects of Internal Components on Designing MIMO Terminal Antennas Using Characteristic Modes

Zachary T. Miers, and Buon Kiong Lau

In *Proceedings of the 10th European Conference on Antennas and Propagation*, Davos, Switzerland, 2016, pp. 1-4.

This article analyzed the impact internal components have on the CMs of a MIMO terminal antenna which has been designed using TCM. It was shown that

the internal components, while physical and electrically small, can have significant impact on the resonant frequencies and excitability of the CMs. Consequently, it is important for these components to be included in TCM-based terminal antenna design.

Post-processing Removal of Non-real Characteristic Modes Via Basis Function Perturbation

Zachary T. Miers, and Buon Kiong Lau

In *Proceedings of the 2016 IEEE Antennas and Propagation Society International Symposium*, Fajardo, Puerto Rico, USA, 2016, pp. 419-420.

In this article, the external fields of the non-real CMs computed using the forced symmetric PMCHWTs MoM impedance matrix are shown to depend on the distribution of the basis functions used. Therefore, it is proposed in this article that mesh perturbation can be utilized to vary the basis functions, and an analysis can be performed in post-processing to determine real CMs from non-real CMs. This is done by analyzing the external fields of a single mode under two different basis function perturbations. If the far-field energy changes across these perturbations, the mode can be attributed to a non-real CM. As an additional criterion, if the correlation of the far-field patterns of a given mode (before and after perturbation) falls below a chosen threshold, the mode can also be considered to be a non-real CM.

Far-Field Orthogonality of Volume-Based Characteristic Modes for Real Materials

Zachary T. Miers, and Buon Kiong Lau

In *Proceedings of the 2016 International Symposium on Antennas and Propagation*, Okinawa, Japan, 2016, pp. 1-2.

In this article, the problem associated with the non-perfect diagonalization of the VIE perturbation and scattering matrix is investigated. When an eigenvalue decomposition is used to define a set of orthogonal characteristic currents for a given lossy VIE impedance matrix, the far-fields as defined by those currents do not provide a perfectly orthogonal set of far-fields. The extent of this problem was studied in this article via two different dielectric resonant structures which were analyzed over six different values of loss. It was found that VIE TCM should only be used for analyzing lossless objects.

7.3 Conclusions

Not all new research, designs, and applications are conceived randomly or miraculously inspired, but rather many are based upon experiences and accumulated knowledge. This is the case for the research contained in this thesis, as well as any new antenna design or application. Often engineers have a predefined knowledge base. Also, when designing antennas some engineers have only a basic understanding of many common antenna topologies, whereas others have what seems to be an uncanny ability to understand complex antenna topologies and how such antennas radiate. However, no matter what an engineer's knowledge base is, it is neither possible nor practical to completely understand how all objects radiate, or how to adapt a preexisting object to radiate efficiently over a defined bandwidth for a specific application. Engineers typically start the antenna design process hypothesizing where to place the initial excitation. This placement often begins with adapting an object to fit within a set of known antenna topologies. However, this ad-hoc approach significantly limits the overall design space, and it also hinders the development of new antenna topologies.

The main goal of this doctoral work has been to demonstrate that TCM is an effective initial design tool which can help an engineer understand the underlying electromagnetic properties of any object. This allows the initial excitation hypothesis and geometrical structure of the object to be guided by physics rather than intuition. Furthermore, this work attempted to create a new antenna design procedure which can be used to systematically shape and excite an object, in order to help design antennas in a truly innovative manner. Furthermore, unlike previous work in this area, the tools created allow TCM to be applied to objects consisting of any material in a computationally efficient manner. Prior to this doctoral work TCM could only be efficiently and accurately computed for arbitrarily shaped conducting bodies.

In this context, Paper I developed a computationally efficient, electromagnetically based, TCM tracking algorithm. This algorithm allows for the real CMs of any object, consisting of any material, to be tracked across a wide frequency range. This tracking allows some Characteristic Attributes (CAs) such as modal quality factor to be obtained, and the tracked modes can then be used in an antenna design process. Paper II, rigorously shows many of the problems associated with deriving the CMs of objects consisting of real materials. Furthermore, this paper presents a method by which the real CMs of dielectric and magnetic object

can be determined using the computationally efficient PMCHWT SIE impedance matrix. However, although this paper proposed a reliable method to solve for the real CMs of any object, many CAs cannot be determined using this approach, because the characteristic eigenvalues are no longer directly related to the object's reactive power. This problem was solved in Paper III, where it was shown that the electric and magnetic current densities could be used to correctly solve for any object's characteristic eigenvalues. Paper IV utilizes the insights from Papers I-III to develop a complete systematic CM design methodology which utilizes a set of CM design tools to assist in understanding the electromagnetic properties of any object. Paper V utilizes many of the developed antenna design techniques from Papers I-IV to design a multi-band multi-element MIMO terminal antenna. Paper VI takes the design process one step further by designing a high efficiency MIMO antenna in the presence of a Cellular Telecommunications Industry Association (CTIA) phantom hand.

7.4 Future Work

While TCM had its humble beginnings as far back as fifty years ago, there is a growing consensus that this field is still in its infancy. The number of barriers which previously existed in TCM analysis has been significantly reduced in recent years. Less than ten years ago, the first overview paper on how to effectively design antennas using CMs was published [129], and only a year later TCM was used to develop a compact MIMO terminal [51]. In the past ten years this field has exploded with interest, as is indicated by the percentage of TCM articles published before 2012 (< 40%) and after (> 60%) within the IEEEExplorer database. This interest has propelled considerable advances in both practical and theoretical aspects of TCM. However, this is just the beginning of a surge in TCM related research, and as such many more updates to this fields should be expected.

TCM's capabilities have matured in many areas, but the area of TCM object-to-object electromagnetic interactions is currently of growing interest throughout the TCM community. Now that it is possible to solve for the CMs of objects containing simple media, antennas can be designed with real components, in real environments. This allows for many object-to-object electromagnetic insights to be obtained, and could provide many new breakthroughs in the area of efficient MIMO terminal antenna design. Other possible new applications for TCM include:

modeling of optical systems, analysis of electrically large objects, phased array design, and development of specialized materials.

New SIE formulations may be found which do not have the internal resonant problem (rather than relying on post-processing removal). However, the internal resonances found using the current SIE formulations could provide insights into why internal resonances form in simple media, and possible applications might be found for these resonances. Furthermore, it is believed that TCM design can be effectively linked with traditional simulation tools and optimization algorithms, to aid in the development of extremely complex systems, which may not be solvable using other analysis techniques. Even though the exact future of TCM cannot be predicted, it is clear that it has several unexplored applications and the potential to solve many problems that plague the field of electromagnetics today.

References

References

- [1] R. J. Garbacz, "Modal expansions for resonance scattering phenomena," *Proceedings of the IEEE*, vol. 53, no. 8, pp. 856–864, Aug. 1965.
- [2] R. Garbacz and R. Turpin, "A generalized expansion for radiated and scattered fields," *IEEE Transactions on Antennas and Propagation*, vol. 19, no. 3, pp. 348–358, May 1971.
- [3] R. Harrington and J. Mautz, "Theory of characteristic modes for conducting bodies," *IEEE Transactions on Antennas and Propagation*, vol. 19, no. 5, pp. 622–628, Sep. 1971.
- [4] R. Harrington and J. Mautz, "Computation of characteristic modes for conducting bodies," *IEEE Transactions on Antennas and Propagation*, vol. 19, no. 5, pp. 629–639, Sep. 1971.
- [5] J. Sturm and J. Liouville, "Mémoire sur la théorie analytique de la chaleur," *Mémoires de l'Académie royale des Sciences*, vol. 21, pp. 145–181, 1831, accessed online, gallica.bnf.fr/ark:/12148/bpt6k3224v.
- [6] G. W. Hanson and A. B. Yakovlev, *Operator Theory for Electromagnetics: An Introduction*. Springer, 2001.
- [7] R. Harrington and J. Mautz, "Control of radar scattering by reactive loading," *IEEE Transactions on Antennas and Propagation*, vol. 20, no. 4, pp. 446–454, Jul. 1972.
- [8] K. Hirasawa, "Reduction of radar cross section by multiple passive impedance loadings," *IEEE Journal of Oceanic Engineering*, vol. 12, no. 2, pp. 453–457, Apr. 1987.
- [9] B. J. Strait and A. T. Adams, "On contributions at Syracuse university to the moment method," *IEEE Transactions on Electromagnetic Compatibility*, vol. EMC-22, no. 4, pp. 228–237, Nov. 1980.
- [10] J. Mautz and R. Harrington, "Modal analysis of loaded n-port scatterers," *IEEE Transactions on Antennas and Propagation*, vol. 21, no. 2, pp. 188–199, Mar. 1973.
- [11] R. Harrington and J. Mautz, "Pattern synthesis for loaded n-port scatterers," *IEEE Transactions on Antennas and Propagation*, vol. 22, no. 2, pp. 184–190, Mar. 1974.
- [12] R. Harrington, "Reactively controlled directive arrays," *IEEE Transactions on Antennas and Propagation*, vol. 26, no. 3, pp. 390–395, May 1978.

-
- [13] D. Liu, R. J. Garbacz, and D. M. Pozar, "Antenna synthesis and optimization using generalized characteristic modes," *IEEE Transactions on Antennas and Propagation*, vol. 38, no. 6, pp. 862–868, Jun. 1990.
- [14] J. Wang, C. Choi, and R. Moore, "Precision experimental characterization of the scattering and radiation properties of antennas," *IEEE Transactions on Antennas and Propagation*, vol. 30, no. 1, pp. 108–112, Jan. 1982.
- [15] A. Yee and R. Garbacz, "Self- and mutual-admittances of wire antennas in terms of characteristic modes," *IEEE Transactions on Antennas and Propagation*, vol. 21, no. 6, pp. 868–871, Nov. 1973.
- [16] R. Garbacz and D. Pozar, "Antenna shape synthesis using characteristic modes," *IEEE Transactions on Antennas and Propagation*, vol. 30, no. 3, pp. 340–350, May 1982.
- [17] D. Pozar, "Antenna synthesis and optimization using weighted Inagaki modes," *IEEE Transactions on Antennas and Propagation*, vol. 32, no. 2, pp. 159–165, Feb. 1984.
- [18] D. Pozar, "Correction to "Antenna synthesis and optimization using weighted Inagaki modes"," *IEEE Transactions on Antennas and Propagation*, vol. 35, no. 6, pp. 742–742, Jun. 1987.
- [19] O. M. Bucci, G. D'Elia, G. Mazzarella, and G. Panariello, "Antenna pattern synthesis: a new general approach," *Proceedings of the IEEE*, vol. 82, no. 3, pp. 358–371, Mar. 1994.
- [20] R. F. Harrington and J. R. Mautz, "Characteristic modes for aperture problems," *IEEE Transactions on Microwave Theory and Techniques*, vol. 33, no. 6, pp. 500–505, Jun. 1985.
- [21] G. Borgiotti, "Integral equation formulation for probe corrected far-field reconstruction from measurements on a cylinder," *IEEE Transactions on Antennas and Propagation*, vol. 26, no. 4, pp. 572–578, Jul. 1978.
- [22] G. Vecchi, P. Pirinoli, L. Matekovits, and M. Orefice, "Use of dynamic modes in the analysis of printed antennas and arrays," in *Proceedings of the IEEE Antennas and Propagation Society International Symposium*, vol. 4, pp. 1834–1837, Jun. 1998.
- [23] E. Newman, "Small antenna location synthesis using characteristic modes," *IEEE Transactions on Antennas and Propagation*, vol. 27, no. 4, pp. 530–531, Jul. 1979.
- [24] B. A. Austin and K. P. Murray, "The application of characteristic-mode techniques to vehicle-mounted NVIS antennas," *IEEE Antennas and Propagation Magazine*, vol. 40, no. 1, pp. 7–21, 30, Feb. 1998.

- [25] Y.-W. Kang and D. Pozar, "Correction of error in reduced sidelobe synthesis due to mutual coupling," *IEEE Transactions on Antennas and Propagation*, vol. 33, no. 9, pp. 1025–1028, Sep. 1985.
- [26] M. Hilbert, M. A. Tilston, and K. G. Balmain, "Resonance phenomena of log-periodic antennas: characteristic-mode analysis," *IEEE Transactions on Antennas and Propagation*, vol. 37, no. 10, pp. 1224–1234, Oct. 1989.
- [27] H. K. Smith, J. R. Mosig, and P. E. Mayes, "Eigenvector analysis of microstrip patch antennas," in *Proceedings of the IEEE Antennas and Propagation Society International Symposium*, vol. 4, pp. 2180–2183, Jun. 1992.
- [28] G. Angiulli and G. D. Massa, "Scattering from arbitrarily shaped microstrip patch antennas using the theory of characteristic modes," in *Proceedings of the IEEE Antennas and Propagation Society International Symposium*, vol. 4, pp. 1830–1833, Jun. 1998.
- [29] J. T. Mayhan, "Characteristic modes and wire grid modeling," *IEEE Transactions on Antennas and Propagation*, vol. 38, no. 4, pp. 457–469, Apr. 1990.
- [30] K. Kabalan, R. Harrington, H. Auda, and J. Mautz, "Characteristic modes for slots in a conducting plane, TE case," *IEEE Transactions on Antennas and Propagation*, vol. 35, no. 2, pp. 162–168, Feb. 1987.
- [31] H. Kawakami and G. Sato, "Broad-band characteristics of rotationally symmetric antennas and thin wire constructs," *IEEE Transactions on Antennas and Propagation*, vol. 35, no. 1, pp. 26–32, Jan. 1987.
- [32] J. Knorr, "Consequences of symmetry in the computation of characteristic modes for conducting bodies," *IEEE Transactions on Antennas and Propagation*, vol. 21, no. 6, pp. 899–902, Nov. 1973.
- [33] R. Harrington, J. Mautz, and Y. Chang, "Characteristic modes for dielectric and magnetic bodies," *IEEE Transactions on Antennas and Propagation*, vol. 20, no. 2, pp. 194–198, Mar. 1972.
- [34] Y. Chang and R. Harrington, "A surface formulation for characteristic modes of material bodies," *IEEE Transactions on Antennas and Propagation*, vol. 25, no. 6, pp. 789–795, Nov. 1977.
- [35] K. A. Obeidat, B. D. Raines, and R. G. Rojas, "Antenna design and analysis using characteristic modes," in *Proceedings of the IEEE Antennas and Propagation Society International Symposium*, pp. 5993–5996, Jun. 2007.
- [36] J. L. T. Ethier and D. A. McNamara, "Antenna shape synthesis without prior specification of the feedpoint locations," *IEEE Transactions on Antennas and Propagation*, vol. 62, no. 10, pp. 4919–4934, Oct. 2014.

- [37] Y. Chen and C. F. Wang, "Characteristic mode synthesis of omni-directional radiation patterns for electrically small UAV," in *Proceedings of the IEEE Antennas and Propagation Society International Symposium*, pp. 1430–1431, Jul. 2015.
- [38] J. Ethier and D. McNamara, "Multiband antenna synthesis using characteristic mode indicators as an objective function for optimization," *IEEE International Conference on Wireless Information Technology and Systems*, pp. 1–4, Aug. 2010.
- [39] M. C. Fabr es, "Systematic design of antennas using the theory of characteristic modes," Ph.D. dissertation, Universidad Politecnica De Valencia, Feb. 2007.
- [40] H. Li, Z. T. Miers, and B. K. Lau, "Design of orthogonal MIMO handset antennas based on characteristic mode manipulation at frequency bands below 1 GHz," *IEEE Transactions on Antennas and Propagation*, vol. 62, no. 5, pp. 2756–2766, May 2014.
- [41] J. J. Adams and J. T. Bernhard, "A modal approach to tuning and bandwidth enhancement of an electrically small antenna," *IEEE Transactions on Antennas and Propagation*, vol. 59, no. 4, pp. 1085–1092, Apr. 2011.
- [42] Y. Chen and C. F. Wang, "Electrically small UAV antenna design using characteristic modes," *IEEE Transactions on Antennas and Propagation*, vol. 62, no. 2, pp. 535–545, Feb. 2014.
- [43] M. Cabedo-Fabres, A. Valero-Nogueira, E. Antonino-Daviu, and M. Ferrando-Bataller, "Modal analysis of a radiating slotted PCB for mobile handsets," in *Proceedings of the 1st European Conference on Antennas and Propagation (EuCAP)*, pp. 1–6, Nov. 2006.
- [44] A. Krewski, W. L. Schroeder, and K. Solbach, "2-port DL-MIMO antenna design for LTE-enabled USB dongles," *IEEE Antennas and Wireless Propagation Letters*, vol. 12, pp. 1436–1439, 2013.
- [45] H. Li, B. K. Lau, Z. Ying, and S. He, "Decoupling of multiple antennas in terminals with chassis excitation using polarization diversity, angle diversity and current control," *IEEE Transactions on Antennas and Propagation*, vol. 60, no. 12, pp. 5947–5957, Dec. 2012.
- [46] K. K. Kishor and S. V. Hum, "A pattern reconfigurable chassis-mode MIMO antenna," *IEEE Transactions on Antennas and Propagation*, vol. 62, no. 6, pp. 3290–3298, Jun. 2014.
- [47] K. K. Kishor and S. V. Hum, "A two-port chassis-mode MIMO antenna," *IEEE Antennas and Wireless Propagation Letters*, vol. 12, pp. 690–693, 2013.

- [48] R. Martens and D. Manteuffel, "Systematic design method of a mobile multiple antenna system using the theory of characteristic modes," *IET Microwaves, Antennas Propagation*, vol. 8, no. 12, pp. 887–893, Sep. 2014.
- [49] R. Martens, J. Holopainen, E. Safin, J. Ilvonen, and D. Manteuffel, "Optimal dual-antenna design in a small terminal multiantenna system," *IEEE Antennas and Wireless Propagation Letters*, vol. 12, pp. 1700–1703, 2013.
- [50] M. H. Rabah, D. Seetharamdoo, and M. Berbineau, "Analysis of miniature metamaterial and magnetodielectric arbitrary-shaped patch antennas using characteristic modes: Evaluation of the Q factor," *IEEE Transactions on Antennas and Propagation*, vol. 64, no. 7, pp. 2719–2731, Jul. 2016.
- [51] J. Ethier, E. Lanoue, and D. McNamara, "MIMO handheld antenna design approach using characteristic mode concepts," *Microwave and Optical Technology Letters*, vol. 50, no. 7, pp. 1724–1727, 2008. [Online]. Available: <http://dx.doi.org/10.1002/mop.23509>
- [52] J. Ethier and D. A. McNamara, "An interpretation of mode-decoupled MIMO antennas in terms of characteristic port modes," *IEEE Transactions on Magnetics*, vol. 45, no. 3, pp. 1128–1131, Mar. 2009.
- [53] J. Ethier and D. A. McNamara, "The use of generalized characteristic modes in the design of MIMO antennas," *IEEE Transactions on Magnetics*, vol. 45, no. 3, pp. 1124–1127, Mar. 2009.
- [54] A. Araghi and G. Dadashzadeh, "Oriented design of an antenna for MIMO applications using theory of characteristic modes," *IEEE Antennas and Wireless Propagation Letters*, vol. 11, pp. 1040–1043, 2012.
- [55] H. Li, Y. Tan, B. K. Lau, Z. Ying, and S. He, "Characteristic mode based tradeoff analysis of antenna-chassis interactions for multiple antenna terminals," *IEEE Transactions on Antennas and Propagation*, vol. 60, no. 2, pp. 490–502, Feb. 2012.
- [56] I. Szini, A. Tatomirescu, and G. F. Pedersen, "On small terminal MIMO antennas, harmonizing characteristic modes with ground plane geometry," *IEEE Transactions on Antennas and Propagation*, vol. 63, no. 4, pp. 1487–1497, Apr. 2015.
- [57] R. Martens and D. Manteuffel, "A feed network for the selective excitation of specific characteristic modes on small terminals," in *Proceedings of the 6th European Conference on Antennas and Propagation (EuCAP)*, pp. 1842–1846, Mar. 2012.
- [58] M. Bouezzeddine and W. L. Schroeder, "Design of a wideband, tunable four-port MIMO antenna system with high isolation based on the theory of characteristic modes," *IEEE Transactions on Antennas and Propagation*, vol. 64, no. 7, pp. 2679–2688, Jul. 2016.

-
- [59] B. Yang and J. J. Adams, "Systematic shape optimization of symmetric MIMO antennas using characteristic modes," *IEEE Transactions on Antennas and Propagation*, vol. 64, no. 7, pp. 2668–2678, Jul. 2016.
- [60] I. Vasilev and B. K. Lau, "On user effects in MIMO handset antennas designed using characteristic modes," *IEEE Antennas and Wireless Propagation Letters*, vol. 15, pp. 758–761, 2016.
- [61] D. Manteuffel and R. Martens, "Compact multimode multielement antenna for indoor UWB massive MIMO," *IEEE Transactions on Antennas and Propagation*, vol. 64, no. 7, pp. 2689–2697, Jul. 2016.
- [62] R. Rezaiesarlak and M. Manteghi, "Design of chipless RFID tags based on characteristic mode theory (CMT)," *IEEE Transactions on Antennas and Propagation*, vol. 63, no. 2, pp. 711–718, Feb. 2015.
- [63] Y. G. Kim and S. Nam, "Determination of the generalized scattering matrix of an antenna from characteristic modes," *IEEE Transactions on Antennas and Propagation*, vol. 61, no. 9, pp. 4848–4852, Sep. 2013.
- [64] A. M. Hassan, F. Vargas-Lara, J. F. Douglas, and E. J. Garboczi, "Electromagnetic resonances of individual single-walled carbon nanotubes with realistic shapes: A characteristic modes approach," *IEEE Transactions on Antennas and Propagation*, vol. 64, no. 7, pp. 2743–2757, Jul. 2016.
- [65] E. Safin and D. Manteuffel, "Reconstruction of the characteristic modes on an antenna based on the radiated far field," *IEEE Transactions on Antennas and Propagation*, vol. 61, no. 6, pp. 2964–2971, Jun. 2013.
- [66] M. W. Young and J. T. Bernhard, "Characteristic mode investigation of a reactively loaded electrically small dipole antenna," in *Proceedings of the 9th European Conference on Antennas and Propagation (EuCAP)*, pp. 1–2, May 2015.
- [67] E. A. Elghannai, B. D. Raines, and R. G. Rojas, "Multiport reactive loading matching technique for wide band antenna applications using the theory of characteristic modes," *IEEE Transactions on Antennas and Propagation*, vol. 63, no. 1, pp. 261–268, Jan. 2015.
- [68] E. Antonino-Daviu, M. Cabedo-Fabres, M. Ferrando-Bataller, and A. Valero-Nogueira, "Wideband double-fed planar monopole antennas," *Electronics Letters*, vol. 39, no. 23, pp. 1635–1636, Nov. 2003.
- [69] H. Li, R. Ma, J. Chountalas, and B. K. Lau, "Characteristic mode based pattern reconfigurable antenna for mobile handset," in *Proceedings of the 9th European Conference on Antennas and Propagation (EuCAP)*, pp. 1–4, May 2015.

- [70] K. A. Obeidat, B. D. Raines, and R. G. Rojas, "Application of characteristic modes and non-foster multiport loading to the design of broadband antennas," *IEEE Transactions on Antennas and Propagation*, vol. 58, no. 1, pp. 203–207, Jan. 2010.
- [71] Y. Chen, "Alternative surface integral equation-based characteristic mode analysis of dielectric resonator antennas," *IET Microwaves, Antennas Propagation*, vol. 10, no. 2, pp. 193–201, 2016.
- [72] J. Eichler, P. Hazdra, J. L. T. Ethier, and M. Mazanek, "Modal resonant frequencies and radiation quality factors of microstrip antennas," *International Journal of Antennas and Propagation*, vol. 2012, no. 490327, pp. 1–9, Jan. 2012.
- [73] K. R. Schab, J. M. Outwater, M. W. Young, and J. T. Bernhard, "Eigenvalue crossing avoidance in characteristic modes," *IEEE Transactions on Antennas and Propagation*, vol. 64, no. 7, pp. 2617–2627, Jul. 2016.
- [74] E. Safin and D. Manteuffel, "Advanced eigenvalue tracking of characteristic modes," *IEEE Transactions on Antennas and Propagation*, vol. 64, no. 7, pp. 2628–2636, Jul. 2016.
- [75] J. L. T. Ethier and D. A. McNamara, "Sub-structure characteristic mode concept for antenna shape synthesis," *Electronics Letters*, vol. 48, no. 9, pp. 471–472, Apr. 2012.
- [76] H. Alroughani, J. L. T. Ethier, and D. A. McNamara, "Observations on computational outcomes for the characteristic modes of dielectric objects," in *Proceedings of the IEEE Antennas and Propagation Society International Symposium*, pp. 844–845, Jul. 2014.
- [77] J. J. Adams and J. T. Bernhard, "Broadband equivalent circuit models for antenna impedances and fields using characteristic modes," *IEEE Transactions on Antennas and Propagation*, vol. 61, no. 8, pp. 3985–3994, Aug. 2013.
- [78] B. Yang and J. J. Adams, "Modal Q as a bounding metric for MIMO antenna optimization," Mar. 2015, pp. 1–2.
- [79] G. A. E. Vandenbosch, "Reactive energies, impedance, and Q factor of radiating structures," *IEEE Transactions on Antennas and Propagation*, vol. 58, no. 4, pp. 1112–1127, Apr. 2010.
- [80] Y. Liu, S. Safavi-Naeini, S. K. Chaudhuri, and R. Sabry, "On the determination of resonant modes of dielectric objects using surface integral equations," *IEEE Transactions on Antennas and Propagation*, vol. 52, no. 4, pp. 1062–1069, Apr. 2004.

-
- [81] R. F. Harrington, *Time-Harmonic Electromagnetic Fields*. New York, NY: McGraw-Hill, 1961.
- [82] W. C. Gibson, *The Method of Moments in Electromagnetics*. Chapman and Hall/CRC, 2007.
- [83] C. Balanis, *Advanced Engineering Electromagnetics*. Hoboken, N.J: John Wiley & Sons, 2012.
- [84] E. Jordan, *Electromagnetic Waves and Radiating Systems*. Englewood Cliffs, N.J: Prentice-Hall, 1968.
- [85] D. Pozar, *Microwave Engineering*. Hoboken, NJ: Wiley, 2012.
- [86] R. F. Harrington, *Field Computation by Moment Methods*. Malabar, FL: Krieger Pub Co, 1968.
- [87] J. Jian-Ming, *Theory and Computation of Electromagnetic Fields*. Hoboken, N.J: Wiley, 2010.
- [88] M. Gustafsson and B. L. G. Jonsson, “Antenna Q and stored energy expressed in the fields, currents, and input impedance,” *IEEE Transactions on Antennas and Propagation*, vol. 63, no. 1, pp. 240–249, Jan. 2015.
- [89] S. Rao, D. Wilton, and A. Glisson, “Electromagnetic scattering by surfaces of arbitrary shape,” *IEEE Transactions on Antennas and Propagation*, vol. 30, no. 3, pp. 409–418, May 1982.
- [90] W. C. Chew, M. S. Tong, and B. Hu, *Integral Equation Methods for Electromagnetic and Elastic Waves (Synthesis Lectures on Computational Electromagnetics)*. Morgan and Claypool Publishers, 2007.
- [91] U. Jakobus, “Comparison of different techniques for the treatment of lossy dielectric/magnetic bodies within the method of moments formulation,” *AEU International Journal of Electronics and Communications*, vol. 54, no. 3, pp. 163–173, 2000.
- [92] J. W. Dettman, *Mathematical Methods in Physics and Engineering*. Dover Publications, 2013.
- [93] K. Kodaira, “The eigenvalue problem for ordinary differential equations of the second order and Heisenberg’s theory of s-matrices,” *American Journal of Mathematics*, vol. 71, no. 4, pp. 921–945, 1949. [Online]. Available: <http://www.jstor.org/stable/2372377>
- [94] A. J. Poggio and E. K. Miller, “Integral equation solutions of three-dimensional scattering problems,” in *Computer Techniques for Electromagnetics*. Elsevier BV, 1973, pp. 159–264. [Online]. Available: <http://dx.doi.org/10.1016/B978-0-08-016888-3.50008-8>

- [95] R. Pike and P. Sabatier, *Scattering, Two-Volume Set: Scattering and Inverse Scattering in Pure and Applied Science*. Academic Press, 2001.
- [96] J. Mautz and R. Harrington, "A combined-source solution for radiation and scattering from a perfectly conducting body," *IEEE Transactions on Antennas and Propagation*, vol. 27, no. 4, pp. 445–454, Jul. 1979.
- [97] C. A. Balanis, *Antenna Theory: Analysis and Design, 3rd Ed.* John Wiley and Sons, 2009.
- [98] R. Fante, "Quality factor of general ideal antennas," *IEEE Transactions on Antennas and Propagation*, vol. 17, no. 2, pp. 151–155, Mar. 1969.
- [99] A. D. Yaghjian and S. R. Best, "Impedance, bandwidth, and Q of antennas," *IEEE Transactions on Antennas and Propagation*, vol. 53, no. 4, pp. 1298–1324, Apr. 2005.
- [100] M. Gustafsson and S. Nordebo, "Optimal antenna currents for Q, superdirectivity, and radiation patterns using convex optimization," *IEEE Transactions on Antennas and Propagation*, vol. 61, no. 3, pp. 1109–1118, Mar. 2013.
- [101] J. Chalas, K. Sertel, and J. L. Volakis, "Computation of the Q limits for arbitrary-shaped antennas using characteristic modes," *IEEE Transactions on Antennas and Propagation*, vol. 64, no. 7, pp. 2637–2647, Jul. 2016.
- [102] M. Gustafsson, D. Tayli, and M. Cismasu, "Q factors for antennas in dispersive media," *Lund University Technical Report LUTEDX*, vol. TEAT-7232, pp. 1–24, 2014, accessed from <http://lup.lub.lu.se/record/4648444/file/4648445.pdf> on 2016-08-29.
- [103] D. B. Davidson, *Computational Electromagnetics for RF and Microwave Engineering*. Cambridge University Press, 2005.
- [104] M. Capek, P. Hamouz, P. Hazdra, and J. Eichler, "Implementation of the theory of characteristic modes in MATLAB," *IEEE Antennas and Propagation Magazine*, vol. 55, no. 2, pp. 176–189, Apr. 2013.
- [105] S. Makarov, "MoM antenna simulations, with Matlab: RWG basis functions," *IEEE Antennas and Propagation Magazine*, vol. 43, no. 5, pp. 100–107, Oct. 2001.
- [106] S. Makarov, *Antenna and EM Modeling with Matlab*. Wiley-Interscience, 2002.
- [107] D. J. Ludick, J. V. Tonder, and U. Jakobus, "A hybrid tracking algorithm for characteristic mode analysis," in *Proceedings of the International Conference on Electromagnetics in Advanced Applications (ICEAA)*, pp. 455–458, Aug. 2014.

- [108] K. A. Obeidat, B. D. Raines, and R. G. Rojas, "Design and analysis of a helical spherical antenna using the theory of characteristic modes," in *Proceedings of the IEEE Antennas and Propagation Society International Symposium*, pp. 1–4, Jul. 2008.
- [109] A. Krewski, W. L. Schroeder, and K. Solbach, "MIMO LTE antenna design for laptops based on theory of characteristic modes," in *Proceedings of the 6th European Conference on Antennas and Propagation (EuCAP)*, pp. 1894–1898, Mar. 2012.
- [110] B. D. Raines and R. G. Rojas, "Wideband tracking of characteristic modes," in *Proceedings of the 5th European Conference on Antennas and Propagation (EuCAP)*, pp. 1978–1981, Apr. 2011.
- [111] Z. Miers and B. K. Lau, "Wideband characteristic mode tracking utilizing far-field patterns," *IEEE Antennas and Wireless Propagation Letters*, vol. 14, pp. 1658–1661, 2015.
- [112] E. Safin, R. Martens, and D. Manteuffel, "Modal source reconstruction based on radiated far-field for antenna design," in *Proceedings of the 6th European Conference on Antennas and Propagation (EuCAP)*, pp. 1645–1649, Mar. 2012.
- [113] T. Cencich and J. A. Huffman, "The analysis of wideband spiral antennas using modal decomposition," *IEEE Antennas and Propagation Magazine*, vol. 46, no. 4, pp. 20–26, Aug. 2004.
- [114] R. B. Lehoucq, D. C. Sorensen, and C. Yang, *Arpack User's Guide: Solution of Large-Scale Eigenvalue Problems With Implicitly Restarted Arnoldi Methods (Software, Environments, Tools)*. Society for Industrial and Applied Mathematics, 1998.
- [115] H. Alroughani, "An appraisal of the characteristic modes of composite objects," Master's thesis, University of Ottawa, Ottawa, Ontario, Canada, Oct. 2013.
- [116] *FEKO User Manual, Suite 7.0*. Stellenbosch, South Africa: EM Software & Systems-S.A. (Pty) Ltd, May 2014.
- [117] Y. Chen and C. F. Wang, *Characteristic Modes: Theory and Applications in Antenna Engineering*. Hoboken, New Jersey: John Wiley and Sons, Inc, 2015.
- [118] W. C. Chew and J. M. Song, "Gedanken experiments to understand the internal resonance problems of electromagnetic scattering," *Electromagnetics*, vol. 27, no. 8, pp. 457–471, Nov. 2007.

- [119] Z. T. Miers and B. K. Lau, "Computational analysis and verifications of characteristic modes in real materials," *IEEE Transactions on Antennas and Propagation*, vol. 64, no. 7, pp. 2595–2607, Jul. 2016.
- [120] Z. Miers and B. K. Lau, "Post-processing removal of non-real characteristic modes via basis function perturbation," in *Proceedings of the IEEE Antennas and Propagation Society International Symposium*, pp. 419–420, Jul. 2016.
- [121] A. Arbabi and S. Safavi-Naeini, "Maximum gain of a lossy antenna," *IEEE Transactions on Antennas and Propagation*, vol. 60, no. 1, pp. 2–7, Jan. 2012.
- [122] J. Rahola, "Effect of antenna Q to the radiation efficiency of tunable antennas," in *Proceedings of the 8th European Conference on Antennas and Propagation (EuCAP)*, pp. 3285–3288, Apr. 2014.
- [123] R. F. Harrington, "Effect of antenna size on gain, bandwidth, and efficiency," *Journal of Research Nat. Bur. Stand. D. Radio Propag.*, vol. 64D, no. 1, pp. 1–12, Jan. 1960.
- [124] A. N. Willson and H. J. Orchard, "Insights into digital filters made as the sum of two allpass functions," *IEEE Transactions on Circuits and Systems I: Fundamental Theory and Applications*, vol. 42, no. 3, pp. 129–137, Mar. 1995.
- [125] A. W. Glisson, D. Kajfez, and J. James, "Evaluation of modes in dielectric resonators using a surface integral equation formulation," *IEEE Transactions on Microwave Theory and Techniques*, vol. 31, no. 12, pp. 1023–1029, Dec. 1983.
- [126] K. Kunz, *The Finite Difference Time Domain Method for Electromagnetics*. Boca Raton: CRC Press, 1993.
- [127] J.-M. Jin, *The Finite Element Method in Electromagnetics*. Hoboken, New Jersey: John Wiley & Sons Inc, 2014.
- [128] M. Cabedo-Fabres, E. Antonino-Daviu, A. Valero-Nogueira, and M. Ferrando-Bataller, "Analysis of wide band planar monopole antennas using characteristic modes," in *Proceedings of the IEEE Antennas and Propagation Society International Symposium*, vol. 3, pp. 733–736, Jun. 2003.
- [129] M. Cabedo-Fabres, E. Antonino-Daviu, A. Valero-Nogueira, and M. F. Bataller, "The theory of characteristic modes revisited: A contribution to the design of antennas for modern applications," *IEEE Antennas and Propagation Magazine*, vol. 49, no. 5, pp. 52–68, Oct. 2007.
- [130] Z. T. Miers and B. K. Lau, "Antenna analysis and design using characteristic modes," in preparation for submission to *IEEE Transactions on Antennas and Propagation*, 2016.